Bose–Einstein Condensates: Excursions beyond the mean field

Ph.D. Thesis

Uffe Vestergaard Poulsen

Department of Physics and Astronomy
University of Aarhus

August 2002
PDF-version in a4wide format: pages don't match printet version

Preface

This thesis is presented for the Faculty of Science at the University of Aarhus, Denmark in order to fulfill the requirements for the Ph.D. degree in Physics. Its main content is work that I have done in cooperation with primarily my supervisor, Klaus Mølmer. The majority of this work has already been published elsewhere as Refs. [1, 2, 3, 4, 5, 6]. Our first publication during my years as a Ph.D. student, Ref. [7], was on magnetic mirrors and is not included in the thesis.

Acknowledgments

First of all I would like to thank my supervisor, Klaus Mølmer, for his enthusiasm and encouragement during the last four years. He is never too busy to discuss or explain a physical problem and his insight and creativity has been a continuous source of inspiration to me.

I also thank Yvan Castin for allowing me to visit Laboratoire Kastler Brossel at the Ecole Normale Supérieure in Paris in the spring of 2001. During my stay, I not only learned a lot of physics, I also met a lot of very friendly people. I would especially like to thank Iacopo Carusotto for numerous invitations to various social events.

My friends and colleagues at the University of Aarhus are likewise acknowledged for the enjoyable atmosphere in which my university studies have taken place. The nearly eight years I have spent at the Departments of Physics and Mathematics have been a pleasure because of the good company provided by both staff and fellow students. Fear of leaving a someone out by mistake prevents me from listing names, you all know who you are.

Finally, I am grateful to family and friends outside the university for being patient with me when I devoted too much attention to physics. In particular, I would like to thank my girlfriend Signe for her love and support.

Uffe Vestergaard Poulsen
Århus, August 2002

Contents

Chapter 1

Introduction to the thesis

This thesis deals mainly with aspects of Bose–Einstein condensates that lie beyond a mean field treatment. Inspired by quantum optics, we[1] have tried to seek out physical situations that cannot be described by the standard Gross–Pitaevskii equation. The uniting themes are correlations and counting statistics more than density distributions, thermodynamics, or superfluidity. Of course, the distinction is never totally clear and we will repeatedly need the concepts of traditional condensed matter physics. The attitude throughout the thesis is, however, that as Bose–Einstein condensation grants us a system with many of the advantages of the unreachable zero temperature, we should embrace this gift and try to make the most of it. For the majority of the work presented, we have assumed a very pure condensate to be at hand and then tried to create more exotic states from this resource.

1.1 Outline of the thesis

The backbone of the thesis is six more or less separate projects done during the authors years as a Ph.D. student. Therefore the number of different subjects covered may seem high and the depth of their treatment may at times be unimpressive. We hope, however, that some continuity of the presentation have been achieved, and that the thesis will be useful beyond its formal purpose.

Not least with this last goal in mind, the introductory Chp. 2 has been included. It will hopefully equip the typical reader with sufficient background knowledge to appreciate (at the very least) why we found the studies worthwhile. For the introduction, a rather direct path to the quantum optical aspects of Bose–Einstein condensates has been chosen: We will start by introducing a many-body wavefunction formulation that should feel pretty familiar to everyone, go on to introduce the second quantized formalism, and soon arrive at the intriguing questions related to measurements on condensates. Although we shall not need it explicitly except in Chp. 6, we include also a discussion of the Bogoliubov approach as it is fundamental for the description of the almost-pure condensate regime that most of our work is carried out in: If one is to ask for corrections to the simple models we sometimes apply, the Bogoliubov approach will usually provide an answer.

Next, in Chp. 3 our numerical tool of choice, the positive P method, is introduced. During the first two years of the thesis work we spend countless hours trying to "fight this dragon",[2] but unfortunately these efforts were mainly fruitless. The presentation is therefore a quite standard one, but intended to be self-contained and readable for the nonspecialist.

The first of the main chapters is Chp. 4 on spin squeezing in two-component condensates. The chapter contains an introduction and four projects, all focussed on describing and utilizing

[1] Throughout the rest of the thesis, the plural "we" and "ours" are used. In the introductory sections this points to "the reader and I", while in the main sections it reflects that most work has be done in collaboration with, primarily, my supervisor, Klaus Mølmer.

[2] A quote from Jean Dalibard.

the correlation between phase and number of atoms produced by the collisional interaction. We first use the positive P method to test a simple model of the physics, and we then propose two applications: A quantum beam splitter for atoms and a source of squeezed light. We also try to estimate the influence of a finite temperature on the longterm behaviour of the system, i.e., on the observation of phase revivals.

In Chp. 5 we take as our optimistic starting point a Bose–Einstein condensate consisting of molecules (not experimentally available at the time of this writing). We then study the special state created when each molecule is split into two atoms. A number of basic quantities are calculated and a particular experiment to demonstrate the peculiar nature of the state is analyzed.

The last project included is perhaps also the simplest one: In Chp. 6 we determine the scattering properties of a condensate when it is bombarded by atoms identical to the ones in the condensate itself. Focusing on a particularly setup, we calculate transmission probabilities etc.

Finally, in Chp. 7 we conclude the thesis by summarizing the main results obtained and some interesting directions for further research.

Chapter 2

Introduction to BEC physics

In this chapter, we give a general introduction which will hopefully make the rest of the thesis accessible to a wider audience. The goal is not so much to be mathematically concise, as to convey a intuitive understanding of the subject. Naturally, other authors may have a different view upon some of the subjects covered, but, if nothing else, this chapter describes the mental framework upon which our research has been build. For more thorough introductions to the many aspects of Bose–Einstein condensation, the reader can consult review articles like Refs. [8, 9, 10] or the recent book by Pethick and Smith [11].

2.1 Many–body wavefunction formulation

We are trying to describe $N \gg 1$ identical, bosonic particles moving in three dimensional space, possibly under the influence of external forces, and in general interacting with each other. A natural starting point is the many–body wavefunction, $\Phi(\mathbf{r}_1, \ldots, \mathbf{r}_N, t)$. If we, for some reason, know that the system is in a particular state, the subsequent time evolution is given by solving the many–body Schrödinger equation,

$$i\hbar \frac{\partial}{\partial t} \Phi(\mathbf{r}_1, \ldots, \mathbf{r}_N, t) = \hat{H} \Phi(\mathbf{r}_1, \ldots, \mathbf{r}_N, t). \tag{2.1}$$

The Hamiltonian, $\hat{H}$, contains single particle terms and interaction terms. We assume the gas to be dilute and therefore three–body and higher interaction terms are neglected:

$$\hat{H} = \sum_{j=1}^{N} \hat{h}(\mathbf{r}_j) + \sum_{\substack{j,k=1 \\ j<k}}^{N} V(\mathbf{r}_j, \mathbf{r}_k) \quad \text{where} \quad \hat{h}(\mathbf{r}) = -\frac{\hbar^2}{2m} \nabla_{\mathbf{r}}^2 + U_{\text{ext}}(\mathbf{r}). \tag{2.2}$$

In the single–particle Hamiltonian, $\hat{h}$, m is the atomic mass and U_{ext} is an external potential. This external potential will (except for the gravitational contribution) depend on some internal structure in the atoms, but we will in this introduction mainly treat the atoms as scalar point particles (for the case of two internal levels, see Sec. 4.1).

2.1.1 The two–body potential

The two–body potential in Eq. (2.2) needs some special care. The real interaction potential between two colliding alkali atoms is rather complicated: The core is strongly repulsive but at intermediate distances the potential is attractive and deep enough to support many bound states. These molecular states imply that the atomic condensate is not the true ground state. In fact, alkali metals at μK temperatures are solids when in true thermal equilibrium and the atomic condensate is only a meta–stable state. This state is long lived due to the relative unlikeliness of

three–body collisions. In Chp. 5 we will have a closer look at the possibility to actually produce molecules from an atomic BEC in a controlled manner, but for the moment we focus on elastic collisions.

The complicated part of the of the inter-atomic potential is fortunately rather short–ranged ($\sim$ nm) compared to typical distances between atoms ($\sim \mu$m). It makes sense, therefore, to assume that we can build a satisfactory theory by focusing on the asymptotic region only. In this region, low energy collision properties are actually described by a single parameter, a_s, the s–wave scattering length. This implies, that we can replace the real interaction potential by another one with correct a_s. The standard choice is a simple contact interaction

$$V_{\text{contact}}(\mathbf{r}) = g\delta(\mathbf{r}) \tag{2.3}$$

where the strength parameter g is given by

$$g = \frac{4\pi\hbar^2 a_s}{m}. \tag{2.4}$$

Strictly speaking this potential needs to be regularized by inclusion of the operator $\frac{\partial}{\partial r} r\cdot$ to remove any irregular component in the wavefunction of the relative motion [12]. This is normally not a concern, especially not when doing numerical calculations on a finite grid.

The sign of g, and thus the repulsive or attractive nature of the interaction, is decided by the sign of a_s. A highly attractive feature of ultracold alkali gases as many–body systems is the possibility to actually tune both magnitude and sign of g by external fields via so-called *Feschbach resonances* [13, 14]. We will return to this subject when we discuss molecule production in Chp. 5. Without special tuning positive values of g are more common than negative ones. Attractive interactions leads to interesting physics, notably the collapse of the system above a certain number of atoms [15, 16, 17]. We shall entirely be working with repulsive interactions, i.e., we will always have $g > 0$ (or put equal to zero for convenience) in the following.

2.1.2 The Gross–Pitaevskii equation

The state of primary interest among all the infinitely many possible ones, is the ground state, i.e., the eigenstate of $\hat{H}$ with the lowest eigenvalue. This is because we can bring the system (at least close to) this state by rather primitive means: we only need some dissipative mechanism, removing energy from the system. In the alkali gas experiments, the dissipative mechanism is initially laser cooling, while the last increase in phase space density is obtained by evaporative cooling. The cooling processes themselves require a more general formalism than the one used here, and we shall be contend with describing the system after the ground state has been produced. At that point, we may apply some manipulation to reach other states: we may shake or deform the trap, or we may apply strong laser or radio-frequency fields to coherently transfer the atoms to other internal states.

The ground state

Let us then start by looking for the ground state. The first thing to try is to make the simple Hartree ansatz

$$\Phi_{\text{GP}}\left(\mathbf{r}_1, \mathbf{r}_2, \ldots, \mathbf{r}_N\right) = \prod_j \phi_0\left(\mathbf{r}_j\right), \tag{2.5}$$

and then minimize $\langle\Phi_{\text{GP}}|\hat{H}|\Phi_{\text{GP}}\rangle$. Assuming $\langle\phi_0|\phi_0\rangle = 1$, we get

$$\langle\Phi_{\text{GP}}|\hat{H}|\Phi_{\text{GP}}\rangle = E_{\text{GP}}[\phi_0, N] \tag{2.6}$$

where the *Gross–Pitaevskii energy functional* is given by

$$E_{\text{GP}}[\phi_0, N] = N\int d^3\mathbf{r}\left\{\frac{\hbar^2}{2m}|\nabla\phi_0(\mathbf{r})|^2 + U_{\text{ext}}(\mathbf{r})\left|\phi_0(\mathbf{r})\right|^2 + \frac{g}{2}\left(N-1\right)\left|\phi_0(\mathbf{r})\right|^4\right\}. \tag{2.7}$$

In $E_{\rm GP}$ we clearly identify kinetic energy, potential energy, and interaction energy. The kinetic and potential energy terms gets equal contributions from all particles and hence a factor N in front, while the interaction term instead has a total factor of $N(N-1)/2$ corresponding to the number of pairs of particles. Introducing a Lagrange multiplier, μ, to take care of the normalization constraint, we end up with the following equation for ϕ_0:

$$\mu\phi_0(\mathbf{r}) = \left[-\frac{\hbar^2}{2m}\nabla^2 + U_{\rm ext}(\mathbf{r}) + g(N-1)\left|\phi_0(\mathbf{r})\right|^2\right]\phi_0(\mathbf{r}). \tag{2.8}$$

This nonlinear Schrödinger equations is the famous Gross–Pitaevskii equation (GPE) [18, 19, 20]. By finding the solution with the lowest possible μ we get very good predictions for the density profile of condensates near their ground state [9]. Referring back to Eq. (2.7) we see that μ is in fact the chemical potential, $\mu = \partial_N E_{\rm GP}$.

Time-dependence

Having obtained a good approximation to the ground state, we would like to be able to manipulate it and to describe these manipulations theoretically. It is clear that if we e.g. move the trapping potential "very slowly" the condensate will following adiabatically. But what happens if we, say, displace the trap rapidly? To describe such a situation, we allow ϕ_0 in Eq. (2.5) to be time-dependent and we do a variational calculation similar to above. Extremalization of the action,

$$A[\Phi_{\rm GP}] = \int dt\left\{\frac{1}{2}\left(\langle\Phi_{\rm GP}|i\hbar\partial_t|\Phi_{\rm GP}\rangle + \text{c.c}\right) - \langle\Phi_{\rm GP}|H|\Phi_{\rm GP}\rangle\right\} \tag{2.9}$$

leads to an approximative solution of Eq. (2.1). We get the time-dependent GPE,

$$i\hbar\partial_t\phi_0(\mathbf{r},t) = \left[-\frac{\hbar^2}{2m}\nabla^2 + U_{\rm ext}(\mathbf{r}) + g(N-1)\left|\phi_0(\mathbf{r},t)\right|^2\right]\phi_0(\mathbf{r},t). \tag{2.10}$$

This equation successfully describes the response of the condensate to changes in the external trapping potential, e.g. the free expansion when the trap is removed completely [21].

Solutions of the Gross–Pitaevskii equation

As nonlinear differential equations, Eqs. (2.8) and (2.10) are not easy to solve analytically and we have to resort to numerical or approximative methods. When interactions are dominant, the main qualitative difference as compared to an ordinary linear Schrödinger equation is a reduced sensitivity to boundary conditions: In a box, the condensate density, $n_0 = N|\phi_0|^2$, will simply be flat except for a region close to the walls.[1] The length scale over which the density attains its bulk value is the *healing length*,

$$\xi = \frac{\hbar}{\sqrt{2gn_0m}} = \frac{1}{\sqrt{8\pi n_0 a_s}}, \tag{2.11}$$

which can be found by balancing kinetic energy and interaction energy. In general, if the external potential varies slowly on the scale of (the local) ξ, the kinetic energy term in Eq. (2.8) can be neglected, and we get the *Thomas–Fermi* approximation:

$$n_0(\mathbf{r}) = N|\phi_0(\mathbf{r})|^2 = \max\left(0, \frac{\mu - U_{\rm ext}(\mathbf{r})}{g}\right). \tag{2.12}$$

Another common approximation is to make a Gaussian ansatz for ϕ_0. This method is obviously good for a harmonic trap and very weak interactions, but can also capture essential features of the dynamics in the strongly interacting case [22]. For a thorough discussion of both the Thomas–Fermi approximation and Gaussian solutions, see Ref. [11].

[1] This can be seen in Fig. 6.1 for the more realistic case of a finite potential depth.

2.1.3 Single particle excitations

The simple Gross–Pitaevskii ansatz, (2.5), is of course not the whole truth. In the low temperature limit, the by far most common next step is the Bogoliubov approach, which will improve on our description of the ground state and encompass both collective and single-particle excitations. We describe this approach in Sec. 2.7 below, after we have introduced some convenient notation. Let us at this point just try one simple thing: Let us make an ansatz like Eq. (2.5) but with one particle out of the condensate. A properly symmetrized expression is

$$\Phi_{\mathrm{GP}*}(\mathbf{r}_1, \mathbf{r}_2, \ldots, \mathbf{r}_N) = \sqrt{\frac{1}{N}} \sum_j \phi_*(\mathbf{r}_j) \prod_{k \neq j} \phi_0(\mathbf{r}_k), \tag{2.13}$$

where $\langle \phi_1 | \phi_0 \rangle = 0$. This ansatz should teach us something about what the world looks like to a single atom out of the condensate. In addition to $E_{\mathrm{GP}}[\phi_0, N-1]$ we get a contribution due to the "noncondensed" atom:

$$E_*[\phi_*, \phi_0] = \int d^3\mathbf{r} \left\{ \frac{\hbar^2}{2m} |\nabla \phi_*(\mathbf{r})|^2 + U_{\mathrm{ext}}(\mathbf{r}) \, |\phi_*(\mathbf{r})|^2 + 2g \, (N-1) \, |\phi_*(\mathbf{r})|^4 \right\}. \tag{2.14}$$

Again we recognize kinetic, potential, and interaction energy. Note, however, the factor of 2 appearing in the interaction term: This comes about because we now have both direct (Hartree) and exchange (Fock) contributions to the scattering. In the resulting equation of motion,

$$i\hbar \partial_t \phi_*(\mathbf{r}) = \left[-\frac{\hbar^2}{2m} \nabla^2 + U_{\mathrm{ext}}(\mathbf{r}) + 2g(N-1) \, |\phi_0(\mathbf{r})|^2 \right] \phi_*(\mathbf{r}), \tag{2.15}$$

the noncondensed atom correspondingly sees twice the mean field of the condensate. As will become apparent in Sec. 2.7, when we discuss the Bogoliubov approach, the Hartree–Fock ansatz, (2.13), is usually only a good approximation at high energies. At low energies, the ansatz wavefunction (2.13) will mix strongly with the totally condensed form (2.5), and the excitations are in fact of a collective nature. This will be dramatically demonstrated in Chp. 6, where an incident atom travels through a condensate that according to Eq. (2.15) would constitute an impenetrable mean field barrier.[2]

2.2 Second quantization

We did not show the details, but to do the variational calculation leading to Eq. (2.14) one has succeed with a fair amount of bookkeeping. This comes about because of the symmetrization of the ansatz wavefunction, (2.13). The task gets increasingly tiresome for more complicated wavefunctions. In this section, we introduce a convenient tool to handle the symmetrization problem, namely *second quantization*.

2.2.1 Productbasis

Quite general (i.e. not only when working with variational ansätze) it is natural to construct a basis for the N–body wavefunctions by making simple products of one–body wavefunctions. Assuming

[2] Strictly speaking, we should not write $2g|\phi_0|^2$ in Eq. (2.15), but rather $g|\phi_0|^2 + g\hat{Q}|\phi_0|^2\hat{Q}$, where $\hat{Q}$ projects on the space orthogonal to ϕ_0. This is because ϕ_* is defined to be orthogonal to ϕ_0, and so the equation of motion needs to conserve this property. Including the $\hat{Q}$'s also makes ϕ_0 itself a stationary solution of Eq. (2.15). In fact we get a complete spectrum of "Hartree–Fock" single-particle states that we will find useful in Sec. 4.5 where we consider the regime of very weak interactions. In the more conventional BEC situation where interactions strongly perturb the trap levels, Eq. (2.15) is mostly useful at high energies and then $\hat{Q}$ can safely be omitted.

$(\phi_k)_{k\in\mathbb{N}}$ to be a basis for the one–body states, the symmetrized many–body basis takes the form

$$\Phi_{(n_k)}(\mathbf{r}_1,\ldots,\mathbf{r}_N) = \sqrt{\frac{1}{N!\prod_k n_k!}}\sum_{\sigma\in S_N}\underbrace{\phi_1(\mathbf{r}_{\sigma(1)})\ldots\phi_1(\mathbf{r}_{\sigma(n_1)})}_{n_1 \text{ factors}}\phi_2(\mathbf{r}_{\sigma(n_1+1)})\ldots \tag{2.16}$$

where the sum is over all permutations. The indistinguishability of the particles implies that only the number of particles in a given ϕ_k matters. Hence, the many–body basis functions are simply labeled by the set of occupation numbers, $(n_k)_{k\in\mathbb{N}} = (n_1, n_2, \ldots)$.

2.2.2 Ladder operators

When working with the basis wavefunctions, $\Phi_{(n_k)}$, it is convenient to introduce ladder operators, $\{\hat{a}_k\}$ and $\{\hat{a}_k^\dagger\}$. If we make the identification

$$\Phi_{(n_k)} \to |n_1, n_2, \ldots\rangle \tag{2.17}$$

they act in the following way:

$$\begin{aligned}\hat{a}_k|n_1,\ldots,n_k,\ldots\rangle &= \sqrt{n_k}|n_1,\ldots,n_k-1,\ldots\rangle\\ \hat{a}_k^\dagger|n_1,\ldots,n_k,\ldots\rangle &= \sqrt{n_k+1}|n_1,\ldots,n_k+1,\ldots\rangle\end{aligned} \tag{2.18}$$

and have the commutation relations

$$[\hat{a}_k, \hat{a}_l] = 0 \quad , \quad [\hat{a}_k, \hat{a}_l^\dagger] = \delta_{kl}. \tag{2.19}$$

In fact, the action of $\hat{a}_k$ takes us out of the N–body Hilbert space and into the $(N-1)$–body Hilbert space. Therefore only N conserving combinations like $\hat{a}_k^\dagger\hat{a}_l$ have a direct representation as operators on symmetric N–body wavefunctions.

A one–body operator respecting the indistinguishability of the particles will be of the form[3]

$$\hat{\mathcal{O}}(\mathbf{r}_1,\ldots,\mathbf{r}_N) = \sum_j \hat{O}(\mathbf{r}_j) \tag{2.20}$$

and the corresponding matrix elements in the basis (2.16) will thus be

$$\sum_{j=1}^N \int d^3\mathbf{r}_1\ldots d^3\mathbf{r}_N \Phi^*_{(n_k)}(\mathbf{r}_1,\ldots,\mathbf{r}_N)\hat{O}(\mathbf{r}_j)\Phi_{(n_l)}(\mathbf{r}_1,\ldots,\mathbf{r}_N) = \sum_{k,l}\sqrt{n_k n_l}O_{kl} \tag{2.21}$$

where $O_{kl} = \int \phi_k^*\hat{O}\phi_l d^3\mathbf{r}$. From (2.18) we see that

$$\hat{\mathcal{O}} = \sum_{k,l}\hat{a}_k^\dagger O_{kl}\hat{a}_l. \tag{2.22}$$

A similar expression holds for two–body operators:

$$\hat{\mathcal{T}} = \sum_{k,l,m,n}\hat{a}_k^\dagger\hat{a}_l^\dagger T_{klmn}\hat{a}_m\hat{a}_n. \tag{2.23}$$

[3]As written here, $\hat{O}(\mathbf{r})$ is a local operator, but it is straightforward to generalize the treatment to any one-body operator.

2.2.3 The field operator

It is often convenient to introduce the *atomic field operator* defined by

$$\hat{\psi}(\mathbf{r}) = \sum_k \hat{a}_k \phi_k(\mathbf{r}). \tag{2.24}$$

The commutation relation reflects the closure property of the (ϕ_k) basis:

$$[\hat{\psi}(\mathbf{r}_1), \hat{\psi}^\dagger(\mathbf{r}_2)] = \sum_k \phi_k^*(\mathbf{r}_1)\phi_k(\mathbf{r}_2) = \delta(\mathbf{r}_1 - \mathbf{r}_2). \tag{2.25}$$

We can express particular states by acting with $\hat{\psi}^\dagger$ on the vacuum, i.e., the state with no atoms present. For example, the one-mode Hartree ansatz, (2.5), reads

$$|\Phi_{\mathrm{GP}}\rangle = |\phi_0, N\rangle = \frac{1}{\sqrt{N!}} \left[\int d^3\mathbf{r}\ \phi_0(\mathbf{r})\hat{\psi}^\dagger(\mathbf{r})\right]^N |\mathrm{vac}\rangle, \tag{2.26}$$

while Eq. (2.13) becomes

$$\begin{aligned} |\Phi_{\mathrm{GP}*}\rangle &= |\phi_0, N-1; \phi_*, 1\rangle \\ &= \frac{1}{\sqrt{(N-1)!}} \left[\int d^3\mathbf{r}\ \phi_0(\mathbf{r})\hat{\psi}^\dagger(\mathbf{r})\right]^{N-1} \left[\int d^3\mathbf{r}\ \phi_*(\mathbf{r})\hat{\psi}^\dagger(\mathbf{r})\right] |\mathrm{vac}\rangle. \end{aligned} \tag{2.27}$$

Operators in the many-body space have a natural representation in terms of field operators. For one-body operators, we find from Eq. (2.22),

$$\mathcal{O} = \sum_{k,l} \int d^3\mathbf{r} \hat{a}_k^\dagger \psi_k^*(\mathbf{r})\hat{O}(\mathbf{r})\psi_l(\mathbf{r})\hat{a}_l = \int d^3\mathbf{r}\ \hat{\psi}^\dagger(\mathbf{r})\hat{O}(\mathbf{r})\hat{\psi}(\mathbf{r}). \tag{2.28}$$

In second quantized form, the Hamiltonian Eq. (2.2) reads

$$\hat{H} = \int d^3\mathbf{r}\ \hat{\psi}^\dagger(\mathbf{r})\hat{h}(\mathbf{r})\hat{\psi}(\mathbf{r}) + \frac{g}{2}\int d^3\mathbf{r}\ \hat{\psi}^\dagger(\mathbf{r})\hat{\psi}^\dagger(\mathbf{r})\hat{\psi}(\mathbf{r})\hat{\psi}(\mathbf{r}), \tag{2.29}$$

when we have put in the contact potential of Eq. (2.3).

2.3 Mixed states

In Sec. 2.1 we worked with the many-body wavefunction and argued that good approximations to the ground state, and even to time-evolution, can be found by making a product ansatz. To pave the road for more sophisticated methods, we introduced the second quantized formalism in Sec. 2.2 as a means to handle the bosonic particle-exchange symmetry of the wavefunction. At this point, we should consider the fact that even if we were able to find theoretically the exact ground state (or the whole set of many-body eigenstates), a realistic experiment would always include some uncertainty. We say that the system is in *mixed state*, i.e., we only have knowledge of the probability, $P(j)$, for the system to be in any one of a number of (many-body!) pure states, $\{|j\rangle\}$. A general observable then has expectation value

$$\langle\hat{\mathcal{A}}\rangle = \sum_j P(j)\langle j|\hat{\mathcal{A}}|j\rangle, \tag{2.30}$$

i.e., a classical average of quantum expectation values.

2.3.1 The density operator

If we introduce the *density operator*,

$$\hat{\rho} = \sum_j P(j)|j\rangle\langle j|, \tag{2.31}$$

Eq. (2.30) be written in a basis independent form,

$$\langle \hat{\mathcal{A}} \rangle = \mathrm{Tr}\left[\hat{\rho}\hat{\mathcal{A}}\right]. \tag{2.32}$$

With the density matrix formalism, it is possible to handle very general situations where interactions with an external environment are included, and we shall touch upon some of these issues below. For a general discussion, see e.g. Ref. [23].

2.3.2 Finite temperature

Depending on the source of our ignorance regarding the precise state of the system, it may be more or less difficult to write down an expression for $\hat{\rho}$. An important model is to assume the system to be in thermal equilibrium at a given temperature T. This usually means, that the system should be able to exchange energy with a reservoir at this T. We then get the *canonical ensemble* density operator,

$$\hat{\rho}_{\mathrm{can}} = \frac{1}{Z} e^{-\beta \hat{H}}, \tag{2.33}$$

where $\beta = 1/k_B T$ and Z ensures normalization. k_B is the Boltzmann constant. We note, that $\hat{\rho}_{\mathrm{can}}$ is diagonal in the basis of eigenstates of (2.29), each eigenstate being given a statistical weight $\exp(-\beta E)$.

Our knowledge of the system will realistically not include the exact number of particles as $N \gg 1$: It is hard to count that many atoms precisely and nondestructively (see, however, Sec. 4.3). The sum in Eq. (2.31) should therefore contain states with different values of N. What the actual distribution of particle numbers should be is a difficult question, depending critically on the history of the system. For mathematical reasons, it proves convenient to embrace the uncertainty by using the *grand canonical* ensemble, where the system can exchange atoms with a particle reservoir. The energy required to extract a particle from the reservoir is assumed to be μ and so (2.33) is replaced by the corresponding *grand canonical* expression,

$$\hat{\rho}_{\mathrm{g.c.}} = \frac{1}{\Xi} e^{-\beta\left(\hat{H} - \mu \hat{N}\right)}, \tag{2.34}$$

where now Ξ ensures normalization. To model a given system, the chemical potential, μ, is adjusted to yield the correct average number of particles. It should be stressed, that there are in general no reason to believe, that the fluctuations in particle number in Bose-condensed systems are well described by the grand canonical ensemble. For interacting particles and in the limit of $N \to \infty$, fluctuations are in fact suppressed in the grand canonical ensemble [12], as one would expect if a system is created out of only moderately correlated particles, but in the more interesting case of intermediate N, the fluctuations can be significant [24, 25].

2.4 Coherence

As soon as we go beyond the simple Gross–Pitaevskii ansatz, (2.26), we need to be a little more precise about the meaning of BEC. In this section we shall formalize the definition "almost all particles in one mode".

2.4.1 The one-body density operator

The *one-body density operator*, $\hat{\rho}_1$, is an operator in the single-particle state space. In position representation, the definition is

$$\langle \mathbf{r}|\hat{\rho}_1|\mathbf{r}'\rangle = \langle \hat{\psi}^\dagger(\mathbf{r}')\hat{\psi}(\mathbf{r})\rangle. \tag{2.35}$$

All one-body observables are determined by $\hat{\rho}_1$

$$\langle \mathcal{O}\rangle = \int d^3\mathbf{r}d^3\mathbf{r}' \ \langle \mathbf{r}|O|\mathbf{r}'\rangle\langle \mathbf{r}'|\hat{\rho}_1|\mathbf{r}\rangle = \mathrm{Tr}\left[\hat{\rho}_1\hat{O}\right]. \tag{2.36}$$

With $\hat{\rho}_1$ we can give well-defined meaning to the number of particles in a given mode: We simply diagonalize $\hat{\rho}_1$,[4]

$$\hat{\rho}_1 = \sum_k \lambda_k|\phi_k\rangle\langle\phi_k|. \tag{2.37}$$

The sum of the eigenvalues gives the average total number of particles, $N = \langle\hat{N}\rangle = \sum_k \lambda_k$. The λ_k's are not necessarily integer, but if we think of measuring one-body properties as first choosing a random particle and then interrogating it, λ_k/N gives the probability that the particle is in mode $|\phi_k\rangle$. A system displays BEC if e.g. λ_0 is of order $O(N)$, while the rest are $O(1)$. Then all one-body properties will be dominated by $|\phi_0\rangle$.[5]

2.4.2 Correlation functions

The concept of mapping the state of the system on the single-particle space can of course be generalized to define m-body density operators. For many purposes, it is sufficient to look at the corresponding *correlation functions*, $g^{(m)}$, $m \in \mathbb{N}$. Basically they measure the probability for finding a particle at $\mathbf{r}$ *and* one at $\mathbf{r}'$ etc. The definition of $g^{(2)}$ is

$$g^{(2)}(\mathbf{r},\mathbf{r}') = \frac{\langle\hat{\psi}^\dagger(\mathbf{r})\hat{\psi}^\dagger(\mathbf{r}')\hat{\psi}(\mathbf{r}')\hat{\psi}(\mathbf{r})\rangle}{\langle\hat{\psi}^\dagger(\mathbf{r})\hat{\psi}(\mathbf{r})\rangle\langle\hat{\psi}^\dagger(\mathbf{r}')\hat{\psi}(\mathbf{r}')\rangle}. \tag{2.38}$$

If we calculate $g^{(2)}$ in the Gross–Pitaevskii state, (2.26), we find

$$g^{(2)}_{\mathrm{GP}}(\mathbf{r},\mathbf{r}') = \frac{|\sqrt{N(N-1)}\phi_0(\mathbf{r})\phi_0(\mathbf{r}')|^2}{|\sqrt{N}\phi_0(\mathbf{r})|^2|\sqrt{N}\phi_0(\mathbf{r}')|^2} = 1 - \frac{1}{N}. \tag{2.39}$$

This result means that the knowledge that one particle is at $\mathbf{r}$ does not change the probability to find another at $\mathbf{r}'$ (except that there is one particle less to choose from). This should be compared to the bunching effect of a noncondensed gas, $g^{(2)}_{\mathrm{th}}(\mathbf{r},\mathbf{r}) = 2$.[6] The difference by a factor of ~ 2 is the same as we found in Sec. 2.1.3 when considering the interaction of a noncondensed particle with the condensate; it is the sum of a direct and an exchange contribution. Looking at the second quantized form of the Hamiltonian, (2.29), we realize that the interaction energy is $\propto \int g^{(2)}(\mathbf{r},\mathbf{r})[n(\mathbf{r})]^2 d^3\mathbf{r}$. Thus the value of $g^{(2)}(\mathbf{r},\mathbf{r})$ can be inferred from a combination of density measurements and a measurement of the released energy when the trap is turned off and the cloud allowed to expand [26, 27].

We also have experimental access to higher order correlation functions. The third order correlation function, $g^{(3)}$, is defined in analogy with $g^{(2)}$. The value at zero separation, $g^{(3)}(\mathbf{r},\mathbf{r},\mathbf{r})$, gives us information on the probability to find 3 atoms at the same point. This should be directly reflected in the rate of three-body recombinations and thus in the rate of trap loss [28]. Here the difference between the fully condensed Gross–Pitaevskii state and a thermal gas is even larger: it is a factor of $3! = 6$. This factor has also been measured with reasonable precision in experiments [29].

[4] This is guaranteed to be possible as $\hat{\rho}_1$is hermitian.

[5] This is the definition of *simple* BEC. It may also be that more than one of the λ_k are $O(N)$; this is refered to as nonsimple or *fragmented* BEC [10].

[6] Strictly speaking, the zero separation ($\mathbf{r} = \mathbf{r}'$) values of the correlation functions are beyond the contact potential approximation. Therefore we don't expect the Gross–Pitaevskii ansatz to give correct predictions in this limit. Accordingly, $\mathbf{r} = \mathbf{r}'$ is here simply shorthand for ,e.g. ,$a_s \ll |\mathbf{r} - \mathbf{r}'| \ll \xi$.

2.4.3 The classical matter wave

The simple form of $g^{(2)}_{\rm GP}$ is a particular example of an (approximate) factorization of correlation functions. If to leading order in N we have

$$\langle \hat{\psi}^\dagger(\mathbf{r}_k)\dots\hat{\psi}^\dagger(\mathbf{r}_1)\hat{\psi}(\mathbf{r}'_1)\dots\hat{\psi}(\mathbf{r}'_k)\rangle \sim \psi^*(\mathbf{r}_k)\dots\psi^*(\mathbf{r}_1)\psi(\mathbf{r}'_1)\dots\psi(\mathbf{r}'_k), \tag{2.40}$$

for some c-number function ψ, we may speak of ψ as a *classical* matter wave describing the system. In the case of $|\Phi_{\rm GP}\rangle$, $\psi = \sqrt{N}\phi_0$, but in general we do not need to assume that the system is in a Gross–Pitaevskii state.

In time dependent situations, we can find the equation of motion for ψ by writing down the Heisenberg equation of motion for the field operator,

$$i\hbar\frac{\partial}{\partial t}\hat{\psi}(\mathbf{r},t) = \left[\hat{\psi}(\mathbf{r},t),\hat{H}\right] \tag{2.41}$$

$$= \hat{h}(\mathbf{r})\hat{\psi}(\mathbf{r},t) + g\hat{\psi}^\dagger(\mathbf{r},t)\hat{\psi}(\mathbf{r},t)\hat{\psi}(\mathbf{r},t). \tag{2.42}$$

The time-dependence of both sides of Eq. (2.40) is given by the productrule of differentiation and therefore we get the equation of motion for ψ by putting $\hat{\psi}\to\psi$ in Eq. (2.41). As expected this results in the Gross–Pitaevskii equation written in terms of ψ,

$$i\hbar\frac{\partial}{\partial t}\psi(\mathbf{r},t) = \left[-\frac{\hbar^2}{2m}\nabla^2 + U_{\rm ext}(\mathbf{r}) + g\left|\psi(\mathbf{r},t)\right|^2\right]\psi(\mathbf{r},t). \tag{2.43}$$

2.4.4 Symmetry breaking

It is definitely not necessary, but the replacement $\hat{\psi}\to\psi$ in normally ordered operator expressions can be summarized as the assumption that the system is in a *coherent state*. A coherent state, $|\psi\rangle$, is an eigenstate of the of field operator, $\hat{\psi}(\mathbf{r})|\psi\rangle = \psi(\mathbf{r})|\psi\rangle$, and we list some of its properties in Appendix A. If the system is really in a coherent state, it has consequences beyond the factorization of number conserving expectation values like (2.40); in fact we get $\langle\hat{\psi}(\mathbf{r})\rangle = \psi(\mathbf{r}) \neq 0$. Assuming a nonvanishing expectation value of the field operator is a so-called *symmetry breaking* point of view. The broken symmetry is the $U(1)$ gauge invariance of the Hamiltonian; $\hat{\psi}\to e^{i\theta}\hat{\psi}$ leaves (2.29) unchanged. To have $\langle\hat{\psi}\rangle \neq 0$ the system must be in a coherent superposition of states with different N. The physical meaning of such superpositions can be questioned in the case of an isolated gas [30, 10]. Nevertheless, coherent states are in many cases easier to work with and except for maybe some conceptual confusion, no harm is usually done by using them. In practical calculations one should of course always average the final result over a random overall phase of ψ. As shown in Appendix A, this means that the corresponding density operator equally well allows an interpretation as a mixture of number states with N's given by a Poissonian distribution.

2.5 Measurements

In principle, any theoretical description of a physical system should include a description of the measurements we can do on the system. For BECs this is even more true as they have the potential for spectacular macroscopic demonstrations of quantum phenomena. We already touched on this subject above, where correlation functions were introduced. In general, measurement theory is unfortunately a rather complicated field, at least if we want to be really careful about the physical implementation and in determining exactly what is being measured [31]. We will therefore only give a brief introduction of the most important concepts.

2.5.1 Simple counting experiments

In the subsequent chapters we shall deal primarily with simple counting experiments: The number of atoms in a certain region of space or in a particular internal state is counted. This can be done

by e.g. shining resonant light onto the sample and looking at the absorption or the fluorescence [32]. The condensation of atoms in meta-stable states also allows sensitive detection on micro-channel plates [33]. If the detection process is very much faster than any dynamics transferring atoms to other internal states or to other regions of space, such a scheme will yield a (destructive) measurement of $\hat{N}_d = \hat{a}_d^\dagger \hat{a}_d$, where $\hat{a}_d$ is the destruction operator for the mode (spatial or internal) in question: The average over many experimental runs will be $\langle \hat{N}_d \rangle$, the variance will be $\langle (\hat{N}_d - \langle \hat{N}_d \rangle)^2 \rangle$, and so on.

2.5.2 Backaction of a measurement

The sudden and single mode approximation made above is often more crude than actual experiments. For example, experiments can include a number of detectors, and these may have good enough time-resolution that we can imagine to count the atoms one by one. It then becomes important to consider the *backaction* of the measurement. The appropriate theory is one of *quantum jumps*, see e.g. Ref. [23]. For illustration, it is useful to imagine a perfect, atom absorbing detector, able to absorb atoms in the mode corresponding to $\hat{a}_d$. The rate of atom absorptions and thus detections is $\Gamma \langle \hat{a}_d^\dagger \hat{a}_d \rangle$. If the detector clicks at time t_k, the state vector of the system changes according to:

$$|t_k\rangle \to |t_k + dt\rangle \propto \hat{a}_d |t_k\rangle. \tag{2.44}$$

Note that we should renormalize before calculating any averages, e.g., the new rate of detections. In the time-intervals between clicks, the state vector also changes: The "nonclicking" of the detector is also a result. This effect is included as a nonhermitian term in the Hamiltonian,

$$\hat{H}_{\mathrm{ba}} = -i\hbar \frac{\Gamma}{2} \hat{n}_d. \tag{2.45}$$

Again, the time evolution will not be norm-conserving and we should in principle renormalize when calculating the instantaneous probability for a detection to occur.

Detection from a Gross–Pitaevskii state

As an example, let us consider atom counting starting from a BEC in a simple product state like in Eq. (2.26). We assume the detector mode, ϕ_d, to be different from the condensate mode, ϕ_0:

$$\phi_0 = \eta_d \phi_d + \eta_\perp \phi_\perp, \tag{2.46}$$

where $|\eta_d|^2 + |\eta_\perp|^2 = 1$. We ignore all dynamics except the one induced by the measurement. At $t = 0$ the state is $|\phi_0, N\rangle$. While we wait for the first detection, the evolution is governed by $\hat{H}_{\mathrm{ba}}$,

$$|t\rangle = e^{-\Gamma \hat{n}_d t/2} |\phi_0, N\rangle \propto |\tilde{\phi}_0(t), N\rangle. \tag{2.47}$$

The new wavefunction, $\tilde{\phi}_0(t)$, is obtained from ϕ_0 by an exponential decay of the component parallel to ϕ_d:

$$\tilde{\phi}_0(t) \propto e^{-\Gamma t/2} \eta_d \phi_d + \eta_\perp \phi_\perp. \tag{2.48}$$

The decay of ϕ_d is expected, but it is somewhat counterintuitive that the decay is driven by the nonclicking of the detector! At some point in time, $t = t_1$, we will detect an atom. We can calculate the effect of the resulting quantum jump:

$$|t_1 + dt\rangle \propto \hat{a}_d |\tilde{\phi}_0(t_1), N\rangle \propto |\tilde{\phi}_0(t_1), N-1\rangle. \tag{2.49}$$

The detection of an atom does not have any other effect on the state than the removal of the atom. We still have $N - 1$ atoms in the mode $\tilde{\phi}_0(t_1)$. The jump is followed by a new period of non-unitary evolution, another jump, etc. All the time, the rate of clicks go down, but we will eventually have removed all atoms. If we stop the detection at time $t = t_f$, the state will be $|\tilde{\phi}_0(t_f), N-k\rangle$, where k is the number of detections up to t_f. This number will vary from experimental run to experimental run, but in this simple model, the new condensate wavefunction is always the same, $\tilde{\phi}_0(t_f)$.

2.5.3 Loss as forgotten detections

What will happen if we forget to record the number of clicks in the detector? Well, as noted above, we still know the system to be in a state of the form $|\tilde{\phi}_0(T), N-k\rangle$, we just don't know k. This is of course one of the situations where the density matrix formalism comes into play. If we as above start in the pure state $|\phi_0, N\rangle$ at $t = 0$, an appropriate description of the system after the detector has been turned on for a time t is

$$\hat{\rho}(t) = \sum_k P(k,t)|\tilde{\phi}_0(t), N-k\rangle\langle\tilde{\phi}_0, N-k|. \tag{2.50}$$

When we forget about the detection record, it is as if the detected atoms were simply lost from the condensate. In fact, it is often possible to model processes involving the environment as measurements. In simplified terms, any system–environment interaction that *allows* us to get information about a given observable of the system by making measurements on the environment will act as measurement of the observable. If we do not actually make the measurement, information is lost and a pure state is turned into a mixed state as in the example above.

2.6 The interference of two condensates

One of the conceptually most important experiments with alkali gas BECs is undoubtly the observation of interference between two independently prepared condensates [34]. In this experiment, two clouds of Sodium atoms were made to condense in a double-well trap. Then the trap was turned off, and the clouds allowed to expanded. At a time where they partly overlapped in space, the density distribution was recorded by absorption imaging. The image showed clear interference fringes. In this section, we analyze a toy model of the experiment, as this will illustrate nicely some of the points made in the previous sections.

2.6.1 An apparent paradox

To model the experiment of Ref. [34], we assume the modes involved to be 1D plane waves moving towards each other:

$$\phi_a(x) = \frac{1}{\sqrt{L}}e^{ik} \quad , \quad \phi_b(x) = \frac{1}{\sqrt{L}}e^{-ik}. \tag{2.51}$$

If we assume the two condensates to be in coherent states, the explanation of the fringes seems simple: With an average of $N/2$ atoms in each condensate, the classical matter waves are $\psi_a = \sqrt{N/2}e^{i\theta_a}\phi_a$ and $\psi_b = \sqrt{N/2}e^{i\theta_b}\phi_b$, and the state can be written (cf. Appendix A)

$$\begin{aligned} |\psi_a, \psi_b\rangle &= e^{\int d^3\mathbf{r}\left(\psi_a\hat{\psi}^\dagger - \psi_a^*\hat{\psi}\right)} e^{\int d^3\mathbf{r}\left(\psi_b\hat{\psi}^\dagger - \psi_b^*\hat{\psi}\right)}|\text{vac}\rangle \\ &= e^{\int d^3\mathbf{r}\left([\psi_a+\psi_b]\hat{\psi}^\dagger - [\psi_a+\psi_b]^*\hat{\psi}\right)}|\text{vac}\rangle \\ &= |\psi_a + \psi_b\rangle. \end{aligned} \tag{2.52}$$

The system is simply in a coherent state with $\langle\hat{N}\rangle = N$ and wavefunction

$$\begin{aligned} \frac{1}{\sqrt{2}}\left[\phi_a + \phi_b\right] &= \frac{1}{\sqrt{2L}}\left[e^{i(kx+\theta_a)} + e^{-i(kx-\theta_b)}\right] \\ &= e^{-i(\theta_a-\theta_b)2}\sqrt{\frac{L}{2}}\cos(kx - kx_0), \end{aligned} \tag{2.53}$$

where $kx_0 = (\theta_b - \theta_a)/2$. In particular, the expectation value of the density shows fringes:

$$\langle\psi_a, \psi_b|\hat{\psi}^\dagger(\mathbf{r})\hat{\psi}(\mathbf{r})|\psi_a, \psi_b\rangle = \frac{N}{L}\left[\cos(kx - kx_0)\right]^2. \tag{2.54}$$

A measurement of the density distribution reveals this fringe pattern.

Consider now what happens if the two condensates are assumed to be in number states. We get

$$\begin{aligned}\langle\phi_a, N/2; \phi_b, N/2|\hat{\psi}^\dagger(\mathbf{r})\hat{\psi}(\mathbf{r})|\phi_a, N/2; \phi_b, N/2\rangle \\ = \frac{N}{2}|\phi_a(\mathbf{r})|^2 + \frac{N}{2}|\phi_b(\mathbf{r})|^2 = \frac{N}{L}\end{aligned} \tag{2.55}$$

Now, there are no fringes! We simply add densities.

2.6.2 Including backaction

Before we jump to the conclusion that coherent states are actually the appropriate description of condensates, we should examine the connection between the calculations of the previous section and the experiment a little closer. We are not simply measuring $\hat{\psi}^\dagger(x)\hat{\psi}(x)$ at a single x; we are actually measuring the density at many positions. "Fringes" are the fact that these measurements are correlated. Several authors have shown how this fringe pattern appears from an initial number states (see, e.g., Refs. [35, 30, 36]), but as the result is so important we recapitulate a simple version of the analysis here.

If we imagine to place identical detectors at each x, we can apply the quantum jump formalism described in Sec. 2.5.2. The rate at which the detector at x will click is $\Gamma\langle\hat{\psi}^\dagger(x)\hat{\psi}(x)\rangle$, and when a it clicks we should apply $\hat{\psi}(x)$ to the state vector. In between clicks, the state evolves according to $\hat{H}_{\rm ba} = -i\int\hat{\psi}^\dagger\hat{\psi}dx\Gamma/2 = -i\hat{N}\Gamma/2$.

Initial number states

We start the experiment, and wait for the first click. During this wait, the number state, $|\phi_a, N/2; \phi_b, N/2\rangle$, being an eigenstate of $\hat{N}$ doesn't change. The expectation values, $\langle\hat{\psi}^\dagger(x)\hat{\psi}(x)\rangle$, that we calculated in the previous sections simply gives the probability of finding *the first* detected atom at x. Assuming the first atom to be detected at $x = x_1$, the associated quantum jump changes the number state to

$$\hat{\psi}(x_1)|N/2, N/2\rangle \propto e^{ikx_1}|(N/2)-1, N/2\rangle + e^{-ikx_1}|(N/2), N/2-1\rangle. \tag{2.56}$$

We now wait for the second atom to be detected. We must calculate the distribution of x_2 from the quantum jumped state, (2.56):

$$\begin{aligned}\langle N/2, N/2|\hat{\psi}(x_1)\hat{\psi}^\dagger(x_2)\hat{\psi}(x_2)\hat{\psi}(x_1)|N/2, N/2\rangle \\ \propto \frac{1}{2} + \left[\cos(kx_2 - kx_1)\right]^2 - \frac{1}{N}.\end{aligned} \tag{2.57}$$

It is clear that the detection of the first atom has a strong influence on the detection of the second: Most likely, it will be detected at position compatible with both x_1 and x_2 being maxima of the same fringe pattern. As more atoms are detected, each detection will become less dependent on the direct previous one and instead obey a fringed distribution picked out early in the process. Once this distribution is established, the state of the system is similar to a number state with the corresponding wavefunction, $\propto \cos(kx - kx_0)$ for some x_0.

Initial coherent states

While we wait for the first detection, the coherent state, $|\psi_a + \psi_b\rangle$, evolves into

$$e^{-\hat{N}\Gamma t/2}|\psi_a + \psi_b\rangle \propto |e^{-\Gamma t/2}(\psi_a + \psi_b)\rangle. \tag{2.58}$$

There is an overall exponential decay of the classical matter wave. Note that this decay doesn't disturb the strong spatial modulation of the probability to detect the first atom at $x = x_1$ as all

detectors are assumed to be equally efficient. The quantum jump has no effect on the coherent state,

$$\hat{\psi}(x_1)|e^{-\Gamma t_1/2}(\psi_a + \psi_b)\rangle \propto |e^{-\Gamma t_1/2}(\psi_a + \psi_b)\rangle, \tag{2.59}$$

and therefore the detection of the first atom at x_1 has no effect on where the second is found: The probability law for detections is frozen from the outset.

2.6.3 Some lessons learned

This example teaches us to be careful when interpreting experiments. Fringes do in fact appear from the number state, the flat distribution found in Eq. (2.55) only telling us about a single detection, or about the average density found when the fringe pattern shifts from experiment to experiment. On the other hand, the preexisting fringes of initial coherent states should also be revisited: Before any measurements has been performed, the phases θ_a and θ_b are unknown to us, and therefore the position of the first detection will seem just as random as for the number state. In the end, the difference between the two ansätze is simply a matter interpretation: Are we revealing an unknown relative phase, or are we establishing a relative phase by measurements. That this should be so is almost clear from the remark at the end of Sec. 2.4.4: The density operator of a mixture of coherent states with random phase is the same as a mixture of number states with Poissonian number distribution.

Another important lesson learned from this example is that even if we are initially sure that the system is in a number state (we have just counted atoms nondestructively), a phase can be established by just a moderate number of detections ($\sim \sqrt{N}$). This means that we can imagine to use a particular condensate as a phase standard for other condensates [37], or to actually unite two initially independent condensates [38].

2.7 The Bogoliubov approach

The Gross–Pitaevskii equation is extremely successful in describing experiments on BEC in dilute alkali gases because the approximation of all atoms being in the same state is for many purposes sufficiently close to the truth. On the other hand, it cannot be the whole truth for at least two reasons: (*i*) The temperature is always finite and not only the exact groundstate is important for the behaviour of the system. (*ii*) The exact ground state will not be an uncorrelated productstate as repulsive interactions make it energetically profitable for atoms to "stay apart", i.e., to be slightly correlated.

We will here give a brief introduction to the so called *Bogoliubov* approach [39]. The idea is to use the dominant role played by the condensate mode in the dynamics also of the noncondensed atoms. Therefore collisions involving more than 2 noncondensate atoms in the ingoing or outgoing channels can be ignored. We shall be using the $U(1)$ symmetry conserving version developed by Gardiner in [40] and by Castin and Dum in [41] (see also [22]). This version differs slightly from the standard one as it doesn't assume $\langle\hat{\psi}\rangle \neq 0$.

2.7.1 Splitting the field

The starting point is the Hamiltonian in second quantized form, (2.29), and a splitting of the atomic field operator,

$$\hat{\psi}(\mathbf{r}) = \hat{a}_0\phi_0(\mathbf{r}) + \delta\hat{\psi}(\mathbf{r}) \quad \text{where} \quad \hat{a}_0 = \int \phi_0^*(\mathbf{r})\hat{\psi}(\mathbf{r})\, d^3\mathbf{r}. \tag{2.60}$$

The first term is the condensate part, the second the noncondensate or fluctuation part. The two parts commute,

$$\left[\delta\hat{\psi}(\mathbf{r}), \hat{a}_0^\dagger\right] = 0. \tag{2.61}$$

The choice of ϕ_0 should ensure that $\hat{a}_0$ is "large" and $\delta\hat{\psi}$ is "small" in the sense that their matrix elements in the actual state of the system are of different order of magnitude.

We now insert (2.60) in the Hamiltonian (2.29) and get:

$$\begin{aligned}\hat{H} = &\int \hat{a}_0^\dagger \phi_0^* \hat{h} \phi_0 \hat{a}_0 \, d^3\mathbf{r} + \int \delta\hat{\psi}^\dagger \hat{h} \delta\hat{\psi} \, d^3\mathbf{r} + \int \left\{ \delta\hat{\psi}^\dagger \hat{h} \phi_0 \hat{a}_0 + \text{h.c.} \right\} d^3\mathbf{r} \\ &+ \frac{g}{2} \int \hat{a}_0^\dagger \hat{a}_0^\dagger |\phi_0|^4 \hat{a}_0 \hat{a}_0 \, d^3\mathbf{r} \\ &+ g \int \left\{ \delta\hat{\psi}^\dagger \hat{a}_0^\dagger |\phi_0|^2 \phi_0 \hat{a}_0 \hat{a}_0 + \text{h.c.} \right\} d^3\mathbf{r} \\ &+ 2g \int \delta\hat{\psi}^\dagger \hat{a}_0^\dagger |\phi_0|^2 \hat{a}_0 \delta\hat{\psi} \, d^3\mathbf{r} + \frac{g}{2} \int \left\{ \delta\hat{\psi}^\dagger \delta\hat{\psi}^\dagger \phi_0^2 \hat{a}_0 \hat{a}_0 + \text{h.c.} \right\} d^3\mathbf{r} \\ &+ g \int \left\{ \delta\hat{\psi}^\dagger \delta\hat{\psi}^\dagger \phi_0 \hat{a}_0 \delta\hat{\psi} + \text{h.c.} \right\} d^3\mathbf{r} \\ &+ \frac{g}{2} \int \left\{ \delta\hat{\psi}^\dagger \delta\hat{\psi}^\dagger \delta\hat{\psi} \delta\hat{\psi} + \text{h.c.} \right\} d^3\mathbf{r}.\end{aligned} \tag{2.62}$$

The terms in Eq. (2.62) all have a clear interpretation. The first line describes the single–particle dynamics, the rest is due to the collisional interaction. As ϕ_0 is supposed to be the only macroscopically populated mode, collisions involving atoms in this mode are much more frequent than collisions among atoms in other modes. Therefore we should work our way down through Eq. (2.62), dealing first with the terms in the upper lines.

2.7.2 Identifying the condensate

So far we have not specified ϕ_0. A natural choice would be as the dominant eigenvector of the one-body density operator, corresponding to the definition of BEC introduced in Sec. 2.4.1. We then have

$$\langle \hat{a}_0^\dagger \delta\hat{\psi} \rangle = 0, \tag{2.63}$$

and the whole theory can be developed by demanding this equation to hold at all times and to all orders in the small parameter $\sqrt{\delta N / N_0}$, where $\delta N = N - N_0$ is the number of noncondensed particles [41]. Here we give a simplified presentation in the same spirit.

If we were to choose ϕ_0 to be an eigenstate of $\hat{h}$, the last term in the first line would vanish, i.e., the single–particle Hamiltonian would not exchange particles between "condensate" and "noncondensate". This nice picture is quickly ruined by the interactions. The second line describes rather harmless collisions, where both incoming and outgoing atoms are in the ϕ_0 state, but already the terms on the third line will exchange atoms between ϕ_0 and other modes. The solution is to choose ϕ_0, not as an eigenstate of $\hat{h}$, but as an approximative "dark" state for a combined action of the last term in the first line and the terms in the third line. Not surprisingly, this condition leads directly to the Gross–Pitaevskii equation: If ϕ_0 solves Eq. (2.8) there will be no terms leading to linear exchange of particles between condensate and noncondensate, i.e., no terms linear in $\delta\hat{\psi}$ or $\delta\hat{\psi}^\dagger$.

2.7.3 Quadratic terms

At the next level of approximation, we need to deal with the terms quadratic in the noncondensate operators. There are both terms conserving the number of noncondensed particles ($\delta\hat{\psi}^\dagger \delta\hat{\psi}$), and terms creating ($\delta\hat{\psi}^\dagger \delta\hat{\psi}^\dagger$) or destroying ($\delta\hat{\psi}\delta\hat{\psi}$) pairs of noncondensed particles.

The full Hamiltonian, (2.62), naturally conserves the total number of atoms. We would like this property to be carried over to our approximate description. This requires some care, but a foolproof approach is to define

$$\hat{\Lambda} = \frac{1}{\hat{N}^{1/2}} \hat{a}_0^\dagger \delta\hat{\psi} \tag{2.64}$$

and express everything in terms of $\hat{\Lambda}$ and $\hat{\Lambda}^\dagger$. In the limit of an almost pure condensate, these operators obey the commutation relation

$$\left[\hat{\Lambda}(\mathbf{r}), \hat{\Lambda}^\dagger(\mathbf{r}')\right] \cong \delta(\mathbf{r}-\mathbf{r}') - \phi_0(\mathbf{r})\phi_0^*(\mathbf{r}') \tag{2.65}$$

as they are orthogonal to ϕ_0. Expressing the Hamiltonian in terms of $\hat{N}$, $\hat{\Lambda}$, and $\hat{\Lambda}^\dagger$, and keeping only terms quadratic in the $\hat{\Lambda}$'s, we end up with

$$\hat{H}_{\text{quad}} = f(\hat{N}) + \frac{1}{2}\int d^3\mathbf{r}\, \left(\hat{\Lambda}^\dagger, -\hat{\Lambda}\right)\hat{\mathcal{L}}\begin{pmatrix}\hat{\Lambda}\\ \hat{\Lambda}^\dagger\end{pmatrix}. \tag{2.66}$$

The term $f(\hat{N})$ only depends on the total number of particles and contributes therefore only an overall phase to a state of definite N. The operator $\hat{\mathcal{L}}$ is given by

$$\hat{\mathcal{L}} = \begin{pmatrix}\hat{H}_{\text{GP}} + g\hat{Q}|\phi_0|^2\hat{Q} & g\hat{Q}\phi_0^2\hat{Q}^* \\ -g\hat{Q}^*\phi_0^{*2}\hat{Q} & -\hat{H}_{\text{GP}} - g\hat{Q}^*|\phi_0|^2\hat{Q}^*\end{pmatrix} \tag{2.67}$$

with $\hat{Q} = 1 - |\phi_0\rangle\langle\phi_0|$, the projector onto the space orthogonal to ϕ_0, and $\hat{H}_{\text{GP}} = \hat{h} + gN|\phi_0|^2 - \mu$.[7]

From $\hat{H}_{\text{quad}}$ we get the equation of motion for $\hat{\Lambda}$ and $\hat{\Lambda}^\dagger$,

$$i\frac{d}{dt}\begin{pmatrix}\hat{\Lambda}\\ \hat{\Lambda}^\dagger\end{pmatrix} = \hat{\mathcal{L}}\begin{pmatrix}\hat{\Lambda}\\ \hat{\Lambda}^\dagger\end{pmatrix}. \tag{2.68}$$

It is clear, that $\hat{\mathcal{L}}$ should not have any eigenvalues with positive imaginary part, as these will lead to an exponential divergence of $\hat{\Lambda}$ and $\hat{\Lambda}^\dagger$. In fact, it can be shown that Eq. (2.68) is also the one obtained from a linear stability analysis of the Gross–Pitaevskii equation: $(\hat{\Lambda}, \hat{\Lambda}^\dagger)$ is simply replaced by $(\delta\phi_\perp, \delta\phi_\perp^*)$, where $\delta\phi_\perp$ is a deviation perpendicular to ϕ_0 [22].

2.7.4 Diagonalizing $\hat{\mathcal{L}}$

We want to diagonalize $\hat{\mathcal{L}}$, so we need to find eigenvectors and eigenvalues:

$$\hat{\mathcal{L}}\begin{pmatrix}|u_k\rangle\\ |v_k\rangle\end{pmatrix} = \epsilon_k\begin{pmatrix}|u_k\rangle\\ |v_k\rangle\end{pmatrix}. \tag{2.69}$$

These two coupled equations are the *Bogoliubov–de Gennes equations.* $\hat{\mathcal{L}}$ is not Hermitian, but it is has some important symmetries. One of these ensures that $\hat{H}_{\text{quad}}$ is Hermitian:

$$\hat{\mathcal{L}}^\dagger = \begin{pmatrix}1 & 0\\ 0 & -1\end{pmatrix}\hat{\mathcal{L}}\begin{pmatrix}1 & 0\\ 0 & -1\end{pmatrix}. \tag{2.70}$$

This symmetry also means that if (u_k, v_k) is an eigenvector of $\hat{\mathcal{L}}$ with eigenvalue ϵ_k then $(u_k, -v_k)$ is an eigenvector of $\hat{\mathcal{L}}^\dagger$ also with eigenvalue ϵ_k. In fact, as quite generally the spectrum of the hermitian conjugate operator is the complex conjugate of the original spectrum, we then find that ϵ_k^* must be in $\hat{\mathcal{L}}$'s spectrum. This refines the condition for dynamical stability; all eigenvalues of $\hat{\mathcal{L}}$ should be real.

Another symmetry,[8]

$$\hat{\mathcal{L}}^* = -\begin{pmatrix}0 & 1\\ 1 & 0\end{pmatrix}\hat{\mathcal{L}}\begin{pmatrix}0 & 1\\ 1 & 0\end{pmatrix}, \tag{2.71}$$

implies that if (u_k, v_k) is an eigenvector with eigenvalue ϵ_k then (v_k^*, u_k^*) is an eigenvector with eigenvalue $-\epsilon_k^*$. In the following, we assume dynamical stability, i.e., all eigenvalues are real.

[7] Note that $\hat{Q}^*$ is not the hermitian conjugate of $\hat{Q}$; rather, it is the projector orthogonal to ϕ_0^*: $\hat{Q}^* = 1 - |\phi_0^*\rangle\langle\phi_0^*|$

[8] This notation is a little imprecise: the complex conjugation is understood to be done in the position representation.

The eigenvectors come in pairs $(u_k, v_k), (v_k^*, u_k^*)$ with eigenvalues $\epsilon_k, -\epsilon_k$. A special case is the two eigenvectors corresponding to the eigenvalue 0: $(\phi_0, 0), (0, \phi_0^*)$. As we assume the set of eigenvectors to be complete, we can write

$$S^{-1}\hat{\mathcal{L}}S = \mathrm{diag}(0, 0, \epsilon_1, -\epsilon_1, \ldots, \epsilon_k, -\epsilon_k, \ldots), \tag{2.72}$$

where the diagonalizing matrix is

$$S = \left[\begin{pmatrix} |\phi_0\rangle \\ 0 \end{pmatrix} \quad \begin{pmatrix} 0 \\ |\phi_0^*\rangle \end{pmatrix} \quad \cdots \quad \begin{pmatrix} |u_k\rangle \\ |v_k\rangle \end{pmatrix} \quad \begin{pmatrix} |v_k^*\rangle \\ |u_k^*\rangle \end{pmatrix} \quad \cdots \quad \right]. \tag{2.73}$$

As $\hat{\mathcal{L}}$ is not hermitian, S is not a unitary matrix, i.e., $S^{-1} \neq S^\dagger$. What we need in order to find S^{-1} are the eigenvectors of $\hat{\mathcal{L}}^\dagger$: Eigenvectors of $\hat{\mathcal{L}}^\dagger$ and $\hat{\mathcal{L}}$ are orthogonal unless the corresponding eigenvalues are complex conjugate.[9] As we assume real eigenvalues this boils down to eigenvectors of $\hat{\mathcal{L}}^\dagger$ and $\hat{\mathcal{L}}$ being orthogonal unless the corresponding eigenvalues are equal. The symmetry expressed in Eq. (2.70) then makes it easy to find the adjoint partners of (u_k, v_k) and (v_k^*, u_k^*): They are $(u_k, -v_k)$ and $(-v_k^*, u_k^*)$ and we have[10]

$$\big(\langle u_k|, -\langle v_k|\big) \begin{pmatrix} |u_{k'}\rangle \\ |v_{k'}\rangle \end{pmatrix} = \langle u_k|u_{k'}\rangle - \langle v_k|v_{k'}\rangle = 0 \quad \text{, for } k \neq k \tag{2.74}$$

$$\big(-\langle v_k^*|, \langle u_k^*|\big) \begin{pmatrix} |u_{k'}\rangle \\ |v_{k'}\rangle \end{pmatrix} = \langle u_k^*|v_{k'}\rangle - \langle v_k^*|u_{k'}\rangle = 0 \quad \text{, for all } k, k', \tag{2.75}$$

as well as $\langle u_k|\phi_0\rangle = \langle v_k^*|\phi_0\rangle = 0$, and similar expressions for ϕ_0^*. The final issue is one of normalization: When we put

$$S^{-1} = \begin{bmatrix} \vdots \\ \big(\langle u_k|, -\langle v_k|\big) \\ \big(-\langle v_k^*|, \langle u_k^*|\big) \\ \vdots \end{bmatrix}, \tag{2.76}$$

we must have

$$\langle u_k|u_k\rangle - \langle v_k|v_k\rangle = +1. \tag{2.77}$$

This can always be arranged by renormalization as we are free to rename $u_k, v_k, \epsilon_k \to v_k^*, u_k^*, -\epsilon_k$, should the sign be negative at first.

2.7.5 Diagonalizing the Hamiltonian

The quadratic Hamiltonian, (2.66), can be diagonalized by the similarity transformation, S. The operators, corresponding to the eigenvalues ϵ_k and $-\epsilon_k$ are denoted $\hat{b}_k$, respectively $\hat{b}_k^\dagger$. We find the *Bogoliubov transformation*

$$\hat{b}_k = \big(\langle u_k|, -\langle v_k|\big) \begin{pmatrix} \hat{\Lambda} \\ \hat{\Lambda}^\dagger \end{pmatrix} = \int d^3\mathbf{r} \, \left[u_k^*(\mathbf{r})\hat{\Lambda}(\mathbf{r}) - v_k^*(\mathbf{r})\hat{\Lambda}^\dagger(\mathbf{r}) \right] \tag{2.78}$$

By virtue of the normalization, Eqs. (2.74), (2.75), and (2.77), the $\hat{b}_k$'s and $\hat{b}_k^\dagger$'s obey the canonical commutation relations,

$$[\hat{b}_k, \hat{b}_{k'}] = 0 \quad , \quad [\hat{b}_k, \hat{b}_{k'}^\dagger] = \delta_{kk'}. \tag{2.79}$$

The final form of $\hat{H}_{\mathrm{quad}}$ is simply

$$\hat{H}_{\mathrm{quad}} = E_0(\hat{N}) + \sum_k \epsilon_k \hat{b}_k^\dagger \hat{b}_k, \tag{2.80}$$

[9] This is simply the generalization of the orthogonality of eigenvectors belonging to different eigenvalues of a Hermitian operator.

[10] In case of degeneracy of eigenvalues some obvious extra selection of partners is necessary.

where again the term $E_0(\hat{N})$ has trivial consequences for a state of definite total N. It is given by:

$$E_0(\hat{N}) = \hat{N}\langle\phi_0, N|\hat{H} + \frac{1}{2}g(N-1)|\phi_0|^2|\phi_0, N\rangle - \sum_k \epsilon_k\langle v_k|\rangle. \tag{2.81}$$

Note the resemblance of the first term with $E_{\rm GP}$ of Eq. (2.7). We comment on the second term below.

2.7.6 Quasi-particles

According to Eq. (2.80) the system can be described as a gas of non-interacting *quasi-particles*. The quasi-particles in the k'th mode are created by $\hat{b}_k$ and $\hat{b}_k^\dagger$. Expressed in terms of $\hat{\Lambda}$ and $\hat{\Lambda}^\dagger$ [Eq. (2.78)], the removal of a quasiparticle corresponds to a super-position of moving a (real) particle into condensate (amplitude u_k) and moving a particle out of the condensate (amplitude v_k^*). This mixed particle–hole character of the excitations reflects the special influence of the condensate on the noncondensed particles which is not fully captured by a Hartree–Fock ansatz.

The Bogoliubov analysis is routinely applied to the case of a homogeneous situation (flat potential) and the case of an infinite trapping potential [9]. In the first case, one obtains solutions with well-defined momenta: phonons in the long wave–length limit, free particles for high momenta. The spectrum is continuous and gap-less. In the second case, the excitations are again collective in the low energy regime, approaching single-particle trap states for high energies [42]. The spectrum is discrete. In Chp. 6 of this thesis we will concentrate on a third situation where the trapping potential has finite width and depth. In this scenario, a finite number of trapped excitations exists and above these a continuum of scattering states.

2.7.7 Ground state and depletion

An important observation is that $\hat{H}_{\rm quad}$ is only bounded from below if all $\epsilon_k \geq 0$: If for some k we have $\epsilon_k < 0$, the energy can be lowered by creating quasi-particles in this mode. In particular, the system will be thermodynamically unstable. Assuming that there is no negative eigenvalues of $\hat{\mathcal{L}}$, the ground state will clearly be the state with no quasi-particles present, i.e., the vacuum of all the destruction operators,

$$\hat{b}_k|{\rm vac}\rangle_{\rm bog} = 0. \tag{2.82}$$

We denote the *Bogoliubov vacuum* $|{\rm vac}\rangle_{\rm bog}$ to distinguish it from the ordinary vacuum with no particles present, $|{\rm vac}\rangle$.

We can calculate the *depletion* of the condensate, i.e., the number of particles not in ϕ_0. We find:

$$\begin{aligned}\langle\delta\hat{N}\rangle &= \int d^3\mathbf{r}\ \langle\delta\hat{\psi}^\dagger(\mathbf{r})\delta\hat{\psi}(\mathbf{r})\rangle \\ &\cong \int d^3\mathbf{r}\ \langle\hat{\Lambda}^\dagger(\mathbf{r})\hat{\Lambda}(\mathbf{r})\rangle \\ &= \sum_k\langle\hat{b}_k^\dagger\hat{b}_k\rangle\big[\langle u_k|u_k\rangle + \langle v_k|v_k\rangle\big] + \sum_k\langle v_k|v_k\rangle.\end{aligned} \tag{2.83}$$

As expected, the connection between the number of quasi-particles and the depletion is not very direct. The number of particles taken out of the condensate by the creation of each quasi-particle is $\langle u_k|u_k\rangle + \langle v_k|v_k\rangle = 1 + 2\langle v_k|v_k\rangle$. In addition, even in the Bogoliubov vacuum there is a *quantum depletion*, $\sum_k\langle v_k|v_k\rangle$. This sum quantifies how much the ground state deviates from the simple Gross–Pitaevskii form. We found a similar sum in E_0 [cf. Eq. (2.81)], and that sum analogously describes the deviation of the ground state energy from the Gross–Pitaevskii result, $E_{\rm GP}[\phi_0, N]$.[11]

When the Bogoliubov mode functions have been found, one should check the consistency of the approach, i.e., that the quantum depletion is small. Depending on the particular situation,

[11] In fact, a few infinities are hidden in these sums and they require the use of the regularized pseudo potential [41].

it may also be possible to evaluate the number of quasi-particles present. An important example is thermal equilibrium, where the canonical density operator, $\hat{\rho}_{\rm can}$, of Eq. (2.33) gives us the well-know Bose-distribution of quasi-particles,

$$\langle \hat{b}_k^\dagger \hat{b}_k \rangle = \frac{1}{e^{\beta\epsilon_k} - 1}. \tag{2.84}$$

For some explicit evaluations of the sums in Eq. (2.83), see Ref. [22].

As the Bogoliubov modes are the fundamental excitations of the system, a (weak) perturbation can selectively create quasi-particles. If the perturbation oscillates at frequency $\epsilon_k/\hbar$, the k'th mode will be populated. In a homogeneous setting, quasi-particles of a specified momentum can also be selected by the spatial periodicity of the perturbation.[12] If we instead insist on the promotion of a single, real particle from the condensate mode, we are creating a superposition of different quasi-particles. For example, the state analogous to $|\Phi_{\rm GP*}\rangle$ of Eq. (2.27) is

$$\int d^3\mathbf{r}\ \phi_*(\mathbf{r})\hat{\Lambda}^\dagger(\mathbf{r})|{\rm vac}\rangle_{\rm bog} = \sum_k \langle u_k|\phi_*\rangle |n_k = 1\rangle_{\rm bog}. \tag{2.85}$$

In Chp. 6, where we study particles sent in from regions outside the condensate, this is a natural starting point.

2.7.8 Phase diffusion

The symmetry preserving Bogoliubov approach that we have presented here is not the one most commonly found in the literature. Instead, one often assumes $\langle\hat{\psi}\rangle = \psi$ and writes

$$\hat{\psi} = \psi + \delta\hat{\psi}. \tag{2.86}$$

The analysis then follows essentially the same lines as above. The major difference is that the $\hat{Q}$'s and $\hat{Q}^*$'s do not appear. This has a curious effect on $\hat{\mathcal{L}}$: without the projection operators, the spectrum is the same, but we only find one eigenvector corresponding to the eigenvalue 0! The missing eigenvector means that we cannot diagonalize the Hamiltonian. The "physical" explanation is the excitation (Goldstone mode) we have introduced by breaking the $U(1)$ symmetry: The phase of the condensate wavefunction can be changed with no energy cost, and will therefore spread out [45, 46].

In the symmetry preserving Bogoliubov theory, the overall phase of the condensate wavefunction is explicitly eliminated from the dynamics. In this language, the equivalent of the spreading of phase is a decay of the two-time correlation function $\langle\hat{\psi}^\dagger(t')\hat{\psi}(t)\rangle$ when averaged over an unknown distribution of the total number of particles [41]. The correlation function decays because the $E_0(\hat{N})$ term in Eq. (2.80) makes the phase evolution of the condensate operators depend nonlinearly on N.[13] In an experiment where time correlations are measured, perfect "fringes" will be seen for each experimental run, but the period of oscillation is different in each realization. This is just as in Sec. 2.6 where the position of spatial fringes shifted from experiment to experiment.

[12] This was recently used at MIT to experimentally measure the u and v contributions separately [43] following a theoretical proposal by Brunello *et al.* [44]

[13] The noncondensed part is smaller and mostly averages to zero

Chapter 3

The positive P method

In this chapter we give an introduction to the *positive P method* that we shall be using in Chapters 4 and 5. The presentation is will necessarily be somewhat brief and we shall focus mainly on aspects directly relevant for describing BEC physics. For a thorough discussion, see Ref.[23] and references therein.

We start in Sec. 3.1 by sketching a program for doing "exact" computer simulations of BEC dynamics. In Sec. 3.2 a first attempt at following this plan comes to grinding halt as the naive coherent state simulations (Glauber–Sudarshan P distribution) proves insufficient. Positive P is presented as the intriguing answer to the problem in Sec. 3.3 and finally we discuss various applications and related methods in Sec. 3.4.

3.1 A Monte Carlo technique for BEC dynamics

For even moderate numbers of particles it is completely out of the question to solve the time-dependent N-body Schrödinger equation, (2.1), for interacting particles. Even storing the wave-function would be a heavy task: N particles in M modes require N^M coefficients to be kept in memory. Luckily, we are rarely interested in anything but few-body observables and for these, approximation schemes exist, as described in the previous chapter. If the gas can be assume to be in thermal equilibrium, it is even possible by Monte Carlo techniques to calculate expectation values of observables exactly [47]. Such techniques are based on a prescription for producing an ensemble of numbers which will have a mean value corresponding to the desired expectation value. To get good precision, a large ensemble is needed and calculation can thus be time-consuming. The big advantage, as compared to a direct solution, is that the calculation is split into manageable pieces. In contrast to many approximation schemes, a very good estimate of the error on the result can be obtained by simple statistical analysis of the ensemble.

Now, let us try to find a Monte Carlo technique that can be used in non-equilibrium, time-dependent situations. It should have the same advantages as the equilibrium sampling techniques, i.e., results should emerge as ensemble averages, and the calculation of each member of the ensemble should be a manageable task. A strategy could be the following: write the density operator as a time-dependent mixture of coherent states,

$$\hat{\rho}(t) = \int d^2\psi \; |\psi\rangle\langle\psi| P[\psi, \psi^*, t], \tag{3.1}$$

and try to sample the distribution, i.e., choose an ensemble of $\mathcal{N}$ time-dependent coherent states such that

$$\int d^2\psi \; |\psi\rangle\langle\psi| P[\psi, \psi^*, t] \cong \frac{1}{\mathcal{N}} \sum_j |\psi^{(j)}(t)\rangle\langle\psi^{(j)}(t)|, \tag{3.2}$$

holds at all times. The critical point is that each member of the ensemble, $\psi^{(j)}(t)$, should evolve independently of the other members of the ensemble: Then we only need to keep one "realization"

in the computer at a time. If coherent states were really consistent solutions of the many-body dynamics, this would be trivially possible if we were just able to sample the initial P. Unfortunately, coherent states do not stay coherent under the Hamiltonian (2.29) and thus the distribution P doesn't simply evolve according to a "phase-space density preserving" drift of the individual coherent states. However, we should not give up all hope: A diffusion-like part of the evolution of P can be included in the realizations as a noise term in the evolution of each $\psi^{(j)}(t)$. As it turns out, the "diffusion" is in our case of a rather peculiar kind and it can be "negative", i.e., it will sometimes tend to sharpen, not soften, P. At a prize, this difficulty can be overcome and, as we shall see below, the plan sketched here be realized.

3.2 The Glauber–Sudarshan P distribution

The distribution, P, appearing in the representation of $\hat{\rho}$ in terms of coherent states, Eq. 3.1, is know as the *Glauber-Sudarshan P distribution*. A large class of states can be represented by the P distribution. However, some states, e.g. states with a very well-defined number of particles, require very singular, generalized distributions.

When P exists, it gives direct translation of normally ordered operator expressions, i.e., expressions where all creation operators are to the left of all annihilation operators:

$$\begin{aligned}&\left\langle \hat{\psi}^\dagger(\mathbf{r}_1)\dots\hat{\psi}^\dagger(\mathbf{r}_s)\hat{\psi}(\mathbf{r}'_1)\dots\hat{\psi}(\mathbf{r}'_t)\right\rangle \\ &\qquad = \int d^2\psi\ \psi^*(\mathbf{r}_1)\dots\psi^*(\mathbf{r}_s)\psi(\mathbf{r}'_1)\dots\psi(\mathbf{r}'_t)P[\psi,\psi^*]. \end{aligned} \tag{3.3}$$

To calculate an arbitrary average we express it in normal ordered form, e.g.,

$$\begin{aligned}&\hat{\psi}^\dagger(\mathbf{r}_1)\hat{\psi}(\mathbf{r}_2)\hat{\psi}^\dagger(\mathbf{r}_3)\hat{\psi}(\mathbf{r}_4) \\ &\qquad =\hat{\psi}^\dagger(\mathbf{r}_1)\Big(\hat{\psi}^\dagger(\mathbf{r}_3)\hat{\psi}(\mathbf{r}_2)+\big[\hat{\psi}(\mathbf{r}_2),\hat{\psi}^\dagger(\mathbf{r}_3)\big]\Big)\hat{\psi}(\mathbf{r}_4) \\ &\qquad =\hat{\psi}^\dagger(\mathbf{r}_1)\hat{\psi}^\dagger(\mathbf{r}_3)\hat{\psi}(\mathbf{r}_2)\hat{\psi}(\mathbf{r}_4)+\hat{\psi}^\dagger(\mathbf{r}_1)\hat{\psi}(\mathbf{r}_4)\delta\big(\mathbf{r}_2-\mathbf{r}_3\big). \end{aligned} \tag{3.4}$$

3.2.1 Operator correspondences

If we know a P-representation of $\hat{\rho}$, we can deduce representations of related operators. Let us for simplicity consider one mode only. From Eq. (3.1) we then have

$$\begin{aligned}\hat{a}\hat{\rho} &= \int d^2\alpha\ \hat{a}|\alpha\rangle\langle\alpha|\ P[\alpha,\alpha^*] \\ &= \int d^2\alpha\ |\alpha\rangle\langle\alpha|\ \alpha P[\alpha,\alpha^*], \end{aligned} \tag{3.5}$$

that is, $\hat{a}\hat{\rho}$ is represented by $\alpha P[\alpha,\alpha^*]$. Such *operator correspondences* will be very useful below when we deduce an equation of motion for P. An second obvious one is $\hat{\rho}\hat{a}^\dagger \leftrightarrow \alpha^* P$. More tricky examples are $\hat{a}^\dagger\hat{\rho}$ and $\hat{\rho}\hat{a}$, but it is not too hard to deduce the complete set of correspondences [23]:

$$\hat{a}\hat{\rho} \quad\leftrightarrow\quad \alpha P[\alpha,\alpha^*] \tag{3.6}$$

$$\hat{\rho}\hat{a}^\dagger \quad\leftrightarrow\quad \alpha^* P[\alpha,\alpha^*] \tag{3.7}$$

$$\hat{a}^\dagger\hat{\rho} \quad\leftrightarrow\quad \big(\alpha^*-\frac{\partial}{\partial\alpha}\big)P[\alpha,\alpha^*] \tag{3.8}$$

$$\hat{\rho}\hat{a} \quad\leftrightarrow\quad \big(\alpha-\frac{\partial}{\partial\alpha^*}\big)P[\alpha,\alpha^*]. \tag{3.9}$$

3.2.2 Equation of motion

From the equation of motion for $\hat{\rho}$, we can deduce an equation of motion for P. One way to do this is to use the operator correspondences of Eq. (3.6). As an example, let us for simplicity specialize to just a single mode and consider a Hamiltonian $\hat{H}_{\rm ah} = \hbar\omega\hat{a}^\dagger\hat{a} + \frac{1}{2}\hbar\chi\hat{a}^\dagger\hat{a}^\dagger\hat{a}\hat{a}$. The von Neumann equation of motion for $\hat{\rho}$ reads

$$\frac{\partial}{\partial t}\hat{\rho} = \frac{1}{i\hbar}\big[\hat{H}_{\rm ah}, \hat{\rho}\big] = -i\omega\hat{a}^\dagger\hat{a}\hat{\rho} - i\frac{1}{2}\chi\hat{a}^\dagger\hat{a}^\dagger\hat{a}\hat{a}\hat{\rho} + \text{h.c.} \tag{3.10}$$

and therefore we get for $\partial_t P$:

$$\begin{aligned}\frac{\partial}{\partial t}P[\alpha,\alpha^*] &= \left\{-i\omega\big(\alpha^* - \frac{\partial}{\partial\alpha}\big)\alpha - i\frac{1}{2}\chi\big(\alpha^* - \frac{\partial}{\partial\alpha}\big)^2\alpha^2\right\}P[\alpha,\alpha^*] + \text{c.c.}\\ &= \left\{\frac{\partial}{\partial\alpha}i\omega\alpha + \frac{\partial}{\partial\alpha}i\chi|\alpha|^2\alpha - \frac{1}{2}\frac{\partial^2}{\partial\alpha^2}i\chi\alpha^2\right\}P[\alpha,\alpha^*] + \text{c.c.}\end{aligned} \tag{3.11}$$

This Fokker–Planck-like equation contains "drift" terms ($\partial_\alpha\ldots$) and "diffusion" terms ($\partial_\alpha^2\ldots$). In principle, we could solve it (numerically) from given initial conditions, but remember that we set out to describe the evolution in terms of an ensemble in which each member behaves independently.

3.2.3 Langevin equations

What we need is a translation from the Fokker–Planck equation for the distribution to a Langevin equation for the individual realizations. Quite generally, a Fokker–Planck equation,

$$\frac{\partial}{\partial t}P(\mathbf{q},t) = \left\{-\frac{\partial}{\partial q_\nu}A_\nu + \frac{1}{2}\frac{\partial^2}{\partial q_\mu\partial q_\nu}D_{\mu\nu}\right\}P(\mathbf{q},t), \tag{3.12}$$

corresponds to a Langevin equation,

$$d\mathbf{q} = \mathbf{A}dt + Bd\mathbf{W}. \tag{3.13}$$

In Eq. 3.13, $\mathbf{A}$ is the drift vector, $d\mathbf{W}$ is a vector of independent Gaussian noise increments,

$$\overline{dW_\mu(t)} = 0 \quad , \quad \overline{dW_\mu(t)dW_\nu(t')} = dt\delta(t-t')\delta_{\mu\nu}, \tag{3.14}$$

and B is the "square root" of the diffusion matrix, $D = BB^T$. The overbar denotes the stochastical average. Now, in the case of Eq. (3.11) it turns out that the diffusion matrix is not positive definite. This means that we cannot find a coefficient for the noise-term that will reproduce the correct second order derivatives in the Fokker–Planck equation. The problem can be illustrated by looking at the Langevin equations we naively deduce for α and α^*:[1]

$$d\alpha = -i\big(\omega + \chi|\alpha|^2\big)\alpha dt + \sqrt{-i\chi}\alpha dW \tag{3.15}$$

$$d\alpha^* = i\big(\omega + \chi|\alpha|^2\big)\alpha^* dt + \sqrt{i\chi}\alpha^* dW^*. \tag{3.16}$$

These equations would reproduce all the terms in Eq. (3.11), but also an additional, mixed second order term, $\partial_\alpha\partial_\alpha^*\ldots$, unless $\overline{dWdW^*} = 0$! This will require dW and dW^* to be independent noise sources and, consequently, α and α^* to be no longer complex conjugate.

3.3 The positive P distribution

To relax the demand that α and α^*, or in the many mode case, ψ and ψ^*, should be complex conjugate, we replace Eq. (3.1) by

$$\hat{\rho}(t) = \int d^2\psi_1 d^2\psi_2\ \frac{|\psi_1\rangle\langle\psi_2^*|}{\langle\psi_2^*|\psi_1\rangle}P_+[\psi_1,\psi_2,t]. \tag{3.17}$$

[1] This is not a strict argument as the translation is not unique.

The doubling of the configuration space leads to the *positive P distribution*, P_+. Everything from above goes through with ψ replaced by ψ_1 and ψ^* replaced by ψ_2. Expectation values of normally ordered expressions, Eq. (3.3), are now calculated as

$$\begin{aligned}\big\langle \hat{\psi}^\dagger(\mathbf{r}_1)\dots\hat{\psi}^\dagger(\mathbf{r}_s)\hat{\psi}(\mathbf{r}'_1)\dots\hat{\psi}(\mathbf{r}'_t)\big\rangle \\ = \int d^2\psi_1 d^2\psi_2\ \psi_2(\mathbf{r}_1)\dots\psi_2(\mathbf{r}_s)\psi_1(\mathbf{r}'_1)\dots\psi_1(\mathbf{r}'_t)P_+[\psi_1,\psi_2],\end{aligned} \tag{3.18}$$

and the many mode operator correspondences are

$$\hat{\psi}\hat{\rho} \quad \leftrightarrow \quad \psi_1 P_+[\psi_1,\psi_2] \tag{3.19}$$

$$\hat{\rho}\hat{\psi}^\dagger \quad \leftrightarrow \quad \psi_2 P_+[\psi_1,\psi_2] \tag{3.20}$$

$$\hat{\psi}^\dagger\hat{\rho} \quad \leftrightarrow \big(\psi_2 - \frac{\partial}{\partial\psi_1}\big)P_+[\psi_1,\psi_2] \tag{3.21}$$

$$\hat{\rho}\hat{\psi} \quad \leftrightarrow \big(\psi_1 - \frac{\partial}{\partial\psi_2}\big)P_+[\psi_1,\psi_2]. \tag{3.22}$$

3.3.1 Noisy Gross–Pitaevskii equations

From the basic trapped gas Hamiltonian, (2.29), with binary collisions described by the contact potential, we get the following Langevin equations for ψ_1 and ψ_2:

$$i\hbar d\psi_1 = \Big\{\hat{h} + g\psi_2\psi_1\Big\}\psi_1 dt + \sqrt{-ig}\psi_1 dW_1 \tag{3.23}$$

$$-i\hbar d\psi_2 = \Big\{\hat{h} + g\psi_1\psi_2\Big\}\psi_2 dt + \sqrt{ig}\psi_2 dW_2, \tag{3.24}$$

where dW_i for $i = 1, 2$ are Gaussian increments,

$$\overline{dW_i(\mathbf{r},t)} = 0 \quad , \quad \overline{dW_i(\mathbf{r},t)dW_j(\mathbf{r}',t')} = dt\delta(t-t')\delta(\mathbf{r}-\mathbf{r}')\delta_{i,j}. \tag{3.25}$$

Note that Eqs. (3.23) and (3.24) are noisy Gross–Pitaevskii equations, i.e., if we drop the noise terms we recover Eq. (2.10). Eqs. (3.23) and (3.24) should be interpreted in the Ito sense, i.e., $d\psi_i(t)$ and $dW_i(t)$ are independent [48]

3.3.2 Initial state

We can now finally simulate BEC dynamics exactly according to the plan outlined in Sec. 3.1. The first thing to do is to get a sampling of the initial P_+. In fact, this is not a trivial task: To do it, we in principle need to know the exact initial state of the system in the given experiment *and* we need to express it in the form (3.17). The latter requirement is easier to meet than for the Glauber–Sudarshan P distribution as singular distributions are never needed [49, 50]. The first requirement is of course a difficult one. It has recently been addressed by Carussotto and Castin for the case of a thermal equilibrium initial state [51]. Focusing on the dynamics, we have been using a more primitive approach, namely,

$$P_+[\psi_1,\psi_2,t=0] = \int \frac{d\theta}{2\pi}\ \delta\big(\psi_1 - e^{i\theta}\psi_0\big)\delta\big(\psi_2 - e^{-i\theta}\psi_0\big). \tag{3.26}$$

Here $\psi_0 = \sqrt{N}\phi_0$ with N being the average number of atoms and ϕ_0 the initial single particle state, usually simply the solution of the GPE. As $\psi_2 = \psi_1^*$, the initial state is of the Glauber–Sudarshan form, (3.1), and in fact equivalent to to a mixture of number states with a Poissonian number distribution (see Appendix A). In praxis, it is not always necessary to actually sample θ initially. Instead the integral in Eq. (3.26) is implemented analytically in the final result.

3.3.3 Numerical simulation

The numerical simulation of the dynamics is now done by propagating each pair, (ψ_1, ψ_2), of the ensemble according to Eqs. (3.23) and (3.24). This not much more demanding than solving the time-dependent GPE. The choice of methods of solution is, however, somewhat limited by the need to include the noise terms. Higher order algorithms grow rapidly in complexity [52, 53] and after having tried some more sophisticated methods (see Ref. [54]) we have settled for a simple explicit approach for the noise terms.[2] Recently, the `xmds` package by Collecutt and Drummond appeared and it definitely seems to be a viable alternative to writing new code from scratch [55].

The crucial drawback of the positive P method is the notorious divergence problem at large non-linearities [56, 52, 57, 23]. The origin of the problem is the doubling of the phase-space in connection with the non-linear term: as ψ_1 and ψ_2 are no longer forced to be complex conjugate during the simulation, the local mean field energy, $g\psi_2(\mathbf{r})\psi_1(\mathbf{r})$, can attain complex values resulting in e.g. $|\psi_1(\mathbf{r})|$ becoming very large and $|\psi_2(\mathbf{r})|$ becoming very small. The good news is that divergencies only sets in after some time and that they can be easily recognized in the simulations. As a rule of thumb, the simulations can be trusted at the level of their statistical error until the time where the the first member of the ensemble takes off to infinity [57]. Positive P simulations (without damping) are thus mostly useful for short-time dynamics, i.e., for studying phenomena that takes place on a time-scale comparable to the one associated with the interaction energy.

3.4 Applications of positive P and related methods to BEC

A number of applications of positive P and closely related methods to BEC appear in the literature. In Chapters 4 and 5 we describe our work on spin squeezing and photodissociation, and there we also give references to the most closely related work by other authors. In this section we point to a broader selection of important references in the field.

In Ref. [58] Steel *et al.* applied both the positive P distribution and the *Wigner distribution* to calculate two-time correlation functions of the field operator. The Wigner function is well-known in physics as the closest thing to a simultaneous probability distribution of non-commuting observables. Here it can be seen as a cousin of P, giving not normally, but symmetrically ordered expectation values. The equation of motion for the Wigner distribution turns out to contain cubic order derivatives. This prevents an exact translation to a Langevin equation. The usual resort is the so-called *truncated Wigner method* where the third order terms are simply ignored. All that is left is a drift term and therefore the Langevin equation is in fact just the GPE. All fluctuations are contained in the initial distribution. In Ref. [58] these fluctuations were purely of quantum nature as T=0, but Sinatra *et al.* has later shown how to sample a thermal equilibrium state in the Bogoliubov approximation [59, 60].

When damping is included in P simulations, the problem of divergencies becomes less severe. In realistic calculations on optical systems, the non-linearities are in fact most often dominated by the damping [57] and positive P can cover much of the interesting physics. In the case of BEC, where the life-time of the condensate can be very long, this is not so in general. A notable exception is the phase of evaporative cooling leading to the very formation of the condensate. Drummond and Corney were thus able to study this process with the positive P formalism [61].

Interesting attempts to tame the divergencies in situations without significant damping has also appeared. Among others, Fleischhauer *et al.* [62] have worked on *noise tuning*, i.e., attempts to utilize a freedom in choosing the exact form of the Langevin equations. These authors derive the positive Langevin equations directly from a path-integral formulation of the problem [63], an approach also used by Stoof Ref. [64]. An advantage of the path-integral formulation seems to be the access to a large arsenal of powerful methods: It is for example rather straightforward to produce a simulation scheme with *linear* equations [62]. The price to be paid is that the formular

[2] In Chp. 5 we will need noise terms that are more complicated than the ones of Eq. (3.25). How to overcome this difficulty is discussed in Appendix D.

for expectation values becomes more involved than Eq. (3.18) and in praxis very susceptible to sampling errors. Recently, highly successful one-mode noise tuning have been presented by Deuar and Drummond [65]. So far, it is fair to say that we are still awaiting major many-mode breakthroughs along these lines.

Another recent development has come from Carusotto *et al.* [56, 51]. They considered the expansion of $\hat{\rho}$ on number state dyadics instead of the coherent state dyadics of Eq. (3.17), and they showed how this leads to an alternative simulation scheme. As a by-product, their work gives a nice alternative derivation of the traditional positive P equations. Using the number state scheme, Carusotto and Castin have been able to calculate quantities which are pratically inaccesible in the coherent state scheme, e.g., the probability distribution for the number of particles in the condensate [66].

Finally, we would like to mention the work of Plimak *et al.* on deriving simulation schemes in cases where there are cubic order derivatives in the equation of motion for the phase-space distribution [63]. It turns out that although no appropiate noise terms exist in the continuum limit, the discretized version of the problem can be treated. This enlarges the number of physical systems that can be handled numerically [67]. As a future prospect, one could hope that these methods will also allow a well-behaved version of the positive P distribution to be simulated.

Chapter 4

Spin squeezing in BEC

We ended the introduction to the Bogoliubov approach, Sec. 2.7, with a discussion of the so-called phase collapse, which in the number conserving language was simply a consequence of the phase evolution of the condensate operators depending on the number of particles in the system: If each experiment is done with a different number of atoms in the trap, observables depending on this phase evolution will average to zero. In this chapter we stop just short of doing the average. We instead take the positive view that interactions create a correlation between phase and number, and we try to utilize this correlation. This is most easily done if initially we have a coherent superposition of states with different N or, more realistically, of states where N is divide in different ways on, say, two modes. As the phase is a fast and sensitive variable, it will turn out that significant number-phase correlations can be build before the spatial dynamics "discovers" the variance in the occupation numbers of the modes.

We begin he chapter in Sec. 4.1, with a rather general introduction to the concept of spin squeezing. This provides an elegant formalism to be used when we in Sec. 4.2 turn to the particular case of two–component BECs. Positive P simulations are applied to confirm the results of a simple model. Next, two applications of spin squeezed BECs are discussed: A matter wave beam splitter with subbinominal distribution of atoms in the output ports (Sec. 4.3), and a source for squeezed light (Sec. 4.4). Finally, in Sec. 4.5, we take a look beyond spin squeezing to Schrödinger cats and phase revivals.

4.1 Introduction to spin squeezing

4.1.1 Coherent spin states

Consider an angular momentum algebra with operators $\hat{S}_x$, $\hat{S}_y$, and $\hat{S}_z$. The operators obey the commutation relation

$$\left[\hat{S}_x, \hat{S}_y\right] = i\hat{S}_z, \tag{4.1}$$

and its cyclic permutations. From all commutation relations follow a corresponding uncertainty relation (see e.g. Ref. [68]). Here Eq. (4.1) leads to

$$\langle \Delta\hat{S}_x^2\rangle\langle \Delta\hat{S}_y^2\rangle \geq \frac{1}{4}\left|\langle \hat{S}_z\rangle\right|^2, \tag{4.2}$$

where $\Delta\hat{S}_i = \hat{S}_i - \langle \hat{S}_i\rangle$. Contrary to the familiar position–momentum uncertainty relation, where the quantity on the right hand side of the inequality is a constant of nature, the limit is here connected to the expectation value of $\hat{S}_z$. In fact, in an eigenstate of either the $\hat{S}_x$ operator or of the $\hat{S}_y$ operator, the left hand side (and thus $\langle \hat{S}_z\rangle$) vanishes.

The relation (4.2) is much more interesting for states that are "pointing" in some direction, e.g., states which have $\langle \hat{S}_x\rangle = \langle \hat{S}_y\rangle = 0$ but where $|\langle \hat{S}_z\rangle|$ is large. Then Eq. (4.2) becomes a statement about the uncertainty in the direction of the angular momentum. For a given total angular

momentum, S, the maximum value of $|\langle \hat{S}_z \rangle|$ is obtained for the stretched states, $|S, m_z = \pm S\rangle$, and in fact these states realizes "=" in Eq. (4.2). The uncertainties are equally distributed, $\langle \Delta \hat{S}_x^2 \rangle = \langle \Delta \hat{S}_y^2 \rangle = S/2$. It is natural to regard $|S, m_z = \pm S\rangle$ as the most classical states representing an angular momentum pointing up, respectively down. Similar states pointing in other directions can be obtained by rotation, and in this way the set of *coherent spin states* (CSSs) is constructed. The CSSs are the angular momentum analogy of the harmonic oscillator coherent states (see Appendix A), and they share many useful properties with these [69].[1] We shall denote by $|S, \mathbf{m}\rangle$ the CSS with total angular momentum S, pointing in the direction given by the unit vector $\mathbf{m}$:

$$\begin{aligned} \hat{\mathbf{S}}^2 |S, \mathbf{m}\rangle &= S(S+1)|S, \mathbf{m}\rangle, \\ \big(\mathbf{m} \cdot \hat{\mathbf{S}}\big)|S, \mathbf{m}\rangle &= S|S, \mathbf{m}\rangle. \end{aligned} \tag{4.3}$$

One of the useful properties of the coherent spin states is (over–)completeness, i.e., we can represent any state of total angular momentum S as a superposition of $|S, \mathbf{m}\rangle$'s. Conceptually, this allows us to think of a quantum mechanical spin state as containing a distribution of classical spins pointing in different directions. Mathematically, this picture can be formalized by introducing pseudo probability distributions as in Chp. 3, but we shall not be needing this here.

4.1.2 Squeezed spin states

In the previous section, we described a CSS as the state with the most well defined direction possible. In fact, this statement is imprecise: An uncertainty relation like Eq. (4.2) only sets a limit on the product of two uncertainties. In the case of spins, it is perfectly possible to have $\langle \Delta \hat{S}_\perp^2 \rangle < |\langle \hat{\mathbf{S}} \rangle|/2$ for a component perpendicular to the mean spin. Such a state is refered to as a *squeezed spin state*.

How do one go about producing a squeezed spin state starting from a coherent spin state? A first observation is that there is no use in considering a Hamiltonian linear in $\hat{S}_x$, $\hat{S}_y$, and $\hat{S}_z$: the time evolution operator, $\exp[-i(\alpha \hat{S}_x + \beta \hat{S}_y + \gamma \hat{S}_z)t]$, merely induces a rotation. One therefore needs some higher order terms, and Kitagawa and Ueda [70] showed how Hamiltonians proportional to $\hat{S}_z^2$ or $\hat{S}_z^2 - \hat{S}_y^2$ will squeeze an initially coherent spin state aligned along the x direction. Let us have a closer look at their prediction for the Hamiltonian

$$\hat{H}_{\text{ss}} = \hbar \chi \hat{S}_z^2. \tag{4.4}$$

The effect of this Hamiltonian is a twisting: $\hat{S}_z$ leads to a rotation, but with $\hat{S}_z^2$ the rotation is in the positive sense on the northern hemisphere and in the negative sense on the southern hemisphere. Fig. 4.1 illustrates how this effect leads to squeezing in a particular component of $\hat{\mathbf{S}}$. The quantitative formulas describing the process will be given in Sec. 4.2.1.

4.1.3 Which systems are spin systems?

The discussion above was quite general, referring only to a general spin (angular momentum) system. A large number of physical systems can be conveniently described via a spin formalism. In fact, if the Hilbert space is n–dimensional, we can map it on the space spanned by $|S, -S\rangle, \ldots, |S, S\rangle$ with $2S + 1 = n$. This is useful if important operators like e.g. the Hamiltonian can be expressed in a simple way in terms of the components of $\hat{\mathbf{S}}$.

A basic example is one particle with two possible states, $|a\rangle$ and $|b\rangle$. These could of course be spin–up and spin–down for a spin–1/2 particle, in which case the mapping is obvious. They could also be two internal states of, e.g., an atom, or they could even be two external modes, e.g., the two arms of a Mach–Zender interferometer. All cases map onto a spin–1/2 system, and we get the

[1] Note, however, that the special property of $\hat{a}|\alpha\rangle = \alpha|\alpha\rangle$ of the harmonic oscillator coherent states has no direct translation. When S is large, the analogy between harmonic oscillator coherent states and CSSs becomes good locally.

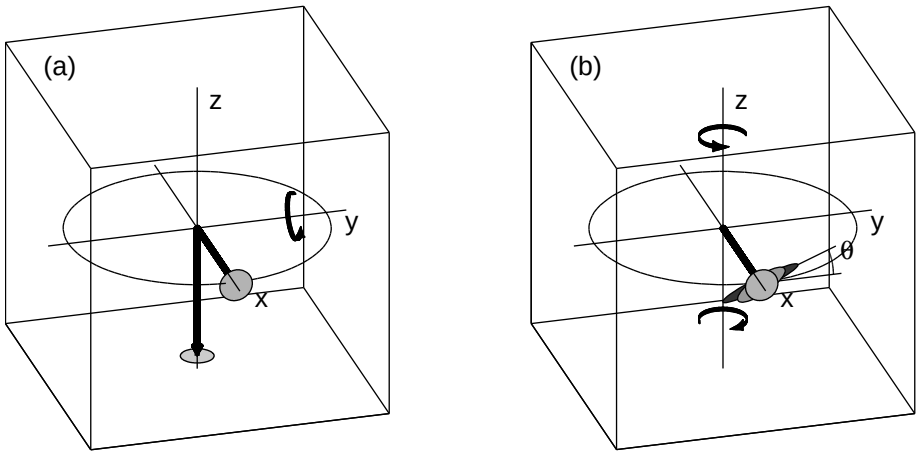

Figure 4.1: Figure illustrating spin squeezing by the a $\hat{S}_z^2$ Hamiltonian. (a) A coherent spin state is illustrated by an arrow with a uncertainty disc at its tip. If we start with the $|S,-S\rangle$ state, i.e., the coherent state pointing down, a rotation by $\pi/2$ around the y–axis will produce a coherent state aligned along x. The rotation is the result of a Hamiltonian proportional to $\hat{S}_y$ acting on the system for a given time. (b) Starting from the coherent state aligned along x, we apply a Hamiltonian proportional to $\hat{S}_z^2$. The resulting "rotation" is dependent on $\hat{S}_z$ itself; in particular the sense of rotation is opposite on opposite sides of the xy–plane. The uncertainty disc is deformed to an ellipse, and a squeezed direction appears. The magnitude of the squeezing and the direction (quantified by θ) is given in Sec. 4.2.2.

angular momentum operators

$$\hat{s}_- = |a\rangle\langle b| \quad , \quad \hat{s}_+ = |b\rangle\langle a| \quad , \quad \hat{s}_z = \frac{1}{2}\left(|b\rangle\langle b| - |a\rangle\langle a|\right). \tag{4.5}$$

For this simple problem, all operators can be expressed as linear combinations of the three spin components and the identity. For example, an energy difference of ϵ between mode a and b will lead to a $\epsilon\hat{s}_z$ term in the Hamiltonian, while a coupling moving the particle from mode a to mode b is represented by $\hat{s}_+$. In the spin language, a unitary time evolution operator is just a rotation and all (pure) states are coherent spin states. The translation for the states is

$$\begin{aligned} \cos\frac{\theta}{2}|b\rangle + e^{i\phi}\sin\frac{\theta}{2}|a\rangle &= |\frac{1}{2},\mathbf{m}(\theta,\phi)\rangle, \\ \mathbf{m}(\theta,\phi) &= \sin\theta\cos\phi\,\mathbf{e}_x + \sin\theta\sin\phi\,\mathbf{e}_y + \cos\theta\,\mathbf{e}_z. \end{aligned} \tag{4.6}$$

We see that the polar angle of $\mathbf{m}$ describes the distribution of weight on a and b, while the azimuthal angle is keeping track of the phase of the superposition.

An important generalization of the example above is N particles in two modes. We then define a *collective* spin operator by

$$\hat{\mathbf{S}} = \sum_{i=1}^{N} \hat{\mathbf{s}}_i. \tag{4.7}$$

If the particles are identical bosons the second quantized formalism can be used,[2]

$$\hat{S}_- = \hat{a}^\dagger\hat{b} \quad , \quad \hat{S}_+ = \hat{b}^\dagger\hat{a} \quad , \quad \hat{S}_z = \frac{1}{2}\left(\hat{b}^\dagger\hat{b} - \hat{a}^\dagger\hat{a}\right). \tag{4.8}$$

Putting all particles in the same one-particle state gives a CSS with $S = N/2$,

$$\frac{1}{\sqrt{N!}}\left[\cos\frac{\theta}{2}\hat{b}^\dagger + e^{i\phi}\sin\frac{\theta}{2}\hat{a}^\dagger\right]^N |\text{vac}\rangle = |\frac{N}{2},\mathbf{m}(\theta,\phi)\rangle. \tag{4.9}$$

[2]This is the Schwinger–bosons construction, see e.g. Ref. [68] page 217.

From the one-particle discussion above, it is clear that this representation is convenient for the one–particle dynamics: everything is just rotations. Looking at (4.8), we see that also two–body interactions are relatively simply described, e.g., interactions between particles in mode a:

$$\hat{a}^\dagger\hat{a}^\dagger\hat{a}\hat{a} = \hat{S}_z^2 + \big(\hat{N}-1\big)\hat{S}_z + \frac{1}{4}\hat{N}\big(\hat{N}-2\big). \tag{4.10}$$

From Sec. 4.1.2, we know that the $\hat{S}_z^2$ will lead to spin squeezing. The interpretation in this many–particle situation is clear: If particles in mode a interact, the effective energy of mode a is changed, hence the $\hat{S}_z$–term. But the change is in fact non–linear in the number of particles in a, and so a $\hat{S}_z^2$ term also appears. This term induces correlations between population differences and phase differences.

4.1.4 Spin squeezing in praxis

How do one detect spin squeezing? The simple answer is of course: by measuring the spin components and looking for the reduced fluctuations. Often some of the components are more easily accessible than others. In the case of N particles in two modes, it will usually be easy to count the number of particles in each mode. Thus $\langle\hat{S}_z\rangle$ and $\langle\Delta\hat{S}_z^2\rangle$ can be found directly. To measure other components, rotations can be applied before the counting. As is apparent from the discussion in the previous section, rotations can be performed by changing the energy difference between the modes and/or applying a coupling that can transfer particles between the modes. For our main interest here, cold atoms, such manipulations are well established as ingredients of spectroscopy, atomic clocks, and matter wave interferometers, see e.g. [71]. Much of the the interest in spin squeezing in fact originates from the desire to improve the precision in these experiments: If the intrinsic fluctuations of a measurement is reduced, it will naturally require fewer repetitions to determine the mean value to a given precision. For spectroscopy Wineland *et al.* have explicitly calculated how spin squeezing can reduce the signal–to–noise ratio [72].

In recent years, a number of practical ways to produce spin squeezing have become known: absorption of squeezed light [73, 74, 75, 76], quantum non-demolition atomic detection [77, 78, 79], controlled dynamics in quantum computers with ions or atoms [80, 81], and the dipole interaction of virtual Rydberg states [82]. Pu and Meystre in [83] and Duan *et al.* in [84] proposed the use of spin–exchange collisions to extract squeezed beams from a Bose–Einstein condensate. We shall mostly be concerned with the idea of Sørensen *et al.* to utilize the collisional interaction to squeeze the collective spin of a two-component condensate [85].

4.2 Spin squeezing and two–component BECs

From the introduction in Sec. 4.1, it almost clear how the proposal of Sørensen *et al.* will work: In a pure one–component condensate, there is only one spatial mode populated. If we introduce a coupling to a different internal state in the atoms, we have effectively a two–mode situation. The N atoms are mapped on a spin of total angular momentum $S = N/2$ and the collisional interaction introduces a $\hat{S}_z^2$ term. A $\pi/2$ pulse will rotate the collective spin to the equator, and spin squeezing will be produced by $\hat{S}_z^2$. Below we shall see that things are in fact almost that simple. For very related work, where the rotation is kept on during the evolution, see Refs. [86] and [87].

4.2.1 Two-mode model

We consider two-level atoms in a trap. To describe the dynamics of such a system we only need to generalize the second quantized Hamiltonian of Eq. (2.29) a little. With creation and annihilation

operators of atoms in the state $i = a$ or b, $\hat{\psi}_i^\dagger$, $\hat{\psi}_i$, we have:

$$\hat{H} = \int d^3\mathbf{r}\Big\{ \sum_{i=a,b} \Big[\hat{\psi}_i^\dagger(\mathbf{r})\hat{h}_i\hat{\psi}(\mathbf{r}) + \frac{g_{ii}}{2}\hat{\psi}_i^\dagger(\mathbf{r})\hat{\psi}_i^\dagger(\mathbf{r})\hat{\psi}_i(\mathbf{r})\hat{\psi}_i(\mathbf{r})\Big] + g_{ab}\hat{\psi}_a^\dagger(\mathbf{r})\hat{\psi}_b^\dagger(\mathbf{r})\hat{\psi}_b(\mathbf{r})\hat{\psi}_a(\mathbf{r})\Big\}. \quad (4.11)$$

Here, h_i is the single particle Hamiltonian for atoms in internal state i and g_{ij} is the effective two-body interaction strength between an atom in state i and one in state j. In terms of the corresponding scattering lengths they are given by $g_{ij} = 4\pi\hbar^2 a_{ij}/m$. We have assumed that collisions cannot transfer atoms between the two modes: All terms in (4.11) commute with both $\hat{N}_a$ and $\hat{N}_b$.

We now start with all atoms in internal state a. At temperatures sufficiently below the critical temperature for Bose-Einstein condensation almost all atoms occupy the same single particle wavefunction, ϕ_0, which to a very good approximation can be obtained from the Gross-Pitaevskii equation, (2.8). We then apply a laser to do a $\pi/2$-pulse on the a–b transition. In this way, all atoms are coherently transfered to an equal superposition of a and b. Of course, for the atoms to behave independently, the transfer should be relatively fast. The spatial mode is ideally not affected by the transfer. At this point, it is very convenient to split the field operators as

$$\hat{\psi}_a(\mathbf{r}) = \hat{a}\phi_a(\mathbf{r}) + \delta\hat{\psi}_a(\mathbf{r}) \quad , \quad \hat{\psi}_b(\mathbf{r}) = \hat{b}\phi_b(\mathbf{r}) + \delta\hat{\psi}_b(\mathbf{r}), \quad (4.12)$$

with $\phi_a = \phi_b = \phi_0$. The fluctuation operators, $\delta\hat{\psi}_a$ and $\delta\hat{\psi}_b$, describe modes of the system that are initially not populated and for most purposes they can be ignored. The state of the system factorizes in a spatial part described by ϕ_0, and an internal part described by $\hat{a}$ and $\hat{b}$. The system is in a coherent spin state with respect to the internal modes. As the superposition is assumed to have equal weight on a and b, the CSS is somewhere on the equator. We now assume that $\delta\hat{\psi}_a$ and $\delta\hat{\psi}_b$ can be ignored also at later times. Then the separation of internal and external dynamics also holds. The wavefunctions $\phi_a(x)$ and $\phi_b(x)$ can evolve with time, and we describe this evolution with two coupled Gross-Pitaevskii equations:

$$i\hbar\partial_t\phi_i = \left(\hat{h}_i + g_{ii}\frac{N}{2}\left|\phi_i\right|^2 + g_{i\underline{i}}\frac{N}{2}\left|\phi_{\underline{i}}\right|^2\right)\phi_i \quad (4.13)$$

where $\underline{a} \equiv b$ and *vice versa*.

The dynamics associated with distribution of atoms among the two modes is studied by replacing in a self-consistent way Eq.(4.11) by an effective Hamiltonian for the $\hat{a}$ and $\hat{b}$ operators:

$$\hat{H}_{\text{two-mode}} = g_{bb}\left(\frac{1}{2}\hat{b}^\dagger\hat{b}^\dagger\hat{b}\hat{b} - \frac{N}{2}\hat{b}^\dagger\hat{b}\right)\int d^3\mathbf{r}\ \left|\phi_b\right|^4 + g_{aa}\left(\frac{1}{2}\hat{a}^\dagger\hat{a}^\dagger\hat{a}\hat{a} - \frac{N}{2}\hat{a}^\dagger\hat{a}\right)\int d^3\mathbf{r}\ \left|\phi_a\right|^4 + g_{ab}\left(\hat{b}^\dagger\hat{a}^\dagger\hat{a}\hat{b} - \frac{N}{2}\hat{b}^\dagger\hat{b} - \frac{N}{2}\hat{a}^\dagger\hat{a}\right)\int d^3\mathbf{r}\ \left|\phi_b\right|^2\left|\phi_a\right|^2. \quad (4.14)$$

The time-dependence of the modes has explicitly been taken into account; In particular the quadratic terms stem from the mean field terms of Eq. (4.13).

4.2.2 Spin operators for the two–mode model

The spin operators describing the dynamics of the two modes are, in complete analogy with Eq. (4.8),

$$\hat{S}_x = \frac{1}{2}\left(\hat{b}^\dagger\hat{a} + \hat{a}^\dagger\hat{b}\right) \tag{4.15}$$

$$\hat{S}_y = \frac{1}{2i}\left(\hat{b}^\dagger\hat{a} - \hat{a}^\dagger\hat{b}\right) \tag{4.16}$$

$$\hat{S}_z = \frac{1}{2}\left(\hat{b}^\dagger\hat{b} - \hat{a}^\dagger\hat{a}\right). \tag{4.17}$$

With these spin operators, the two–mode Hamiltonian, (4.14), can be written

$$\hat{H}_{\text{two-mode}} = e(t)\hat{N} + k(t)\hat{S}_z + E(t)\hat{N}^2 + D(t)\hat{N}\hat{S}_z + \hbar\chi(t)\hat{S}_z^2, \tag{4.18}$$

where the time dependent coefficients are given by integrals involving the time dependent mode functions found from Eq.(4.13). All the terms in the Hamiltonian (4.18) commute which is an important simplification as the coefficients are time-dependent. The term proportional to $\hat{S}_z$ will result in a rotation of the spin around the z-axis and it can be removed by working in a rotating frame. The $\hat{N}$ and $\hat{N}^2$ terms give different dynamical overall phases to states with different total numbers of atoms. Such phases are immaterial if we have no external phase-standard to compare with and we neglect these terms for the purpose of the present work. The $\hat{N}\hat{S}_z$-term adds to the spin rotation with an angle linear in N. It cannot be neglected as the direction of the spin (the phase between a- and b-components) can be probed by a second $\pi/2$ pulse phase locked to the first $\pi/2$ pulse, but it is small for the particular cases studied below. Finally, the $\hat{S}_z^2$ produces spin-squeezing as described in Sec. 4.1.2. The strength parameter of the squeezing operator is given by

$$\hbar\chi(t) = \int d^3\mathbf{r}\,\frac{1}{2}\left(g_{bb}\left|\phi_b\right|^4 + g_{aa}\left|\phi_a\right|^4 - 2g_{ab}\left|\phi_a\right|^2\left|\phi_b\right|^2\right). \tag{4.19}$$

Given the time integral $\mu = 2\int\chi(t')dt'$ Kitagawa and Ueda [70] provide the analytical expressions for the variance of the squeezed spin component

$$\langle\Delta S_\theta^2\rangle = \frac{S}{2}\left\{1 - \frac{2S-1}{4}\left[\sqrt{A^2+B^2} - A\right]\right\} \tag{4.20}$$

where $A = 1 - \cos^{2S-1}\mu$ and $B = 4\sin\mu/2\cos^{2S-2}\mu/2$. They also specify the direction of the squeezed spin component $\hat{S}_\theta = \cos\theta\hat{S}_z - \sin\theta\hat{S}_y$ (assuming the mean spin to be along x, see Fig. 4.1):

$$\theta = \frac{1}{2}\arctan\frac{B}{A}. \tag{4.21}$$

It is of some interest to use simple analytical approximations for $\chi(t)$ and we will do so in the specific cases studied below.

4.2.3 Full multi-mode description

The two–mode model is based on a simplifying assumption. The actual observables of the system are more complicated to deal with than $\hat{\mathbf{S}}$, but we can also define a set of operators obeying angular momentum commutation relations by

$$\hat{J}_x = \frac{1}{2}\int d^3\mathbf{r}\,\left(\hat{\psi}_b^\dagger\hat{\psi}_a + \hat{\psi}_a^\dagger\hat{\psi}_b\right) \tag{4.22}$$

$$\hat{J}_y = \frac{1}{2i}\int d^3\mathbf{r}\,\left(\hat{\psi}_b^\dagger\hat{\psi}_a - \hat{\psi}_a^\dagger\hat{\psi}_b\right) \tag{4.23}$$

$$\hat{J}_z = \frac{1}{2}\int d^3\mathbf{r}\,\left(\hat{\psi}_b^\dagger\hat{\psi}_b - \hat{\psi}_a^\dagger\hat{\psi}_a\right). \tag{4.24}$$

The total number operator $\hat{N} = \int d^3\mathbf{r}\ (\hat{\psi}_a^\dagger \hat{\psi}_a + \hat{\psi}_b^\dagger \hat{\psi}_b)$ commutes with these three operators and when the two-mode approximation applies well, the two-mode and multi-mode operators are comparable by the replacements

$$\hat{J}_+ = \rho e^{i\nu} \hat{S}_+ \qquad \hat{J}_- = \rho e^{-i\nu} \hat{S}_- \qquad \hat{J}_z = \hat{S}_z \tag{4.25}$$

where $\rho e^{i\nu} = \int d^3\mathbf{r}\ \phi_b^*(\mathbf{r})\phi_a(\mathbf{r})$. The factor ρ takes into account that $\langle \hat{J}_x \rangle$ and $\langle \hat{J}_y \rangle$ vanish unless the atoms in state a and b occupy the same region in phase space and ν is a dynamical phase from the spatial dynamics.

4.2.4 Positive P simulations

The two-mode approximation provides an intuitive picture of the evolution of the system. It is however not easy to justify the neglect of the fluctuations in Eq. (4.12) and we therefore need an exact method to determine more precisely what happens to the mean values and the variances of the components of $\hat{\mathbf{J}}$. The positive P function (P_+) introduced in Chp. 3 is a possible answer. With two internal states, one has instead of Eq. (3.18)

$$\langle : f[\hat{\boldsymbol{\psi}}(t)] : \rangle = \int d^2[\boldsymbol{\psi}] f[\boldsymbol{\psi}] P_+[\boldsymbol{\psi}, t] \tag{4.26}$$

where $: \cdot :$ denotes normal ordering. Instead of pairs of "wavefunctions" we now have quadruples,

$$\hat{\boldsymbol{\psi}}(t) = \begin{pmatrix} \hat{\psi}_a(t) \\ \hat{\psi}_a^\dagger(t) \\ \hat{\psi}_b(t) \\ \hat{\psi}_b^\dagger(t) \end{pmatrix} \quad \text{and} \quad \boldsymbol{\psi} = \begin{pmatrix} \psi_{a1} \\ \psi_{a2} \\ \psi_{b1} \\ \psi_{b2} \end{pmatrix}. \tag{4.27}$$

Likewise, the Langevin equations are for 4 c-number fields,

$$d\psi_{i\mu} = (-1)^\mu \frac{idt}{\hbar} \left(\hat{h}_i + g_{ii}\psi_{i2}\psi_{i1} + g_{ab}\psi_{\underline{i}2}\psi_{\underline{i}1} \right) \psi_{i\mu} + dW_{i\mu} \tag{4.28}$$

where again $\underline{a} = b$ and *vice versa*. In order to treat the interactions exactly [within the approximation given by the form of Eq.(4.11)] the noise terms have to be Gaussian and to fulfill:

$$\overline{dW_{i\mu}(\mathbf{r}, t)} = 0 \tag{4.29}$$

$$\begin{aligned} \overline{dW_{i\mu}(\mathbf{r}, t) dW_{j\nu}(\mathbf{r}', t')} &= \delta(\mathbf{r} - \mathbf{r}')\delta(t - t')\delta_{\mu,\nu} \\ &\quad \times (-1)^\mu \frac{idtg_{ij}}{\hbar} \psi_{i\mu}(\mathbf{r}, t)\psi_{j\mu}(\mathbf{r}, t). \end{aligned} \tag{4.30}$$

On the computer we can simulate the Langevin equations to obtain an ensemble of realizations of $\boldsymbol{\psi}$. This ensemble is a finite sampling of P_+ and can therefore be used to calculate expectation values via the prescription (4.26) and with a precision limited only by the number of realizations in the ensemble.

Although we have so far written all equations in 3D it would be computationally heavy to simulate a sufficient number of realizations of Eq. (4.28). In what follows we will thus restrict ourselves to 1D. It is reasonable to assume that this may alter the quantitative results significantly but a 1D calculation can be used to investigate the validity of the two-mode model which may hereafter be applied in 3D with more confidence.

4.2.5 Results for favourable collision strengths

Let us first focus on a situation with simple spatial dynamics. If we set $V_a = V_b = m\omega^2 x^2/2$ and if we assume that the values of the collision strengths can be controlled so that, $g_{aa} = g_{bb} = 2g_{ab} = g$, the spatial dynamics is limited to a slight breathing. The spin-dynamics is almost a pure squeezing, that is, the mean spin stays in the x-direction. To get an estimate of the strength parameter χ of

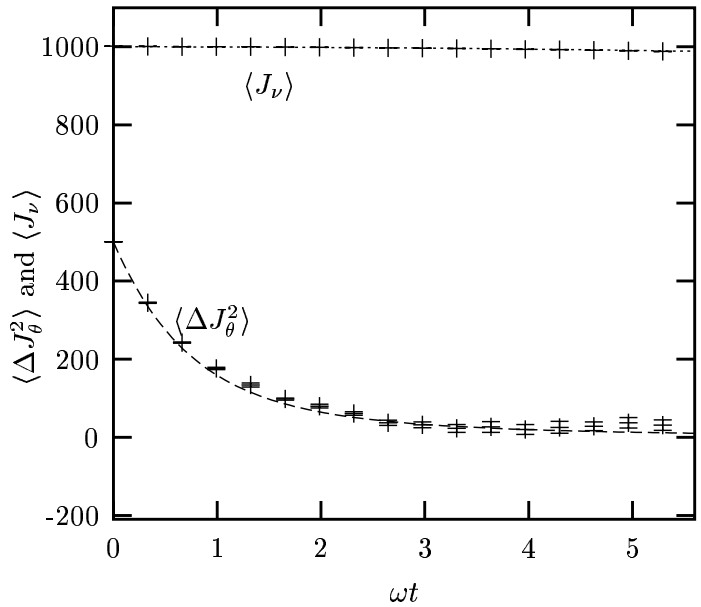

Figure 4.2: Squeezing of the collective spin for favourable interaction parameters: N=2000 atoms and $(g_{aa}, g_{ab}, g_{bb}) = (1.0, 0.5, 1.0) \times 5 \times 10^{-3} \hbar\omega a_0$ (1D model). + (with errorbars) show P_+ results, lines show results of the two-mode model.

Eq. (4.19) we find $\phi_a(t = 0) = \phi_b(t = 0)$ as the Thomas-Fermi approximation to the stationary solution of the GPE with all atoms in the a-state. We then have:

$$\hbar\chi = \frac{1}{5}\frac{1}{N^{1/3}}\left(\frac{2}{3}\frac{g}{\hbar\omega a_0}\right)^{2/3}\hbar\omega \tag{4.31}$$

where $a_0 = \sqrt{\hbar/m\omega}$ is the harmonic oscillator length in the trap and m is the atomic mass. Choosing $g = 0.005\hbar\omega a_0$ and $N = 2000$ we get $\chi = 6.1 \times 10^{-4}\hbar\omega$ which should give a sizable squeezing within a quarter of a trapping period.

In Fig. 4.2 we show results of both the two-mode approximation, (4.20), and of the P_+ simulation for the parameters mentioned above. χ was assumed to be constant and of the value determined by Eq. (4.31). $\hat{J}_\theta = \cos\theta \hat{J}_z - \sin\theta \hat{J}_y$ refers to the squeezed component of the spin. The direction θ in the yz-plane is determined in the two mode model, i.e., from Eq. (4.21) and it is not independently optimized for the full P_+ results. The agreement is seen to be surprisingly good considering the crudeness of the estimate of the parameters in the two mode model. Within the uncertainty of the positive P results (the $\langle \Delta \hat{J}_\theta^2 \rangle$ data are presented with errorbars in Fig. 4.2) the noise suppression is seen to be almost perfect.

4.2.6 Controlling mode functions overlaps

In the experiments on the $|F = 1, m_f = -1\rangle$ and $|F = 2, m_f = 1\rangle$ states in ^{87}Rb [88] the scattering lengths and thus the interaction strengths are actually in proportion $g_{aa} : g_{ab} : g_{bb} = 1.03 : 1 : 0.97$. This is far from ideal conditions for squeezing as we can see from Eq. (4.19): $\chi = 0$ when in addition $\phi_a = \phi_b$ as is the case initially. To produce a sizable squeezing effect, we can instead make the two mode functions differ (see also Ref. [89]). In Sec. 4.3, this idea is taken to the extreme by working with two motional modes and only one internal state. Here we just apply different potentials to the two internal states. This has actually already been done for magnetically trapped Rb making use of gravity and different magnetic moments of the two internal states [88]. If V_b is displaced

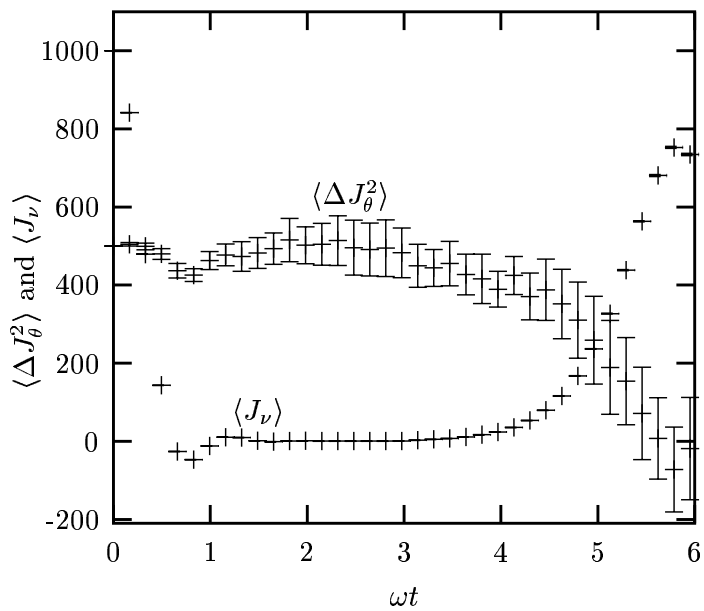

Figure 4.3: Squeezing due to spatial separation of the two internal state potentials by $x_0 = 3a_0$. The total number of atoms is 2000 and the interaction strengths are $(g_{aa}, g_{ab}, g_{bb}) = (1.03, 1, 0.97)\times 5 \times 10^{-3}\hbar\omega a_0$ (1D model).

from V_a, the b-component created by the initial $\pi/2$-pulse will move away from the a component thereby reducing the overlap $\int dx\, |\phi_a|^2 |\phi_b|^2$ and increasing χ. It is remarkable that the squeezing then takes place while the two components are away from each other.

To demonstrate the accomplishments of the scheme described above, we have chosen simply to displace V_b by a certain amount x_0 from V_a. In this model both potentials are still harmonic and of the same strength. The spatial dynamics is now more complicated, but it can be approximated by the solutions to coupled Gross-Pitaevskii equations. To get a rough idea of the parameters we can use the well known evolution of a displaced ground state wavefunction in a harmonic trap. We then get

$$\rho e^{i\nu} = e^{-x_0^2(1-\cos(\omega t))/2} e^{i x_0^2 \sin(\omega t)/2} \tag{4.32}$$

and

$$\int |\phi_b|^2 |\phi_a|^2 \, dx = \frac{1}{\sqrt{2\pi}} \, e^{-x_0^2(1-\cos(\omega t))/4}. \tag{4.33}$$

If we choose $(g_{aa}, g_{ab}, g_{bb}) = (1.03, 1, 0.97) \times 5 \times 10^{-3}\hbar\omega a_0$ and $x_0 = 3a_0$ this model gives an order of magnitude estimate for the integrated strength parameter of $\int_0^{2\pi/\omega} \chi(t)dt \cong 10^{-2}\hbar\omega$ when the two components are again overlapped. For 2000 atoms this corresponds to a reduction of the uncertainty in the squeezed spin component by roughly a factor of 10 according to Eq. 4.20.

In Fig.4.3 we use these estimates to analyze the P_+ simulations, i.e., we plot the expectation value of the spin component predicted to be maximal, $\langle \hat{J}_\nu \rangle$, and the variance of the perpendicular component predicted to be squeezed, $\langle \Delta \hat{J}_\theta^2 \rangle$. As can be seen, after a fast drop a large fraction of the original mean spin is recovered in $\langle \hat{J}_\nu \rangle$ when the two wave packets are again overlapped. This confirms our prediction of ν and it implies that a sizable signal can be obtained in an experiment. At the same time the variance in the predicted perpendicular component is strongly suppressed confirming our prediction for θ and implying that the noise in the experiment can be significantly reduced below the standard quantum limit.

4.2.7 Discussion

From the result of the P_+ simulations, we conclude that the predictions of the simple two-mode model reproduce the full multimode result also quantitatively. This means that the spatio-temporal dynamics and the population dynamics couple the way they should to produce spin squeezing, but the resulting entanglement between spatial and internal degrees of freedom is small enough that purely internal state observables show strong squeezing. In particular the calculations of Fig. 4.3 reveal that quite significant distortions of the distributions when the components separate and merge do not prevent sizable spin squeezing.

Although we claim quantitative agreement, it should of course be realized that this is within the 1D model. In the original proposal by Sørensen *et al.* [85], the simple model was successfully tested against a 3D calculation within an approximation developed by Sinatra and Castin in Ref. [90]. The aim of the positive P simulations was to check whether all the relevant quantum features were captured. It is reasonable to assume that no big surprises would show up in a 3D positive P simulation of the scenarios considered here.

Recently, Sørensen [91] applied a the two–component version of the number conserving Bogoliubov approach to the spin squeezing problem. He also found the two–mode model to be good for a rather wide range of parameters when the squeezing was not too strong, but in addition he identified conditions where Bogoliubov theory predicts a breakdown of the simple picture. It would be interesting to do positive P simulations also for such cases. In the following sections on applications of atomic spin squeezing, we comment more on these limitations to squeezing.

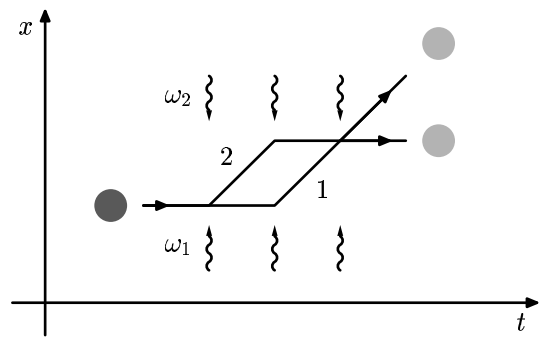

Figure 4.4: Atom-interferometer realized via Bragg scattering of the condensate.

4.3 Quantum beam splitter

In this section we elaborate on the idea of Sec. 4.2.6, namely that squeezing can take place while the two components are spatially separated. In fact, we abandon the second internal state and propose a method to realize a beam-splitter for a one-internal-state condensate, causing a splitting of the condensate in two spatially separated components with a better matching of occupancies than in the binomial distribution resulting from a splitting of independent particles. Such subbinominal splitting has indeed been proposed to occur if one adiabatically raises a potential barrier inside a single condensate. This dynamics is governed by the time scale for which the system is able to adiabatically follow the lowest energy state due to the collisional repulsion among atoms, and this time scale may be very long, making an experimental implementation very difficult [92].

In contrast, we propose a fast method working in four steps: (i) apply a normal splitting to create a binomial distribution of atoms separated in space, (ii) make use of the collisional interaction in each spatial component to cause in few ms a non-linear phase evolution of the different amplitudes, (iii) reflect the atoms so they again overlap in space, and (iv) remix them on a second beam splitter, so that the resulting separate components are populated by a subbinomial distribution. It will turn out below that the last beam splitter should only have very small reflectivity.

4.3.1 Bragg interferometer

The principle of the proposal is sketched in Fig. 4.4., where the vertical arrows indicate Bragg diffracting laser fields with appropriate detunings and phases. We suggest to use Bragg diffraction to split and to recombine the atomic clouds because this method has already been successfully demonstrated in experiments [93, 94, 95].

The atoms are initially in a single component BEC, i.e., all atoms populate the same one-particle wavefunction ϕ_0. Counterpropagating laser beams along the x-direction with a frequency difference around 100 kHz are applied to the atomic cloud and cause diffraction of the atoms. In the moving frame of the optical standing wave pattern, Bragg diffraction conserves kinetic energy and the atoms coherently populate two components at the incident momentum $-\hbar k$ (corresponding to zero momentum in the laboratory frame) and at $\hbar k$, differing by twice the photon momentum. For suitably chosen parameters the diffraction process is fast and interactions can be ignored. The diffraction is then a linear process and each atom is put in a superposition of remaining at rest, and having received twice the photon momentum. Allowed to propagate freely the atoms will coherently populate two spatially separated regions of space after less than 1 ms. This splitting by a Bragg pulse is equivalent to the $\pi/2$ pulse on the internal transition in the previous section.

To compute the effect of collisions on the spatial dynamics we assume as in the previous section that it is an adequate approximation to let half of the atoms, $N/2$, populate each component. Once the two momentum components have separated, their evolution is therefore described by

two identical, single–component Gross–Pitaevskii equations,

$$i\hbar\frac{\partial}{\partial t}\phi_i = (\hat{h}_i + \frac{Ng}{2}|\phi_i|^2)\phi_i. \tag{4.34}$$

The atoms may be free, in which case $\hat{h}_i$ equals the kinetic energy operator, they may fall under gravity, or they may be trapped in a weak trapping potential. For the component remaining at rest, the initial condition is $\phi_1(x, t = 0) \sim \phi_0(x)$, for the Bragg diffracted component, $\phi_2(x, t = 0) \sim \exp(2ikx)\phi_0(x)$.

Effectively, the wavefunctions ϕ_1 and ϕ_2 define two modes for the atoms, just as the two internal states and their associated spatial wavefunctions in Sec. 4.2.1. The two modes have creation and annihilation operators $a_i^\dagger$ and a_i and the dynamics associated with the distribution of atoms among the modes is accounted for by a two–mode Hamiltonian, analogous to (4.14):

$$H = \sum_{i=1,2} g\mathcal{I}_i \left(\frac{1}{2}(a_i^\dagger)^2 a_i^2 - \frac{N}{2}a_i^\dagger a_i\right). \tag{4.35}$$

As we are working with only one internal state, a difference in the strength parameter for $i = 1, 2$ is caused only by differences in the self–interaction integrals, $\mathcal{I}_i = \int |\phi_i|^4 d^3\mathbf{r}$, not by differences in s-wave scattering lengths.

4.3.2 Collective spin picture of interferometer operation

Having reduced the problem to two modes, the mapping to a collective spin applies. Let us walk through the interferometer operation in the spin picture. Before the first Bragg pulse, all atoms are at rest, and the collective spin, defined now by

$$\begin{aligned}\hat{S}_x &= \frac{1}{2}\left(\hat{a}_2^\dagger\hat{a}_1 + \hat{a}_1^\dagger\hat{a}_2\right)\\ \hat{S}_y &= \frac{1}{2i}\left(\hat{a}_2^\dagger\hat{a}_1 - \hat{a}_1^\dagger\hat{a}_2\right)\\ \hat{S}_z &= \frac{1}{2}\left(\hat{a}_2^\dagger\hat{a}_2 - \hat{a}_1^\dagger\hat{a}_1\right),\end{aligned} \tag{4.36}$$

is in a CSS pointing down. The Bragg pulse puts all atoms a superposition of remaining at rest and moving with momentum $2\hbar k$, i.e., it rotates the spin to the equatorial plane. By convention, we take the spin to point in the x–direction; this is of course arbitrary to the extent that we can choose a different phase for the mode functions. It is, however, important to realize that the Bragg scattering is a coherent process, and given a definition of the modes, we can choose the relative phase of the Bragg lasers to rotate the spin around *any* vector in the equatorial plane.[3]

After the Bragg pulse, the two components are allowed to propagate for a for a time interval of duration T (typically some ms). We then apply a new Bragg diffraction pulse to induce a complete transfer between states with momenta $\pm\hbar k$ in the moving frame, i.e., 0 and $2\hbar k$ in the laboratory frame, so that the two components now approach each other. This operation is carried out on the two spatially separated components, and it is accounted for by inclusion of the interaction with the Bragg fields in $\hat{h}_i$ in Eq. (4.34). Note that with the convention that the collective spin refers to the spatially separated components, this Bragg pulse has no effect on the values of the spin components; the solutions $\phi_i(\mathbf{r}, t)$ constitute a 'rotating frame' for our calculation of populations and coherences. The spin picture is suggestive that spin measurements and rotations can be carried out at any time, but with the paths–as–modes convention, it is only when the two spatial components overlap that all the spin variables represent physically accessible quantities.

During the separated propagation of the two components along the interferometer paths, spin squeezing takes place by the $\hat{S}_z^2$ mechanism. The strength parameter, χ, of Eq. (4.4) can be found from the two–mode Hamiltonian, (4.35):

$$\hbar\chi = \frac{g}{2}\left\{\mathcal{I}_1 + \mathcal{I}_2\right\}. \tag{4.37}$$

[3]This relative phase corresponds to the position of standing wave pattern.

In Sec. 4.3.3, we shall give realistic estimates for how much squeezing can be accumulated during the propagation.

After the second Bragg pulse, the components are approaching each other. If the external potential is turned off, they overlap again in space after a time T. As we saw in Sec. 2.6, it is at this point possible to observe interference fringes in the spatial density profile. At the time of full overlap we can apply a final beam splitter Bragg pulse to recombine the two components into two new output components. As explained above, we can choose to rotate around any vector in the equatorial plane:

$$\begin{aligned}\hat{U}_{\text{Bragg}} &= \exp\left[i\alpha\left(\cos\phi\ \hat{S}_x + \sin\phi\ \hat{S}_y\right)\right] \\ &= \begin{bmatrix} \cos\frac{\alpha}{2} & i\sin\frac{\alpha}{2}e^{-i\phi} \\ i\sin\frac{\alpha}{2}e^{i\phi} & \cos\frac{\alpha}{2} \end{bmatrix}\end{aligned} \tag{4.38}$$

Here we have written the Bragg evolution operator in the spin picture and as a 2×2 matrix giving the mode annihilation operators $\hat{b}_1$ and $\hat{b}_2$ after the pulse in terms of the operators $\hat{a}_1$ and $\hat{a}_2$ before the pulse. We are interested in creating a state with two separate components with subbinomial counting statistics, that is, we want to chose ϕ, the phase of the pulse, and α, controlled by the duration, such that the counting statistics of $\hat{b}_1$ and $\hat{b}_2$ will benefit from the correlations in $\hat{a}_1$ and $\hat{a}_2$. In the spin picture it is clear that this operation should be a rotation around the mean spin to align the squeezed direction with the z-axis which represents population differences. If we denote by S_α the spin component that the last Bragg pulse rotates into the z-direction, then from the definition (4.36) we get the mean and variance of the populations of one of the output beams

$$\begin{aligned}\langle\hat{n}_{\text{det}}\rangle &= \frac{1}{2}N + \langle\hat{S}_\alpha\rangle \\ \text{Var}(n_{\text{det}}) &= \text{Var}(S_\alpha).\end{aligned} \tag{4.39}$$

If $\phi = 0$ we rotate around the x-axis and the angle α should ideally be chosen equal to θ of Fig. 4.1b and Eq. (4.21). With no spin squeezing one finds $\text{Var}(n_{\text{det}}) = N/4$ in agreement with the initial binomial distribution.

In the previous section, we learned from the positive P simulations that the rotation angle is predicted with adequate precision in the simple model, so that application of Bragg pulses with these variables should suffice to yield substantial reduction of the population fluctuations of the two atomic outputs. It is also straightforward to optimize the parameters in experiments. The phases of the diffracting lasers are adjusted so that the two output beams have the same mean occupancy, independently of the duration of the last Bragg pulse. The solid curve in Fig. 4.5 shows the squeezing factor $(N/4)/\text{Var}(n_{\text{det}})$ (large for strong squeezing) as a function of α. With a spin squeezed sample the variance of the populations show a strong dependence on the duration of the last Bragg pulse, which should therefore be adjusted to identify the output with minimal fluctuations.

4.3.3 Expected results

Let us turn to the discussion of the experimental feasibility of our proposal. Splitting and recombination of one-component condensates have been done in several laboratories, and the coherence properties have been verified and explicitly utilized in a number of imaging experiments: our proposal follows closely the experiments at NIST, where the phase variation of the condensate gives rise to a density variation in the recombined output [94]. These experiments have been done in the limit of interacting condensates which is of course essential for our proposal: In Ref. [95] the mean field repulsion was observed and it was shown not to prevent a nearly perfect overlap of the spatial modes at the recombination, and in Ref. [94] a soliton was imprinted in one of the components to be subsequently detected in the output. We note that also the phase variation around quantized vortices has been studied by similar interference imaging, both in the case where a vortex was prepared prior to the splitting and a dislocation appears in the interference fringes [96], and in

the case where a condensate was split and a vortex was subsequently created by stirring only one component [97].

One might wonder whether our proposal puts more strict demands on the beam splitting Bragg pulses than the above mentioned experiments. Bragg pulses can be made highly selective in momentum and can even be used for momentum spectroscopy, but a beam splitter should instead have the same reflectivity for all momentum components of the condensate so that a good mode match can be achieved. In this respect, our proposal is not more demanding than already realized interferometers and we show this explicitly in Sec. 4.3.4.

To assess the strength of the squeezing interaction we need to evaluate the parameter χ of Eq. (4.37). We assume $\mathcal{I}_1 = \mathcal{I}_2 = \mathcal{I}$ for simplicity, and in the Thomas-Fermi approximation, valid for an interaction dominated condensate, one finds the simple result:[4]

$$\mathcal{I} = \int |\phi|^4 d^3\mathbf{r} = \frac{10}{7}\frac{1}{V_{\mathrm{TF}}} \tag{4.40}$$

where $V_{\mathrm{TF}} \equiv (4\pi/3)R_x R_y R_z$ with R_i the Thomas-Fermi radius of the condensate in the i-direction. As typical numbers we can take parameters of the sodium experiment reported in [94]: $R_x = 23\mu m$, $R_y = 33\mu m$, $R_z = 47\mu m$, and $a_s(\mathrm{Na}) = 2.8nm$. We then get $\chi = 1.0 \times 10^{-3}s^{-1}$ and with $N = 1.8 \times 10^6$ Eq. (4.20) gives a factor of ~ 5 reduction on the population fluctuations in the output ports for $1ms$ separation of the components.

In reality, ϕ, and thus $\mathcal{I}$, will be functions of time and χt is replaced by $\int \chi(t)dt$. In Sec. 4.2.6 we used a simple non-interacting approximation to handle the case where one component finds itself in a displaced harmonic trap. Here we are rather dealing with free expansion starting from a Thomas–Fermi initial state, and the solution is given by a scaling of the initial wavefunction [21]. Therefore the form of Eq. (4.40) is preserved and $V_{\mathrm{TF}}(t)$ can found by solving 3 coupled differential equations for the 3 scaling parameters. (A note of caution: When the condensate is split in two, $N \to N/2$, and this must be taken explicitly into account when using the scaling equations derived in, e.g., Ref. [21].)

If the components are separated for more than the 1 ms assumed above, the squeezing gets stronger but the process is slowed down by the reduction of $\chi(t)$ as the clouds expand. The expansion happens on a time-scale given by the trapping frequency before the release of the condensate and the simple two-mode picture predicts that high squeezing factors can be reached before the non-linearity becomes negligible. However, this is one of the regimes identified by Sørensen [91] as not too well described by the two–mode model. Squeezing still takes place, but at an reduced rate: A squeezing factor of 10 requires almost 7 ms of separation while the two-mode model predicts 2 ms.

4.3.4 Effect of imperfect overlap

As a final issue for the operation of the quantum beam splitter, we wish to discuss the matching of the spatial wave functions of the two components. After the physical interactions described above, one will detect a number of atoms with momenta around zero, and a number of atoms with momenta around $2\hbar k$, and the analysis shows that these numbers will fluctuate less than if they were given by a binomial distribution. This reduction is due to the correlations between the atoms following the lower and the upper paths in the interferometer, and it is hence important that atoms from the lower path, being diffracted by the last Bragg pulse, occupy the same spatial state as the undiffracted component of the upper path, cf. Fig. 4.4. In the extreme case where these two contributions are orthogonal and distinguishable, there will be no squeezing effect at all, and in the case where they overlap 100 %, the squeezing is given by the above simple analysis.

Atoms leaving the interferometer at zero momentum can in general be described by a superposition of ϕ_2, the undiffracted upper path wavefunction, and a state $\phi_{2\perp}$ orthogonal to ϕ_2. This gives rise to two orthogonal modes which both contribute to the detected number of atoms around zero momentum. We can express the field operators, $\hat{b}_2, \hat{b}_{2\perp}$, for these two modes in terms of the

[4] This is the 3D version of Eq. (4.31)

operators $\hat{a}_1, \hat{a}_2$ given above for the modes prior to the last Bragg pulse *and* operators for two additional "vacuum" modes, $\hat{a}_{1\perp}, \hat{a}_{2\perp}$, which are necessary to ensure unitarity of the beam splitter pulse. Letting c denote the overlap of the (normalized) diffracted lower path component with the upper path undiffracted component and s the overlap with the orthogonal complement we have

$$e^{-2ikx}\phi_1(\mathbf{r}) = c\phi_2(\mathbf{r}) + s\phi_{2\perp}(\mathbf{r}), \tag{4.41}$$

were $|s|^2 + |c|^2 = 1$. In terms of α and ϕ of the last Bragg pulse (4.38) we have:

$$\hat{b}_2 = \cos\frac{\alpha}{2}\,\hat{a}_2 + i\sin\frac{\alpha}{2}e^{-i\phi}\left(c\,\hat{a}_1 + s\,\hat{a}_{1\perp}\right) \tag{4.42}$$

$$\hat{b}_{2\perp} = \cos\frac{\alpha}{2}\,\hat{a}_{2\perp} + i\sin\frac{\alpha}{2}e^{-i\phi}\left(s^*\,\hat{a}_1 - c^*\,\hat{a}_{1\perp}\right). \tag{4.43}$$

Focusing on $\hat{b}_2$ we see that for $|c| < 1$ we can still control the mixing and pick the squeezed combination of $\hat{a}_1$ and $\hat{a}_2$. However, some contributions from the unoccupied modes have been introduced, and the situation is similar to the detection of squeezed light: A non-unit overlap ν between the squeezed mode of light and a detector mode as, e.g., modeled by a beam splitter transmitting a fraction $|\nu|^2$ of the squeezed light to the detector, leads to admixture with a vacuum field and the deterioration of the squeezing, $\mathrm{Var}(X)_{\mathrm{det}} = |\nu|^2\mathrm{Var}(X)_{sq} + (1 - |\nu|^2)$, where the X is the scaled quadrature field component with unit variance in the vacuum state.

In a real experiment it is difficult to count the atoms in mode ϕ_2 exclusively. It is more realistic that one will only have access to the total number of atoms in ϕ_2 and $\phi_{2\perp}$. We then have to include $\hat{b}_{2\perp}$ in the analysis, and if the phase of the Bragg diffraction is chosen to compensate the phase of the complex overlap c, we find:

$$\begin{aligned}\langle\hat{n}_{\mathrm{det}}\rangle &= \langle\hat{b}_2^\dagger\hat{b}_2 + \hat{b}_{2\perp}^\dagger\hat{b}_{2\perp}\rangle \\ &= \langle\cos\alpha\;\hat{S}_z - |c|\sin\alpha\;\hat{S}_y\rangle + \frac{N}{2} \\ &= \lambda\langle\hat{S}_{\alpha'}\rangle + \frac{N}{2}.\end{aligned} \tag{4.44}$$

in terms of the spin component $\hat{S}_{\alpha'}$ *prior* to the last Bragg pulse. The angle α' is related to α, the rotation angle given by the duration of the last Bragg pulse, by $\tan\alpha' = |c|\tan\alpha$, and we have introduced the factor $\lambda = \sqrt{|c|^2/(\sin^2\alpha' + |c|^2\cos^2\alpha')}$.

The spin component $\hat{S}_{\alpha'} \equiv \cos\alpha'\hat{S}_z - \sin\alpha'\hat{S}_y$ is in a direction perpendicular to the mean spin. We therefore have $\langle\hat{S}_{\alpha'}\rangle = 0$ and $\langle\hat{n}_{\mathrm{det}}\rangle = N/2$ independently of α. The variance of n_{det} is given by

$$\begin{aligned}\mathrm{Var}(n_{\mathrm{det}}) &= \langle\hat{n}_{\mathrm{det}}^2\rangle - \langle\hat{n}_{\mathrm{det}}\rangle^2 \\ &= \lambda^2\mathrm{Var}(\hat{S}_{\alpha'}) + (1-\lambda^2)\frac{N}{4}.\end{aligned} \tag{4.45}$$

If the overlap is complete, $|c| = 1 = \lambda$, we can pick out the maximally squeezed spin component to yield the minimal variance of n_{det}. In case of a non-perfect overlap, we see that Eq. (4.45) introduces a non-squeezed contribution, scaling as $N/4$, and it makes the number fluctuations depend on the noise of the spin component $S_{\alpha'}$ rather than of S_α. We therefore want α' to be close to the actual direction of squeezing θ in Fig. 4.1 and Eq. (4.21), which is obtained by choosing a Bragg pulse with longer duration than what is optimal in the ideal case.

In Fig. 4.5 we show the variation of $(N/4)/\mathrm{Var}(n_{\mathrm{det}})$ with α for different values of the overlap c. When $|c|$ is reduced the squeezing factor drops, but the curves illustrate that the results improves if one chooses a larger rotation angle α. Note that the mode function mismatch does not have the same detrimental effect as in the detection of a single mode squeezed field: the admixture of the vacuum modes, and hence the vacuum contribution $N/4$ to $\mathrm{Var}(n_{\mathrm{det}})$, does not scale with $|s|^2 = 1 - |c|^2$ but rather with $|s|^2\sin^2\alpha$, and for small rotation angles this is a small number.

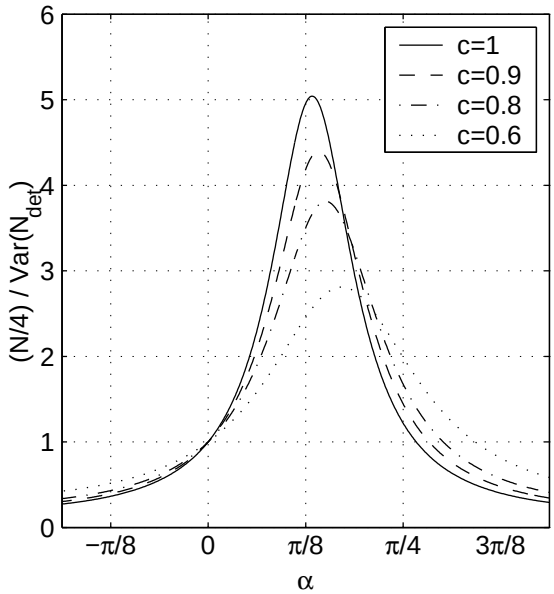

Figure 4.5: The reduction of $\mathrm{Var}(n_{\mathrm{det}})$ is illustrated by plotting the reciprocal ratio $(N/4)/\mathrm{Var}(n_{\mathrm{det}})$ as a function of the applied Bragg pulse rotation angle for parameters as in Sec. 4.3.3 with 1 ms separation. The results are shown for different values of the overlap, $c = 1$ (solid line), $c = 0.9$ (dashed line), $c = 0.8$ (dash-dotted curve), and $c = 0.6$ (dotted curve). The value of α at the maximum of the $c = 1$ curve displays the orientation of the squeezing ellipse, i.e. θ of Fig. 4.1. As is apparent from the other curves, one may compensate for a non-perfect overlap by applying a larger Bragg pulse rotation.

For strong squeezing the uncertainty ellipse is almost horizontal and only rotation by a small α is needed to observe squeezing in the number fluctuations. In this case even a significantly reduced overlap does not prevent a sizable noise reduction for $n_{\rm det}$. This is illustrated when we write the maximal squeezing factor attainable for given c and given $\mathrm{Var}(S_\theta)$:[5]

$$\begin{aligned}\mathrm{Var}(n_{\rm det}) &= \mathrm{Var}(S_\theta)\left(1+(1-|c|^2)\frac{\frac{N}{4}-\mathrm{Var}(S_\theta)}{|c|^2\frac{N}{4}+\mathrm{Var}(S_\theta)}\right)\\ &\sim \frac{\mathrm{Var}(S_\theta)}{|c|^2} \qquad (\mathrm{Var}(S_\theta)\ll\frac{N}{4}).\end{aligned} \tag{4.46}$$

4.3.5 Discussion

In this section we have described our proposal for a quantum beam splitter for matter waves, and in fact, as is apparent from Sec. 4.3.3, spin squeezing is already taking place in experiments; it is just not detected. It is experimentally feasible to do the rotations around the mean spin to reveal the α dependence of $\mathrm{Var}(n_{\rm det})$, and detection is mainly limited by the inability to count atoms with sufficient precision. High counting efficiency is attractive for many reasons, and we expect much progress to be made in this area in the near future. The condensation of meta–stable Helium holds great promise for single–atom detection, as meta–stable atoms are virtual bombs at the energy scales otherwise relevant to BEC, and e.g. a micro channel plate can have a time-resolution at the ns level [98, 99].

In our analysis, we have relied on the two–mode model. This was motivated by the successful comparison of this simple picture with the full positive P method in Sec. 4.2. As mentioned in Sec. 4.3.3, one should be more careful at long times. Bogoliubov theory shows [91] that free expanding clouds are not an ideal setting for production of really strong spin squeezing. This is because the mode functions in this case becomes sensitive to the number of atoms. Therefore the separation of population and spatial dynamics breaks down, ruining our ability to adjust fluctuations in a simple way. This problem is less pronounced if the atoms are trapped during the experiment and strong squeezing may be possible in e.g. an atomic waveguide interferometer.

[5] In Eq. (4.46) we assume that the spin state described by Eqs. (4.21,4.20) is a minimum uncertainty state. This not exactly true, but a good approximation for moderate squeezing as considered here [70].

4.4 Squeezed light from spin squeezed atoms

In this section we describe how to generate squeezed light from a spin squeezed sample of atoms. The motivation for such a proposal could be sought in the many uses of squeezed light. To mention a few, squeezed light and entangled beams of light can be used to probe mechanical motion with better resolution than classical light [100], for lithography with a resolution below the optical wavelength [101, 102], and in the active field of quantum information [103, 104, 105].[6] The standard means to produce nonclassical light are nonlinear crystals in optical parametric oscillators and laser diodes with suitable feed-back. As a figure of merit for the degree of nonclassicality of these light sources, one may refer to the noise suppression observed in direct or homodyne photon detection measurements. Compared to classical sources it has so far been possible to reduce the noise (variance) by about one order of magnitude. In order to make a significant difference in practical applications, further noise reduction is really necessary, and it will surely be worthwhile to look for new approaches to squeezing of light. Among the promising candidates are resonant Raman systems. These systems can display both large nonlinearity and low absorption leading to ideal four-wave mixing and substantial squeezing [107, 108, 109]. We suggest instead to transfer the squeezing of atomic spins to squeezing of a mode of the light field by applying stimulated Raman scattering.

4.4.1 Stimulated Raman scattering

The theoretical treatment of the light emission will be a generalization of traditional Raman scattering theory, see Refs. [110, 111, 112]. This part of our proposal can be analyzed without specifying the model for spin squeezing, but in Sec. 4.4.3 we will specifically return to the case of a spin squeezed BEC from Sec. 4.2.

Our ensemble of two-state atoms is assumed to be strongly elongated and it is treated in a 1D approximation. It is illuminated by a strong laser field E_s propagating along the z-axis of the system. This opens up a channel for an atom in the b state to go to the a state by absorbing a photon of frequency ω_s and emitting a photon of frequency $\omega_q \sim \omega_s + \omega_{ba}$. As a result, a field at this frequency builds up and propagates through the sample. This process is described by the following coupled set of equations for the atomic and field operators

$$\begin{aligned}\frac{\partial}{\partial t}\left[\hat{\psi}_a^\dagger(z,t)\hat{\psi}_b(z,t)\right] &= i\kappa_1^* E_s^*(z,t)\times \\ &\quad\times\left(\hat{\psi}_a^\dagger(z,t)\hat{\psi}_a(z,t) - \hat{\psi}_b^\dagger(z,t)\hat{\psi}_b(z,t)\right)\hat{E}_q(z,t)\end{aligned} \tag{4.47}$$

$$\left(\frac{\partial}{\partial z} + \frac{1}{c}\frac{\partial}{\partial t}\right)\hat{E}_q(z,t) = -i\kappa_2\hat{\psi}_a^\dagger(z,t)\hat{\psi}_b(z,t)E_s(z,t), \tag{4.48}$$

where $\kappa_1 = \sum_i \mu_{ai}\mu_{bi}/(\hbar^2\Delta_i)$ and $\kappa_2 = 2\pi\hbar\omega_q\kappa_1/c$. μ_{ji} are dipole moments of the atomic transitions and Δ_i are the (large) detunings with respect to intermediate levels, see Fig. 4.6. In Eq. (4.47) we have assumed that there is no dephasing of the a–b coherence, and in Eq. (4.48) we have assumed the validity of the slowly varying envelope approximation for the emitted field.

4.4.2 Finding the output field

If we restrict our analysis to the case where the atoms are almost entirely in the a state when the E_s field is applied, we can replace the population difference appearing in Eq. (4.47) by the density of atoms, $n(z)$. This density we represent as a c-number throughout the duration of the output coupling. This allows us to define a dipole operator "per atom" by $\hat{\psi}_a^\dagger(z,t)\hat{\psi}_b(z,t) = n(z)\hat{Q}(z,t)$

[6] For a general review of squeezed light, see Ref. [106].

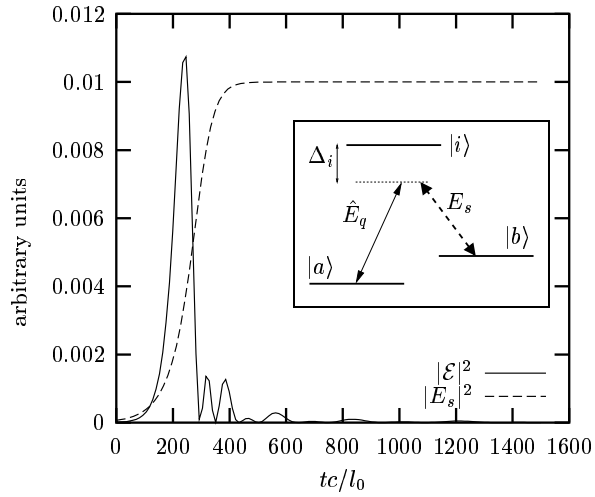

Figure 4.6: The shape of the E_s pulse and the mode function $\mathcal{E}$ of the emitted $\hat{E}_q$ pulse. The mode function is found by diagonalizing the first-order correlation function of the field, but coincides with the signal expected when the single atom operator $\hat{Q}$ is uniform over the sample. The insert shows the atomic level scheme of the proposal.

and we obtain the linear operator equations

$$\frac{\partial}{\partial t}\hat{Q}(z,t) = i\kappa_1^* E_s^*(z,t)\hat{E}_q(z,t) \tag{4.49}$$

$$\left(\frac{\partial}{\partial z} + \frac{1}{c}\frac{\partial}{t}\right)\hat{E}_q(z,t) = -i\kappa_2 n(z)E_s(z,t)\hat{Q}(z,t). \tag{4.50}$$

To solve Eqs. (4.49) and (4.50), we need to generalize the analysis of stimulated Raman scattering in Refs. [110, 111, 112] slightly: we do not want to assume a homogeneous media. A uniform density of atoms is to be expected when dealing with room temperature atoms or molecules in a gas cell, but we want also to be able to treat a BEC held in, e.g., a harmonic trap. Within the approximations made, the alterations are minor, mainly consisting in the scaling of lengths by density. We can thus solve Eqs. (4.49) and (4.50) analytically in terms of the input field $\hat{E}_q(0,t)$ at the entrance face of the sample at $z = 0$, the initial position dependent atomic polarization $\hat{Q}(z,0)$, and the strong laser field $E_s(0,t)$ which is treated as classical and undepleted by the interaction with the sample. In particular, for the field operator we get

$$\hat{E}_q(z,\tau) = \hat{E}_q(0,\tau) - i\kappa_2 E_s(\tau)\int_0^z \psi_b^\dagger(z',0)\psi_a(z',0)\times \\ \times J_0\left(2\sqrt{a(\tau)\int_{z'}^z n(z'')dz''}\right)dz' \tag{4.51}$$

where the new time coordinate is $\tau \equiv t - z/c$, $J_0(\cdot)$ is a Bessel function of the first kind, and $a(\tau) = \kappa_1^*\kappa_2\int_0^\tau |E_s(\tau')|^2 d\tau'$.

The expression (4.51) must be evaluated at the position $z = L$ of a detector outside the atomic sample. In the absence of atoms, the field equals the incident quantum vacuum field $\hat{E}_q(0,\tau)$. The atomic sample is able to replace the vacuum with an entirely different field. In order to analyze the quantum properties of $\hat{E}_q$ it is convenient to imagine a time integrated homodyne detection at the detector. By choosing the temporal form of the strong local oscillator field in this detection

we select a certain spatio-temporal mode of the field represented by the field operator

$$\hat{a} = \sqrt{\frac{c}{2\pi\hbar\omega_q}} \int_0^\infty \mathcal{E}^*(\tau)\hat{E}_q(L,\tau)d\tau \tag{4.52}$$

where $\int |\mathcal{E}|^2 d\tau = 1$. In choosing $\mathcal{E}(\tau)$ we should seek to ensure that $\hat{a}$ is a mapping of the precise collective operator of the atomic sample that is known to be squeezed. Mathematically, it is easy to show that in order to probe $\int h(z')\hat{Q}(z',0)dz'$ we should choose $\mathcal{E}(\tau)$ as the normalized solution of Eqs. (4.49) and (4.50) with the initial condition $n(z')\hat{Q}(z',0)$ replaced by $h(z')$. Physically, this reflects that the question of mode matching coincides with the problem of identifying the classical field radiated by a classical dipole distribution. In particular, if the uniform integral of atomic operators $\int \psi_a^\dagger(z',0)\psi_b(z',0)dz'$ is squeezed, mode matching is accomplished by taking $\mathcal{E}(\tau)$ to be the (normalized) solution to the classical Raman scattering problem. In that case we get the mapping

$$\hat{a} = \frac{1}{\sqrt{N}} J_- \tag{4.53}$$

where $\hat{J}_- = \int \hat{\psi}_a^\dagger(z,t)\hat{\psi}_b(z,t)dz$, and N is the total number of atoms.

4.4.3 Light from a spin squeezed BEC

In the introduction to spin squeezing, Sec. 4.1, we mentioned a number of different schemes for the generation of spin squeezing in atomic samples. The above analytical treatment is general and independent of the method of spin squeezing, and as shown by Eq. (4.53) (valid only if the majority of atoms occupy the state a), the atomic state is transfered perfectly to the light field. To see more precisely how this works out in a specific case, we can return to the positive P treatment of spin squeezing by collisional interactions in a two-component Bose Einstein condensate, Sec. 4.2. The suggested procedure for squeezing was: Start in internal state a and apply a $\pi/2$ pulse to put the atoms in an equal superposition of a and b. The collisional interaction now produces spin squeezing. After a suitable time interval, we apply a second $\pi/2$ pulse to put the atoms back in state a, i.e., to rotate the collective spin back to the south pole of the Bloch sphere. In fact, we do not necessarily want to apply exactly a $\pi/2$ pulse; we only want to have $\hat{\psi}_a^\dagger(z,t)\hat{\psi}_a(z,t) - \hat{\psi}_b^\dagger(z,t)\hat{\psi}_b(z,t) \sim n(z)$ to get from Eq. (4.47) to Eq. (4.49). Finally, we apply the E_s field and generate the outcoupled $\hat{E}_q$ field, carrying quantum correlations.

4.4.4 Using the positive P simulations as input

In the positive P description, the state of the system just before we apply the last $\pi/2$ pulse is represented by an ensemble of pairs of two–component wavefunctions, $\boldsymbol{\psi} = (\psi_{a1}, \psi_{a2}, \psi_{b1}, \psi_{b2})$. From this ensemble, we can calculate expectation values of all operator expressions and make plots like e.g. Figs. 4.2 and 4.3. We can also propagate the ensemble through a subsequent linear evolution, that do not in itself demand the heavy machinery of positive P simulations. In this way, no information is thrown away before it is necessary. For our spin squeezed condensate, we will start by applying the final $\pi/2$ pulse "by hand", i.e., we rotate the individual sets of wavefunction realizations of the simulation ($i = 1, 2$):

$$\begin{pmatrix} \psi_{ai} \\ \psi_{bi} \end{pmatrix} \rightarrow \begin{pmatrix} \psi'_{ai} \\ \psi'_{bi} \end{pmatrix} = \begin{pmatrix} \cos\frac{\theta}{2} & \sin\frac{\theta}{2} \\ -\sin\frac{\theta}{2} & \cos\frac{\theta}{2} \end{pmatrix} \begin{pmatrix} \psi_{ai} \\ \psi_{bi} \end{pmatrix} \tag{4.54}$$

with $\theta \cong \pi/2$. Now the E_s pulse is send in, and the atom–field interaction in the coupled equations (4.47) and (4.48) leads to a natural positive P representation of the field $\hat{E}_q(z,t)$: Replace in Eq. (4.51) $\hat{E}_q(z,t)$ by a c-number field $E_{q1}(z,t)$ and $\hat{\psi}_a^\dagger(z',0)\hat{\psi}_b(z',0)$ by $\psi_{a2}(z',0)\psi_{b1}(z',0)$, and make a similar replacement in the hermitian conjugate equation where $\hat{\psi}_b^\dagger(z',0)\hat{\psi}_a(z',0)$ is replaced by $\psi_{b2}(z',0)\psi_{a1}(z',0)$ to yield the c-number field $E_{q2}(z,t)$. In both cases, the incident vacuum field can be represented by a zero, since the positive P representation yields normally

ordered expectation values as simple products. From our original ensemble of quadruples of wavefunctions, $\boldsymbol{\psi}$, describing the atoms just after the spin squeezing, we obtain in this way an ensemble of pairs $(E_{q1}(z,\tau), E_{q2}(z,\tau))$ describing the generated light field $\hat{E}_q(z,\tau)$. With this ensemble any normally ordered field expectation value can be found.

4.4.5 An example

As an example, we have used the simulations of Sec. 4.2.4, i.e., the "favourable g's" case. The parameters were 2000 atoms of mass m and with 1D interaction strengths $(g_{aa}, g_{ab}, g_{bb} = (1.0, 0.5, 1.0)\times 5\times 10^{-3}\hbar\omega l_0$ where ω is the frequency of the harmonic trap and $a_0 = \sqrt{\hbar/m\omega}$ is the associated characteristic length. The atoms are spin squeezed by collisional interactions for a time $t = 3.0\omega^{-1}$. They are subsequently driven towards the state a, and hereafter they are illuminated with the E_s light which builds up a maximum strength of $E_{max} = 10^2\sqrt{2\pi\hbar\omega_q/l_0}$ in a time of roughly $t_{rise} = 100a_0/c$. The matter-light coupling is chosen to be $\kappa_1 = 10^{-3}c/2\pi\hbar\omega_q$.

As we know the atoms to be spin squeezed we also know one mode of the $\hat{E}_q$ field which will be squeezed: The one corresponding to the simple uniform integral of $\int \psi_a^\dagger(z',0)\psi_b(z',0)dz'$ as described in the discussion after Eq. (4.52). Even with the simplifications leading to Eqs. (4.49) and (4.50) the atomic state could in principle radiate into many other modes and do so with varying quantum statistics. To check whether such other modes are present in this case we calculate the first order correlation function of the field $\langle \hat{E}_q^\dagger(L,\tau')\hat{E}_q(L,\tau)\rangle = \overline{E_{q2}(L,\tau_2)E_{q1}(L,\tau_1)}$. When it is diagonalized we find that almost all population is in fact in the expected mode $\mathcal{E}(\tau)$ which is plotted in Fig. 4.6. In other scenarios it might be difficult to calculate beforehand exactly which collective atomic operator is squeezed and then an analysis like this would be necessary in order to pick the local oscillator field for the homodyne detection.

Having confirmed that only one mode is populated we now turn to the quantum character of the field. It depends on how we choose θ in Eq. (4.54): For $\theta = \pi/2$ it will approximate squeezed vacuum, for θ slightly different from $\pi/2$ it will approximate a squeezed coherent state. Remember, that the spin squeezing ellipse is at an angle to the coordinate axes (cf. Fig. 4.1). This carries over to the light field which is squeezed in an appropriate quadrature component $X_\phi = (\hat{a}e^{i\phi} + \hat{a}^\dagger e^{-i\phi})/\sqrt{2}$. With the above parameters, we find from the positive P simulations that the minimum variance is 0.04 ± 0.01 corresponding to a reduction by a factor of more than 12 from the standard quantum limit. Eq. (4.53) predicts that this factor should coincide with the squeezing of the atomic spin. From Fig. 4.2 we see that this is so.

To illustrate the positive P results we show in Fig. 4.7 both a histogram and a scatter plot obtained from the positive P ensemble of pairs (a_1, a_2) representing $(\hat{a}, \hat{a}^\dagger)$ for the mode of the field. a_1 and a_2, on average, are complex conjugate quantities, so that the expectation values of Hermitian field operators like $\langle X_\phi\rangle = \overline{a_1 e^{i\phi} + a_2 e^{-i\phi}}$ are real for all ϕ. To represent our simulated results we have made a histogram for the values of $x = X_0$ and $p = X_{\pi/2}$, indicated by the *real part* of $(a_1 + a_2)/\sqrt{2}$ and $(ia_1 - ia_2)/\sqrt{2}$. The histogram in Fig. 2 has been obtained from 10^5 independent realizations of the noisy Gross-Pitaevskii equation for the atomic spin squeezing, while the scatter plot contains only 6800 points each representing a single realization.

4.4.6 Generalization to 3D

We have now seen how the spin squeezing of an atomic sample can be transfered to another quantum system, a mode of the light field. The analytical results are encouraging, a mapping like Eq. (4.53) being exactly what we could have hoped for. Naturally, we should at this point examine the approximations carefully. One assumption that really stands out is the restriction to 1D. A full 3D analysis is by no means guaranteed to preserve the possibility to couple to only a single spatio-temporal field mode. This issue is also considered in the classical treatments of stimulated Raman scattering. In Ref. [111] a diagonalization of the first order coherence function of the field (Karhunen–Loeve transformation) is performed and it shows that a single mode dominates the output, provided the Fresnel number of the (active part of the) atomic sample is not larger than of order unity. Fresnel numbers smaller than unity could not be directly treated. By choosing the

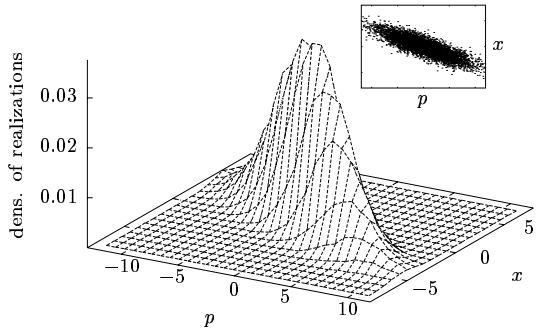

Figure 4.7: Histogram illustrating the prediction for the squeezing of light. The quadrature components of the output field are represented by pairs of numbers $\mathrm{Re}(a_1 + a_2)/\sqrt{2}$, $\mathrm{Re}(ia_1 - ia_2)/\sqrt{2}$, the distribution of which forms a squeezed ellipsoid shape in phase space. The actual amount of squeezing cannot be directly determined from this plot; it requires a computation of mean values and variances, making use of the fact that the distribution of the complex numbers a_1 and a_2 represent mean values of normally ordered field operators. 10^5 realizations contributed to the histogram and in the insert is for illustration shown a scatter plot of 6800 of the representative points.

experimental parameters carefully, we thus expect the 1D results also to apply for the quantum field in three dimensions.

4.4.7 Discussion

Related to our proposal are the recent experiments on slowing, and even halting and subsequently releasing, a light pulse propagating through an atomic sample [113, 114]. It has been theoretically predicted that the quantum state of the light is preserved in this process [115], and by applying e.g. a spin squeezing scheme to the atoms it could be possible to do powerful quantum state manipulations. One may even imagine a CW source of squeezed light. As described here, however, our proposal will only produce a pulse of squeezed light in a specific mode. The mode function can be predicted, and it is entirely possible to do experiments with such pulses. Ideally, one would however like to have some control over the shape of the pulse. Eq. (4.51) shows how the shape of the strong laser pulse, E_s, and the distribution of atoms, $n(z)$, determine the output field. Based on this equation, it should be possible to make educated guesses for optimal shapes E_s when trying to, e.g., eliminate the "ringing" of $\mathcal{E}$ evident in Fig. 4.6, but we have not pursued such an analysis further.

One may argue that a squeezing factor of 12, in the specific example of outcoupling from a spin squeezed BEC, is not so spectacular, comparable as it is to the performance of traditional sources of squeezed light. For us, this limit is mainly set by the precision obtainable from the limited ensemble of positive P simulations. In reality, the collisional interaction can produce stronger spin squeezing under ideal conditions. The same comments as in the discussion of the quantum beam splitter apply: The collisional interaction should have as limited influence on the spatial dynamics as possible. For other mechanisms for spin squeezing, other limitations to the degree of squeezing exist, but in general there is now reason to expect strong squeezing of atomic spins to be an easier task than strong squeezing of light. If this turns out to be the case, spin squeezing will certain be an interesting source of squeezed light.

On the more technical side, we would like to point out that the method of using a positive P ensemble as input for further, but "simple", evolution of the physical system is quite useful.[7] Even

[7] The problem of feeding a quantum state to a new system is of course quite general, see e.g. Refs. [116] and [117]

when the nonlinear dynamics is over and done with, we can still keep the whole ensemble with a modest computational overhead, as the positive P Langevin equations are then noiseless. If the final observables are complicated functions of the ones directly available just after the nonlinear dynamics this approach provides a straightforward way to obtain expectation values. In the example in this section, the outcoupled light field is connected to a complicated spatial integral of the atomic operators. Had an analytical solution of Eqs. (4.49) and (4.50) not been available, we could instead have solved these equations for each realization in the ensemble. Such an approach would have to be taken in a 3D calculation, or when light production and spin squeezing are taking place simultaneously.

and references therein.

4.5 Beyond spin squeezing

What lies beyond spin squeezing, i.e., what will happen if we let the two component system evolve far beyond the regime describable as a deformed coherent spin state? Pictorially, very strong spin squeezing corresponds to the uncertainty ellipse of Fig. 4.1 being bend all the way around the Blochs sphere and therefore the spin picture is in fact not very useful anymore. To gain more insight, we focus on CSSs on the equator and we make a change of notation to define the *phase states* [compare with Eq. (4.9)]

$$|\phi; N\rangle = \frac{1}{\sqrt{N!2^N}} \left[e^{i\phi}\hat{a}^\dagger + e^{-i\phi}\hat{b}^\dagger\right]^N |\text{vac}\rangle. \tag{4.55}$$

Being special cases of CSSs, phase states are not orthogonal for different ϕ's unless the phase-difference is exactly $\pi/2$,

$$\langle\phi'; N'|\, \phi, N\rangle = \delta_{NN'} \left[\cos(\phi - \phi')\right]^N. \tag{4.56}$$

4.5.1 Phase revivals

We want to study the longtime effect of the $\hat{S}_z^2$ Hamiltonian, i.e., of the time-evolution operator

$$\hat{U}_{\text{nl}}(t) = \exp\Big\{-i\chi\Big(\frac{\hat{n}_b - \hat{n}_a}{2}\Big)^2 t\Big\} = \exp\Big\{-i\chi\hat{n}^2 t/4\Big\}, \tag{4.57}$$

where we have introduced $\hat{n} = \hat{n}_b - \hat{n}_a$. As $\hat{U}_{\text{nl}}$ is nonlinear in $\hat{n}_a$ and $\hat{n}_b$, phase states will not evolve into phase states. For small t we get the spin squeezing effect, gradually deforming the state. However, as the spectrum of $\hat{n}$ consist of integers, we clearly have that $\hat{U}_{\text{nl}}(8\pi/\chi) = 1$ and at that time we recover the original state. In fact, the binomial expansion of Eq. (4.55),

$$|\phi; N\rangle = \sum_{\substack{n_a, n_b = 0 \\ n_a + n_b = N}}^{N} \sqrt{\binom{N}{n_a}} e^{-in_a\phi} e^{in_b\phi} |n_a, n_b\rangle, \tag{4.58}$$

contains either only even or only odd values of n. In addition, alternating signs on the terms of Eq. (4.58) equals $\phi \to \phi + \pi/2$. As a result, already at $t = t_{\text{rev}} = \pi/\chi$ we have

$$\hat{U}_{\text{nl}}(t_{\text{rev}})|\, \theta; N\rangle = \begin{cases} |\, \theta + \pi/2; N\rangle & , N \text{ even} \\ e^{-i\pi/4}|\, \theta; N\rangle & , N \text{ odd.} \end{cases} \tag{4.59}$$

For a given N, we can conclude that *phase revivals* will take place at all $t = qt_{\text{rev}}$ for $q = 1, 2, 3, \ldots$.

4.5.2 Schrödinger cats

Between revivals there is in general no well-defined phase between a and b. In an interference experiment, a phase can be established as explained in Sec. 2.6.2, but the value will not be predictable from the initial ϕ. A closer analysis [118], or numerical calculations [36, 119], reveals, however, some structure in the phase distribution: At certain times, only a few phase states are needed to represent the evolved state and consequently only a few phases are possible outcomes of interference experiments. Most interesting is the case of a superposition of two orthogonal phase states as it corresponds to a so-called *Schrödingers cat*, i.e., a superposition of two macroscopically distinguishable states. The cat state is created at $t = t_{\text{rev}}/2 = \pi/(2\chi)$ at which time we have

$$\hat{U}_{\text{nl}}(t_{\text{cat}})|\, \phi; N\rangle = \frac{1}{\sqrt{2}} \begin{cases} e^{-i\pi/4}|\, \phi; N\rangle + e^{i\pi/4}|\, \phi + \pi/2; N\rangle & , N \text{ even} \\ e^{-i\pi/8}|\, \phi + \pi/4; N\rangle + e^{-i\pi/8}|\, \phi + 3\pi/4; N\rangle & , N \text{ odd.} \end{cases} \tag{4.60}$$

Remembering the phase revivals above, we conclude, that cat states will be produced at all $t = (q + 1/2)t_{\text{rev}}$ for $q = 0, 1, 2, 3, \ldots$.

4.5.3 Detection of cat and confirmation of coherence

Just as important as the ability to create the cat state is the ability to experimentally detect it. The signature of the cat state will be that each measurement of the relative phase (interference experiment) will yield either 2ϕ or $2\phi + \pi$ (for N even). This is not enough, however, to conclude that the system was in a coherent superposition of the two phase states. A 50-50 incoherent mixture of the two would yield exactly the same result so it is necessary to somehow confirm the coherence of the system. This is not a trivial task: all M-body density matrices with $M < N$ are identical whether the system is in the superposition state or is a mixture, and no linear evolution (single-particle Hamiltonian) can change this.

To check coherence, we can instead rely on the intrinsic nonlinearity that produced the cat state in the first place: We simply wait for the phase revival. Only if the system is coherent, it is possible for the phase distribution to evolve back to be single peaked and the revival is therefore strong evidence of coherence.

To quantify the phase revival, we look to the interference contrast

$$C(t) = \frac{\left|\langle \hat{a}^\dagger \hat{b}\rangle(t)\right|}{N/2} \tag{4.61}$$

which is the maximal visibility obtainable when averaging over many interference experiments. (Again: in a single experiment we can obtain perfect fringes, but if these are at random positions C will be zero.)

4.5.4 Calculating the contrast

The time-evolution of the contrast under U_{nl} can be calculated. It is convenient to work in the Heisenberg picture, i.e., to write

$$\hat{a}^\dagger(t)\hat{b}(t) = e^{i\chi\hat{n}^2 t/4}\hat{a}^\dagger \hat{b} e^{-i\chi\hat{n}^2 t/4}, \tag{4.62}$$

the average of which should then be taken in the phase state, (4.55). This is done by using the commutation relations in the form of "pull-through" tricks

$$\hat{a}^\dagger \hat{n}^{(a)} = \big(\hat{n}^{(a)} - 1\big)\hat{a}^\dagger \quad \text{and} \quad \hat{b}\hat{n}^{(b)} = \big(\hat{n}^{(b)} + 1\big)\hat{b}. \tag{4.63}$$

We find

$$\begin{aligned} C(t) =& \frac{2}{N}\left|\langle \phi; N| e^{-i\chi(\hat{n}+1)t}\hat{a}^\dagger \hat{b}|\ \phi; N\rangle\right| \\ =& \frac{2}{N}\left|e^{-i\chi t}\langle \theta - \chi t, N|\hat{a}^\dagger \hat{b}|\ \theta, N\rangle\right| \\ =& \left|\cos(\chi t)\right|^{N-1}. \end{aligned} \tag{4.64}$$

As expected, the phase revivals show up as peaks in the contrast and we shall use $C(t_{\mathrm{rev}})$ at the revival times as a measure of the coherence in the system.

4.5.5 Enemies of revivals

There are many decoherence effects that can prevent us from observing the perfect revivals predicted above.

Fluctuations from external sources

Any change in the relative energy of the modes will affect the phase between them (Sec. 4.1.3) and hence the fringe pattern will be shifted. If we can predict the shift it is harmless, if not the result will be a loss of contrast. As ultra-cold atomic gases can be very well isolated from the out-side world it would seem that these effects are not intrinsic and could be made arbitrarily small.

Losses

From the discussion in Sec. 2.5.3, it is intuitively clear that the phase revivals will be highly sensitive to losses as the system passes through a cat state at $t_{\text{cat}} = t_{\text{rev}}/2$: At this point, a clever measurement on the escaping particle can in principle reveal from which of the orthogonal states it came and will therefore collapse the whole system on the corresponding state.

In Ref. [120] Sinatra and Castin analyzed the effect of general m-body losses. Physically, $m = 1$ corresponds to background gas collisions, $m = 2$ describes spin-flip collisions, and $m = 3$ is the case of three-body collisions with molecule formation. The authors employed a Monte Carlo wavefunction method like the one of Sec. 2.5.2 and they showed that the effect on the phase revivals is an exponential damping of the signal:

$$C(t_q) = e^{-\lambda_m t_q} \tag{4.65}$$

where $t_q = q t_{\text{rev}}$ is the qth revival time and λ_m is the mean number of m-body loss events per unit time. Eq. (4.65) implies that we can only allow less than one loss event on average. Based on a consideration of realistic loss rates, Sinatra and Castin concluded that condensates with small numbers of atoms are the best candidates for observation of phase revivals.

Finite temperature

The two-mode picture above assumes that we can prepare the initial phase state starting from a pure single-mode condensate. In reality, we learned already in Chp. 2 that the Gross–Pitaevskii ansatz of all atoms in one mode is only an approximation: Even at $T = 0$ interactions will modify the state and at $T > 0$, thermal fluctuations will also be present. As phase revivals take place on a long time-scale they are particularly sensitive to such fluctuations. In the next section we shall use a simple toy-model to investigate the influence of noncondensed particles on the phase revivals of the condensate.

4.6 Toy-model for the effect of noncondensed particles[8]

As condensates with small numbers of atoms are our candidates for producing phase-revivals, we can at least dream of being in the very weakly interacting regime, where all excitations are particle-like, i.e., can be described by a Hartree–Fock ansatz like Eq. (2.13). Thermal fluctuations are then fluctuations of the populations in these excited single-particle states.

Inspired by the trick of Eq. (4.62) we write a Hamiltonian that we expect will allow us to still calculate the contrast analytically. In Sec. 4.6.4 below we will argue that this Hamiltonian describes the truly perturbative regime of ultra-cold, interacting gases, but for now, consider it simply a toy-model we can solve. If we ignore the linear part of the dynamics,[9] and if we for simplicity assume that there are no interactions between atoms in mode a and in mode b, our Hamiltonian reads

$$\begin{aligned}\hat{H}_{nn} =& \hat{H}^{(a)}_{nn} + \hat{H}^{(b)}_{nn} \\ =& \frac{1}{2}\sum_j \hbar K^{(a)}_{jj} \hat{n}^{(a)}_j (\hat{n}^{(a)}_j - 1) + \sum_{j\neq k} \hbar K^{(a)}_{jk} \hat{n}^{(a)}_j \hat{n}^{(a)}_k \\ &+ \; a \leftrightarrow b.\end{aligned} \tag{4.66}$$

The $\hat{n}^{(a)}_j$ and $\hat{n}^{(b)}_j$ are number operators for the trap levels. As $\hat{H}_{nn}$ commutes with all of them, it conserves the population in each trap level. The dynamics consists entirely of densities interacting

[8] The work in this section was mainly done in cooperation with Yvan Castin during my stay at Ecole Normal Supérieure in Paris.

[9] The influence of linear terms on phase revivals is trivial, but will need to be included below when we seek to determine actual thermal populations of the excited levels.

with densities. The K_{jk}'s quantify the strength of the coupling and "typical" values are discussed in Sec. 4.6.5.

4.6.1 Calculation of contrast under $\hat{H}_{nn}$

Working in the Heisenberg picture we need to evaluate

$$\hat{a}_j^\dagger(t) = e^{i\hat{H}_{nn}t/\hbar}\hat{a}_j^\dagger e^{-i\hat{H}_{nn}t/\hbar}. \tag{4.67}$$

We employ Eq. (4.62) to write

$$\hat{a}_j^\dagger \hat{H}_{nn}^{(a)} = \hat{H}_{nn}^{(a)}\Big|_{\hat{n}_j^{(a)}\to\hat{n}_j^{(a)}-1}\ \hat{a}_j^\dagger, \tag{4.68}$$

and we find

$$\hat{a}_j^\dagger(t) = \exp\Big\{i\Big[K_{jj}^{(a)}(\hat{n}_j^{(a)}-1) + 2\sum_{k\neq j} K_{jk}^{(a)}\hat{n}_k^{(a)}\Big]t\Big\}\hat{a}_j. \tag{4.69}$$

In a completely analogous way $\hat{b}_j(t)$ can be calculated, and we thus have

$$\begin{aligned}\hat{a}_j^\dagger(t)\hat{b}_j(t) = \exp\Big\{-iK_{jj}^{(a)}t\Big\}\exp\Big\{-i\Big[\tilde{\chi}_j\hat{N}_j + \sum_{k\neq j}\tilde{\kappa}_{jk}\hat{N}_k\Big]t\Big\}\\ \times\exp\Big\{-i\Big[\chi_j\hat{n}_j + \sum_{k\neq j}\kappa_{jk}\hat{n}_k\Big]t\Big\}\hat{a}_j^\dagger\hat{b}_j,\end{aligned} \tag{4.70}$$

where we have defined

$$\begin{aligned}\chi_j &\equiv \frac{1}{2}\left(K_{jj}^{(b)} + K_{jj}^{(a)}\right) \qquad & \tilde{\chi}_j &\equiv \frac{1}{2}\left(K_{jj}^{(b)} - K_{jj}^{(a)}\right)\\ \kappa_{jk} &\equiv K_{jk}^{(b)} + K_{jk}^{(a)} \qquad & \tilde{\kappa}_{jk} &\equiv K_{jk}^{(b)} - K_{jk}^{(a)},\end{aligned} \tag{4.71}$$

and

$$\hat{N}_j \equiv \hat{n}_j^{(b)} + \hat{n}_j^{(a)} \qquad \hat{n}_j \equiv \hat{n}_j^{(b)} - \hat{n}_j^{(a)}. \tag{4.72}$$

In a perfectly symmetric situation, the quantities defined in the second column of Eq. (4.71) all vanish, and thus the second exponential in Eq. (4.70) is simply equal to 1. In the following we will for simplicity assume this to be the case, and we drop the (a) and (b) superscripts.

4.6.2 Arbitrary distribution on excited levels

With Eq. (4.70) we can easily calculate $\langle\hat{a}_j^\dagger\hat{b}_j\rangle$ directly from an initial state where all levels are in phase states. This is not an unnatural starting point: The splitting of the condensate into a superposition of mode a and b could very well have the same effect on the noncondensed particles. To be specific, assume that we before the splitting have a given distribution, $(N_j)_{j\in\mathbb{N}}$, of particles in the mode a levels. The splitting is now assumed to put each atom in a superposition of mode a and mode b, but in such a way that the level index is retained, i.e., after the pulse N_j particles are in a superposition of being in mode a level j and in mode b level j. The system is in a many-mode phase state,

$$|\phi;(N_j)\rangle = \prod_j \frac{1}{\sqrt{2_j^N N_j!}}\left(b_j^\dagger e^{i\theta} + a_j^\dagger e^{-i\theta}\right)^{N_j}|\text{vac}\rangle. \tag{4.73}$$

Proceeding exactly as in the one mode case (Sec. 4.5.3) we get

$$\langle\hat{a}_j^\dagger\hat{b}_j\rangle = e^{-2i\theta}\frac{N_j}{2}\left[\cos(\chi_j t)\right]^{N_j-1}\prod_{k\neq j}\left[\cos(\kappa_{jk}t)\right]^{N_k}. \tag{4.74}$$

This is a somewhat discouraging formula for efforts to observe the phase-revivals: Even if we could prepare almost all particles in, say, level 0, the contrast will be reduced due to interactions with the remaining particles in other levels. Note that Eq. (4.74) is for a fixed distribution of particles. The loss of coherence is thus caused directly by the entanglement of the different levels, no thermal fluctuations of particle numbers are needed. Another interesting feature revealed by Eq. (4.74) is the "separability revivals" between modes j and k at times where $t = q2\pi/\kappa_{jk}$, $q = 1, 2, \ldots$. At these times, the k'th mode has no influence on the contrast observable in the j'th mode.

4.6.3 Canonical ensemble in simple Bogoliubov approximation

It is of course not realistic that we should know exactly the distribution (N_j): we must average Eq. (4.74) over some probability law, $P(N_j)$. A reasonable choice would be to use the canonical ensemble at some temperature $T > 0$, Eq. (2.33). As even a moderate number of excited particles will kill phase revivals, we focus on situations where $N_0 \sim N$. Then a simple Bogoliubov-like approach is justified: Write $\hat{N}_0 = N - \sum_j \hat{N}_j$ and linearize the Hamiltonian in the number of excited atoms. At this point we should put in some "bare" level energies, $\hbar\nu_j$, in addition to the nonlinear part of the evolution described by $\hat{H}_{nn}$: These were left out above as they have a trivial influence on the phase dynamics, but they are of course essential for the thermal distribution. All in all we have[10]

$$\begin{aligned}\hat{H}_{\text{lin}} &= \hbar\nu_0 N + \frac{1}{2}K_{00}N(N-1) \\ &\quad + \sum_{j>0}\Big(\hbar\nu_j - \hbar\nu_0 + 2\hbar N K_{0j} - \hbar N K_{00}\Big)\hat{N}_j \\ &= E(N) + \sum_{j>0}\tilde{\nu}_j\hat{N}_j,\end{aligned} \tag{4.75}$$

where $E(N)$ is an irrelevant constant for given N and the $\tilde{\nu}_j$ serve as effective energies. We can perform the average of Eq. (4.74) analytically if we make the further assumption that the N_j for $j > 0$ can be treated as independent variables which can take on all integer values from 0 to ∞. This is means that we are in effect doing a grand canonical calculation with the condensate acting as a particle reservoir, an approximation which is only good when the probability of $\sum_{j>0} N_j > N$ is negligible. Close enough to the revival times so that $e^{-\beta\tilde{\nu}_j}/|\cos(\chi_0 t)| < 1$ for all j, we then get:[11]

$$C(t) \cong |\cos(\chi_0 t)|^{N-1}\prod_{j>0}\frac{1-e^{-\beta\tilde{\nu}_j}}{\left|1-e^{-\beta\tilde{\nu}_j}\frac{\cos(\kappa_{0j}t)}{\cos(\chi_0 t)}\right|}. \tag{4.76}$$

For low numbers of atoms where the grand canonical approximation cannot be used, the average must instead be perform numerically, a quite manageable task if necessary. In Fig. 4.8 we show $C(t)$ for a number of temperatures using "typical" values of the parameters found in Sec. 4.6.5.

4.6.4 Physical relevance of toy-model

At first sight, $\hat{H}_{nn}$ of Eq. (4.66) seems a very strange approximation for describing a real situation with atoms in a trap, much different than anything we encountered in the introductory Chp. 2. Consider, however, the truly perturbative regime, i.e., the regime where the mean field energy is much smaller than the typical trap level spacing,

$$\frac{gN}{\Delta\hbar\nu V} \ll 1. \tag{4.77}$$

Here g is the interaction strength of Eq. (2.4), N is the number of particles, V is a measure of the volume of the trap, and $\Delta\hbar\nu$ is the typical level spacing. In the regime of (4.77), the trap levels

[10] Remember, initially all atoms are in mode a and therefore only $\hat{H}_{nn}^{(a)}$ with $\hat{n}_j^{(a)} \to \hat{N}_j$ is relevant.

[11] We also put the $N_0/2$ appearing in Eq. (4.74) for $j = 0$ equal to $N/2$.

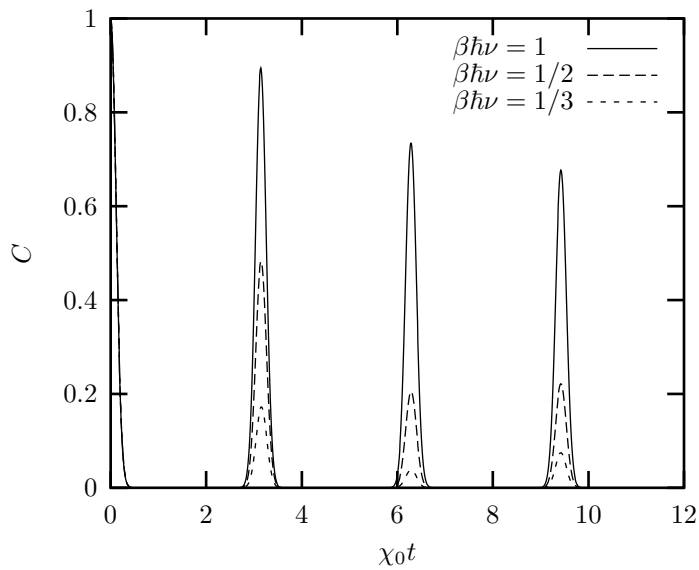

Figure 4.8: Contrast as a function of scaled time, $\chi_0 t$, for three different temperatures. The total number of atoms is $N = 80$ and the bare trap level spacing $\hbar\nu = 1.6 \times 10^4 \hbar\omega$. We have used the simple harmonic trap estimates of Sec. 4.6.5 for coupling strengths while the trap level energies are adjusted according to Eq. (4.75) before calculating the populations. The three temperatures corresponds to averages of approximately 0.8, 2.8, and 5.4 excited atoms.

are relevant also in a many-body situation as resonance criteria apply for the possible scattering processes. For a harmonic trap, lots of processes changing the populations of the trap levels are still possible because of the equidistant energies, but one could imagine a scenario where effectively, the populations are frozen on a time-scale longer than the one given by $V/g\hbar$. Then $\hat{H}_{nn}$ would be a reasonable approximation for the nonlinear part of the Hamiltonian.

4.6.5 Typical parameter values

If we denote the j'th trap-level wavefunction by ϕ_j, the first approximation to the interaction parameters of $\hat{H}_{nn}$ would be the generalization of the $\hat{S}_z^2$ coefficient, χ, we have used in previous sections [see Eqs. (4.19) and (4.37)],

$$\hbar K_{jk} = g \int \left|\phi_j(\mathbf{r})\right|^2 \left|\phi_k(\mathbf{r})\right|^2 d^3\mathbf{r}. \tag{4.78}$$

Even though we assume to be in the very weakly interacting regime, we should take the ϕ_j's as Hartree–Fock eigenstates, see Eq. (2.15) and the accompanying footnote 2. In particular, the macroscopically populated ϕ_0 should solve the GPE. Then, by the kinematic argument of Sec. 2.7.2, we have eliminated processes involving 3 condensate particles. This is important as the condition to neglect these processes is even stronger than Eq. (4.77).

In addition to using Hartree–Fock single-particle states in Eq. (4.78), we should expect some corrections on the K_{jk}'s from the neglected, nonresonant scattering processes. To get an estimate of the values we can, however, simply use bare eigenstates of a harmonic trap $\phi_j^{\text{h.o.}}$. The most important quantities are the couplings of involving the ground state. If we assume a 1D configuration, the relevant integrals are:

$$\int \left[\phi_j^{\text{h.o.}}(x)\phi_0^{\text{h.o.}}(x)\right]^2 dx = \frac{1}{\sqrt{2\pi}a_0}\frac{\Gamma(j+\frac{1}{2})}{\sqrt{\pi}j!}. \tag{4.79}$$

From this we find the values used in Fig. 4.8,

$$\frac{\kappa_{0j}}{\chi_0} = \frac{2\Gamma(j+1/2)}{\sqrt{\pi}j!}. \tag{4.80}$$

4.6.6 Discussion

The main result of our study is that under the nonlinear many-mode Hamiltonian $\hat{H}_{nn}$ we can still calculate the evolution of some important observables analytically. This can be used when we expect $\hat{H}_{nn}$ to give a good description of the dynamics: here Eq. (4.74) gives in a transparent manner the influence of the noncondensed particles on the contrast, but in general, $\hat{H}_{nn}$ can be useful as a testing ground for various simulation schemes [121].

When applied to real physical systems, the justification for the toy-model Hamiltonian, $\hat{H}_{nn}$, offered in Sec. 4.6.4 and Sec. 4.6.5 should be made more precise. We have done some work towards this end by using second order perturbation theory on the terms declared nonresonant. Keeping track of all possible contributions is extremely tedious and probably not very illuminating so we have chosen not to present the calculations here. In the work done so far, it has been possible to include all nonnegligible contributions in small adjustments of the K_{jk}'s.

Another approach to checking the predictions of $\hat{H}_{nn}$ is to implement thermal fluctuations in a propagation of GPE solutions in each Fock space of the expansion (4.58). The method of treating each Fock state independently and with a Gross–Pitaevskii approximation was introduced in Ref. [90] and as mentioned in Sec. 4.2, it was used by Sørensen *et al.* in their work on spin squeezing in two-component BECs [85]. When thermal fluctuations were included in the initial condensate wavefunction, we obtained good agreement with the results of Fig. 4.8, but more work still remains to be done.

Finally, another unfinished aspect of our study is the "size" of the Schrödinger cat when a noncondensed cloud is present. Just as the contrast of the phase revivals goes down, so must every reasonable measure of the quality of the cat states. Exactly what the right measure should be is an interesting subject for further study.

Chapter 5

Dissociation of a molecular BEC

The analogy between a BEC and the properties of a laser is often emphasized.[1] Indeed, seeking inspiration in quantum optics can prove fruitful. In Sec. 4.4, where we discussed the production of squeezed light from a spin squeezed condensate, we briefly mentioned that one of the traditional ways of producing squeezed light and entangled light beams is downconversion in nonlinear crystals. In this process, one photon is split in two with interesting correlations as a result. In this chapter, we present our analysis [1, 2] of the corresponding process in BEC physics: The dissociation of a molecular condensate.

We start with a brief introduction to molecules in connection with BEC (Sec. 5.1), before we go into detail with dissociation: In Sec. 5.2 we introduce the simplified model we have used, in Sec. 5.3 we derive the equations to be solved, and in Sec. 5.4 we show the numerical results. To illustrate the special properties of the created state we devote Sec. 5.5 to a particular experiment. In Sec. 5.6 we report on some extensions of our simplified model and in Sec. 5.7 we conclude.

5.1 Introduction to molecules in BEC

One of the areas of BEC physics that has been receiving much attention lately is the production of a condensate of molecules. In principle, by cooling bosonic molecules to low enough temperatures one could create a condensate just as for atoms. Unfortunately, the laser cooling techniques that have so successfully been applied to atoms cannot be used with the same ease for molecules. This is because molecules in general lack a closed transition on which to do the cooling; the molecules would soon be distributed on a large number of rotational and vibrational levels and the cooling would cease to be effective. A more promising road to cold molecules is to produce them in a controlled manner from already cold atoms. Below we give brief introduction to *photoassociation* and *Feschbach resonances*.

5.1.1 Photoassociation of cold atoms

Photoassociation has already for some time been used as a spectroscopic method. The basic idea is to let the colliding atoms absorb a photon so that the collision complex is transfered to an excited bound state of the molecule. If the kinetic energy of the colliding atoms is very well known, the resonance frequency of the transition gives detailed information on the molecular potential curves and thus the method is particularly interesting for ultracold atomic samples [122, 123]. Left alone, the excited state will decay spontaneously, but by applying a second laser, it can be stimulated to emit at a particular frequency and thus end up in a particular bound state as illustrated in Fig. 5.1. Ideally, one would like the population of the excited state to remain very low to avoid any spontaneous emission. It has been proposed to use stimulated Raman adiabatic photoassociation (STIRAP) to achieve this goal [125] and this proposal has been shown to survive

[1] Perhaps most often as a reply to the dreaded "what is it good for" question.

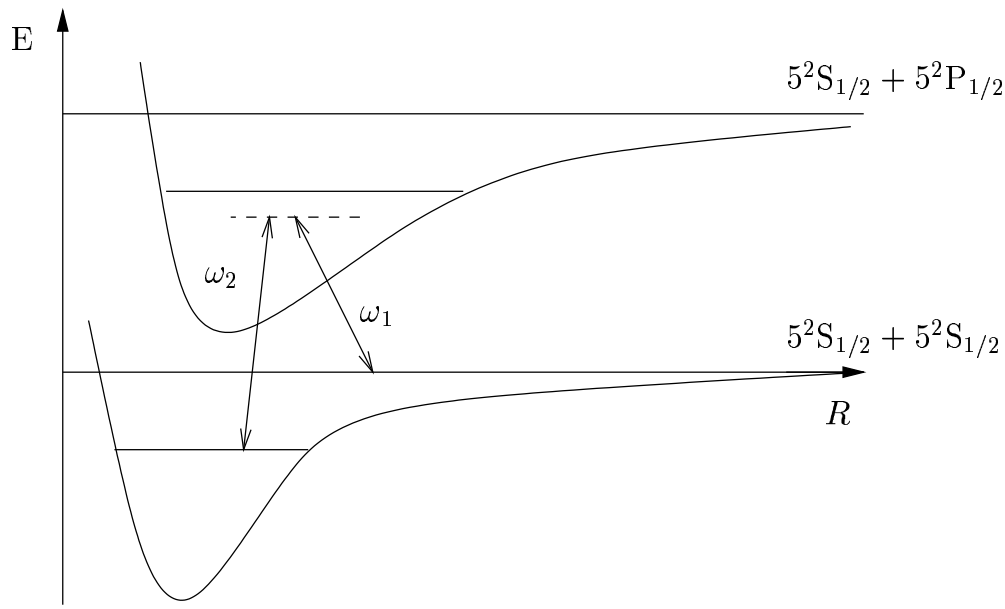

Figure 5.1: Stimulated Raman photoassociation. As an example, the states used in the ^{87}Rb experiment of Ref.[124] are used (but the figure is purely schematic). The two potential curves correspond to two different electronic states in the molecule. Each curve supports numerous bound vibrational and rotational levels and each has an associated continuum of free atoms. Initially, all atoms are free and in the $^2S_{1/2}$ state. Collisions take place, but as the gas is dilute, they are mainly binary and elastic: The waste majority is simply described by a scattering state belonging to the lower potential curve. If lasers at frequencies ω_1 and ω_2 are turned on, the colliding atoms can absorb an ω_1 photon and then be stimulated into emitting an ω_2 photon. In this way, the collision complex is transfered to a bound level in the molecules electronic ground state. The efficiency of the process depends on the detuning from the intermediate level on the excited curve and on wavefunction overlaps (Franck–Condon factors). Photodissociation by the inverse mechanism is of course equally possible. In fact, if laser are kept on for sufficiently long, one would expect to see some kind of Rabi oscillations between free atoms and molecules.

also in a multimode setting [126, 127]. Alternatively, at high one-photon detunings only the full two–photon process is resonant and we effectively have a coupling between free atoms and rather stable molecules [128]. In this way, Wynar *et al.* [124] were able to create extremely cold molecules in a BEC of ^{87}Rb atoms.

5.1.2 Feschbach resonances

Already in the introductory Chp. 2, we mentioned the possibility to tune the interaction strength in a condensate via a so called Feschbach resonance. Such resonances are close relatives of photoassociation and occur when a bound state is tuned into resonance with the colliding atoms. The bound state has a different spin arrangement and so the tuning is done by varying the strength of an applied homogeneous magnetic field. In a semiclassical picture, two atoms collide and while they are close, the hyperfine interaction can flip the spins in one of them. The created molecular state will decay by another spin flip and the two atoms move apart. From the atoms perspective, the presence of the resonance will have a violent effect on the atom–atom interaction strength, but if the intermediate molecular state is long–lived it should in fact be treated as a component of the system in its own right [13, 129]. Just as for photoassociation we get a coupling turning atoms into molecules and *vice versa*.

5.1.3 Atom–molecule oscillations

As both far–detuned photoassociation and longlived Feschbach resonances can be described as a coupling between an atomic component and a molecular component, we simply introduce a new term in the Hamiltonian [130, 131, 132, 129],

$$\int d^3\mathbf{r}\ \chi_{\rm am}(\mathbf{r})\hat{\psi}_m^\dagger(\mathbf{r})\hat{\psi}_a(\mathbf{r})\hat{\psi}_a(\mathbf{r}) + \text{h.c.}. \tag{5.1}$$

The strength parameter, $\chi_{\rm am}$, can in both cases be tuned: For photoassociation by varying laser intensities and detunings, for Feschbach resonances by varying the applied magnetic field. $\chi_{\rm am}$ need not be spatially uniform.

A Hamiltonian like (5.1) is well known from nonlinear optics where it describes second–harmonic generation and downconversion, i.e., the conversion of two photons at frequency ω to one at 2ω and *vice versa*. Starting from a state with only atoms present, it will create a molecular component. How large a fraction of the atoms that will be converted is a complicated question. In the simplest approximation with only two modes and ignoring all other interactions, an analytical solution shows a perfect conversion to molecules after which the populations freeze [133]. When including many modes or fluctuations, an oscillatory behaviour is expected [133, 134, 129, 135]. Very recently, the first experimental evidence for such oscillations has appeared [136].

5.2 A model focussed on photodissociation

It is of course a matter of taste, but one could argue that the most interesting point of atom–molecule oscillations is when (if ever) the system consist entirely of molecules. In a one mode model, quantum effects (spontaneous dissociation) are needed to get the past this point. To focus on these effects in a clearcut manner, we will assume that we have a molecular condensate at our disposal. Whether it is obtained by perfect atom–molecule conversion, by removal of the atomic component in a less ideal experiment, or by some purely molecular scheme is not important.

5.2.1 The Hamiltonian

To describe the atomic component, we use the by now familiar second quantized Hamiltonian including atom–atom collisions, Eq. (2.29), and an equivalent of Eq. (5.1) to describe the dissociation. As we will focus on the initial stages of photo–dissociation, the molecules will be treated

semiclassically and in the undepleted pump approximation, i.e., as a time–independent c–number field. This approximation is good as long as the number of molecules is very much larger than the number of atoms.[2] We assume a harmonic trap of frequency ω for the atoms and we measure all quantities in the corresponding set of units: Time in units of ω^{-1}, lengths in units of $a_0 = \sqrt{\hbar/m\omega}$, and energy in units of $\hbar\omega$. In 1D we then have

$$\hat{H} = \int dx \left\{ \hat{\psi}^\dagger(x)\hat{h}\hat{\psi}(x) + \frac{g}{2}\hat{\psi}^\dagger(x)\hat{\psi}^\dagger(x)\hat{\psi}(x)\hat{\psi}(x) \right\} + \hat{H}_{\mathrm{PD}}, \tag{5.2}$$

where

$$\hat{h} = -\frac{1}{2}\frac{\partial^2}{\partial x^2} + \frac{1}{2}x^2, \tag{5.3}$$

and g is an appropriate 1D interaction strength [137]. The coupling Hamiltonian is

$$\hat{H}_{\mathrm{PD}} = \frac{1}{2}\int dx dx' \ \left\{ b(x,x',t)\hat{\psi}^\dagger(x)\hat{\psi}^\dagger(x') + b^*(x,x',t)\hat{\psi}(x)\hat{\psi}(x') \right\}. \tag{5.4}$$

Besides the semiclassical treatment of the molecular field, Eq. (5.4) differs from Eq. (5.1) in the use of a more general spatial dependence than the contact approximation. For the function b, we use the ansatz

$$b(x,x',t) = \frac{B}{2\pi\sigma_r\sigma_{cm}} \exp\left(-2i\Delta t\right) \exp\left(-\frac{1}{2}\frac{(x-x')^2}{\sigma_r^2}\right) \exp\left(-\frac{1}{2}\frac{(\frac{1}{2}(x+x'))^2}{\sigma_{cm}^2}\right), \tag{5.5}$$

where B denote the strength the photodissociation while 2Δ is the effective energy of the molecular level. Physically, the finite width, σ_r, describes the spatial separation of the products of a single molecular photodissociation. The scattering wave function of two atoms has a node at $r = a_s$, the scattering length, and for convenience we apply a simple Gaussian wavefunction for the atoms which localizes the amplitude to within $\sigma_r \cong a_s$. More formally, $\sigma_r > 0$ introduces a finite momentum cut-off in spontaneous dissociation [129, 127]. The product of the spatial field envelope and the molecular wavefunction is here taken to be a Gaussian of width σ_{cm}, corresponding to a weakly interacting molecular condensate in a homogeneous field or a uniform condensate in a Gaussian beam. The precise values applied in the model are not crucial, but realistically one would assume $\sigma_r \cong a_s \ll \sigma_{cm} \cong a_0$.

5.3 Equations of motion

5.3.1 Operator equations of motion

From the Hamiltonian (5.2) we can derive the Heisenberg equation of motion for the atomic field operator. It reads:

$$\begin{aligned} i\frac{\partial\hat{\psi}(x,t)}{\partial t} &= \left(-\frac{1}{2}\frac{\partial}{\partial x} + \frac{1}{2}x^2 + g\hat{\psi}^\dagger(x,t)\hat{\psi}(x,t)\right)\hat{\psi}(x,t) \\ &\quad + \int dx' \ b(x,x',t)\hat{\psi}^\dagger(x',t). \end{aligned} \tag{5.6}$$

The last term in this equation is due to the exchange of atom pairs with the molecular condensate.

Our motivation for focusing on the dissociation process was its inherent quantum nature. We would therefore not expect a semiclassical approximation like the Gross–Pitaevskii equation to be useful here. To verify this, we try to derive a GPE as in Sec. 2.1.2, i.e., we simply take the average

[2] In Sec. 5.6 we will comment on work without this constraint.

value of Eq. (5.6). Apart from the discomfort in using a mean field equation when initially no atoms are present, we notice that a more serious problem arises: We start in the atomic vacuum,

$$\hat{\psi}(x,0)|\text{vac}\rangle = 0, \tag{5.7}$$

and so the incoupling term on the right hand side has vanishing average value. Therefore $\langle\hat{\psi}(x,t)\rangle$ will stay zero also at all later times and no useful information can be extracted. Notice, that this problem is peculiar to processes, where two (or more) atoms are created simultaneously.

As no mean field will be created, we proceed to study expressions quadratic in the field operators. To shorten notation we define

$$\hat{R}(x,y,t) \equiv \hat{\psi}^\dagger(x,t)\hat{\psi}(y,t) \tag{5.8}$$

$$\hat{S}(x,y,t) \equiv \hat{\psi}(x,t)\hat{\psi}(y,t). \tag{5.9}$$

For these operators we get the following Heisenberg equations of motion:

$$\begin{aligned} i\frac{\partial\hat{R}(x,y,t)}{\partial t} &= \left(\frac{1}{2}\frac{\partial^2}{\partial x^2} - \frac{1}{2}x^2 - \frac{1}{2}\frac{\partial^2}{\partial y^2} + \frac{1}{2}y^2\right)\hat{R}(x,y,t) \\ &+ g\left(\hat{R}(y,y,t)\hat{R}(x,y,t) - \hat{R}(x,y,t)\hat{R}(x,x,t)\right) \\ &+ \int dz\ \left\{b(z,y,t)\hat{S}^\dagger(x,z,t) - b^*(x,z,t)\hat{S}(z,y,t)\right\} \end{aligned} \tag{5.10}$$

and

$$\begin{aligned} i\frac{\partial\hat{S}(x,y,t)}{\partial t} &= \left(-\frac{1}{2}\frac{\partial^2}{\partial x^2} + \frac{1}{2}x^2 - \frac{1}{2}\frac{\partial^2}{\partial y^2} + \frac{1}{2}y^2\right)\hat{S}(x,y,t) \\ &+ g\left(\delta(x-y) + \hat{R}(x,x,t) + \hat{R}(y,y,t)\right)\hat{S}(x,y,t) \\ &+ \int dz\ \left\{b(z,y,t)\hat{R}(z,x) + b(x,z,t)\hat{R}(z,y)\right\} + b(x,y,t). \end{aligned} \tag{5.11}$$

Note that $b(x,y,t)$ now appears as an inhomogeneous source term in the $\hat{S}$ equation. This term can be interpreted as spontaneous dissociation, and is what will get the process started.

5.3.2 c-number equations

The evolution of $\hat{R}$ and $\hat{S}$ cannot be found analytically. To make numerical progress, we need c–number equations. The simplest thing to do is to consider average values. We first ignore direct interactions among atoms.

Exact equations for $g = 0$

When $g = 0$, Eq. (5.10) and Eq. (5.11) are in fact linear. By taking averages, we immediately get two coupled, but closed, linear equations for the moments

$$R(x,y,t) \equiv \langle\hat{R}(x,y,t)\rangle \quad , \quad S(x,y,t) \equiv \langle\hat{S}(x,y,t)\rangle. \tag{5.12}$$

The equations read:

$$\begin{aligned} i\frac{\partial R(x,y,t)}{\partial t} &= \left(\frac{1}{2}\frac{\partial^2}{\partial x^2} - \frac{1}{2}x^2 - \frac{1}{2}\frac{\partial^2}{\partial y^2} + \frac{1}{2}y^2\right)R(x,y,t) \\ &+ \int dz\ \{b(z,y,t)S^*(x,z,t) - b^*(x,z,t)S(z,y,t)\} \end{aligned} \tag{5.13}$$

$$\begin{aligned} i\frac{\partial S(x,y,t)}{\partial t} &= \left(-\frac{1}{2}\frac{\partial^2}{\partial x^2} + \frac{1}{2}x^2 - \frac{1}{2}\frac{\partial^2}{\partial y^2} + \frac{1}{2}y^2\right)S(x,y,t) \\ &+ \int dz\ \{b(z,y,t)R(z,x) + b(x,z,t)R(z,y)\} \\ &+ b(x,y,t). \end{aligned} \tag{5.14}$$

A nice observation is that R and S in fact uniquely determine all higher order expectation values: they are simply calculated according to the vacuum version of Wicks theorem [138]. This can be seen in a number of ways. One is to note that the Wigner distribution is a multi-dimensional Gaussian distribution fully characterized by its second order moments [139, 23]. Another follows from the Heisenberg equation of motion (5.6) and is given in Appendix C.

Approximate equations for $g \neq 0$

When $g \neq 0$, we have to include the interaction term of Eqs. (5.10) and (5.11) in Eqs. (5.13) and (5.14). Unfortunately, in this case the Wick decomposition is no longer exact, and there is no simple way to reduce the mean values of four-operator products to products of R and S. If the state created by photodissociation was anything like a coherent state, a natural replacement would be, e.g., $\hat{R}(y,y)\hat{R}(x,y) \to S^*(x,y)S(y,y) + \delta(x-y)R(y,y)$, but this is probably not a good approximation here. We instead choose to apply the Wick prescription as this is correct to lowest order. We then get

$$\begin{aligned} g\left\langle \hat{R}(y,y,t)\hat{R}(x,y,t) - \hat{R}(x,y,t)\hat{R}(x,x,t)\right\rangle \to & \\ & g\left(S^*(x,y,t)S(y,y,t) - S(x,y,t)S^*(x,x,t)\right) \\ & + 2g\left(R(y,y,t) - R(x,x,t)\right)R(x,y,t) \end{aligned} \tag{5.15}$$

and

$$\begin{aligned} g\left\langle \left(\hat{R}(x,x,t) + \hat{R}(y,y,t) + \delta(x-y)\right)\hat{S}(x,y,t)\right\rangle \to & \\ & 2g\left(R(y,y,t) + R(x,x,t)\right)S(x,y,t) \\ & + g\left(R(x,y,t)S(x,x,t) + R^*(x,y,t)S(y,y,t)\right) \\ & + g\delta(x-y)S(x,y,t). \end{aligned} \tag{5.16}$$

These expressions are inserted into Eqs. (5.13) and (5.14), and we have arrived at the equations we want to solve numerically. We use a split-step approach where the kinetic energy is treated by a Fourier method. The remaining terms are dealt with by a fourth order Runge-Kutta scheme. In this one-dimensional problem the equations are quite manageable.

5.3.3 Positive P Langevin equations

To overcome the difficulties of including the interactions, we can resort to the positive P method. The new feature as compared to Chp. 3 is the photodissociation. The Langevin equations now read

$$\begin{aligned} id\psi_1(x) &= \left\{\hat{h}\psi_1(x) + g\psi_2(x)\psi_1(x)\psi_1(x)\right\}dt \\ &\quad + \left\{\int b(x,x')\psi_2(x')dx'\right\}dt + dW_1(x) \end{aligned} \tag{5.17}$$

$$\begin{aligned} -id\psi_2(x) &= \left\{\hat{h}\psi_2(x) + g\psi_1(x)\psi_2(x)\psi_2(x)\right\}dt \\ &\quad + \left\{\int b^*(x,x')\psi_1(x')dx'\right\}dt + dW_2(x) \end{aligned} \tag{5.18}$$

where $\hat{h}$ is still defined in Eq. (5.3) and the noise terms are Gaussian and given by

$$\overline{dW_{1,2}(x,t)} = 0, \tag{5.19}$$

$$\overline{dW_1(x,t)dW_2(x',t')} = 0, \tag{5.20}$$

$$\overline{dW_1(x,t)dW_1(x',t')} = idt\left[b(x,x',t) + g\psi_1(x,t)\delta(x-x')\right]\delta(t-t'), \tag{5.21}$$

$$\overline{dW_2(x,t)dW_2(x',t')} = -idt\left[b^*(x,x',t) + g\psi_1(x,t)\delta(x-x')\right]\delta(t-t'). \tag{5.22}$$

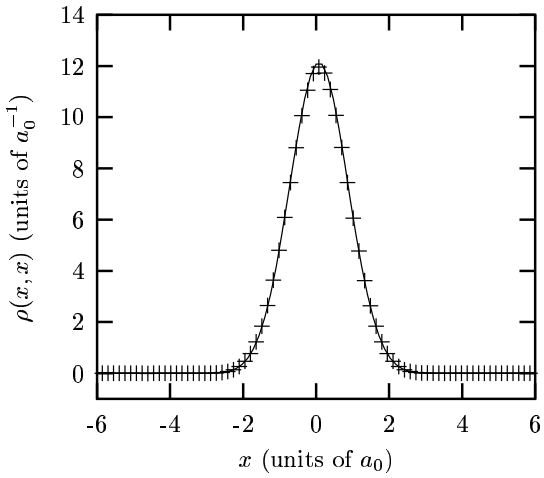

Figure 5.2: The density profile at time $\omega t = 2.4$ for interaction strength $g = 0.01\hbar\omega a_0$ and incoupling parameters $B = 3.0\hbar\omega a_0$, $\Delta = \omega$, $\sigma_{cm} = a_0$ and $\sigma_r = 0.2a_0$. The solid curve shows the results of the coupled R&S equations, the crosses are obtained with the positive P simulations.

In Appendix D we describe our procedure to synthesize these more complicated noise terms.

5.4 Results

In this section we show results for some of the quantities of interest that we are able to calculate in our model. Although the main new feature lies in the quantum correlations we first show a very classical quantity, namely the density profile. We then proceed to look at the eigenvalues of the one-particle density matrix. As described in Sec. 2.4.1, the largest of these eigenvalues defines the condensate fraction and the corresponding eigenvector is the condensate wavefunction. Finally we turn to a two-body quantity, the second order correlation function.

5.4.1 The density profile and the number of atoms

The atomic density is given by the diagonal elements of the one-body density operator in the position representation, that is

$$\rho_1(x,x) = \langle \hat{\psi}^\dagger(x)\hat{\psi}(x)\rangle = R(x,x) = \overline{\psi_2(x)\psi_1(x)}. \tag{5.23}$$

In Fig. 5.2 is shown a typical plot of this profile at $\omega t = 2.4$. It has the characteristic Gaussian shape of the harmonic oscillator ground state and as we shall see in Sec. 5.4.2, a large fraction of the atoms indeed occupy a common wavefunction close to this state. The R&S equations (5.13) and (5.14) with the interaction terms (5.15) and (5.16) give results in excellent agreement with the positive P simulations.

The total number of photo-dissociated atoms is obtained as the trace of the one-body density-operator or, according to Eq. (5.23), simply as

$$N = \int dx\, \rho_1(x,x). \tag{5.24}$$

In Fig. 5.3 this number is shown as a function of time for $g = 0$ and for $g = 0.01\hbar\omega a_0$. The agreement between the R&S equations and the positive P method is seen to be quite good.

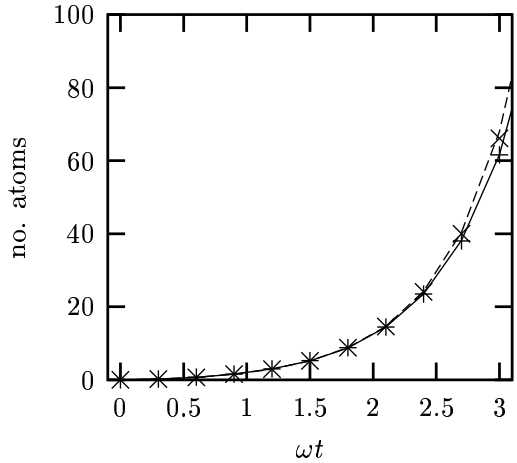

Figure 5.3: The number of photo-dissociated atoms as a function of time. The solid and dashed curves show the results of the R&S equations for $g = 0.00$ and $g = 0.01\hbar\omega a_0$ while the symbols + and $\times$ indicate the corresponding results of the positive P Langevin equations. Incoupling as in Fig.5.2.

5.4.2 The condensate fraction and wavefunction

In Fig. 5.4 we show the condensate fraction, i.e., the ratio of the largest eigenvalue of the one-body density matrix to the sum of the eigenvalues for different values of the interaction strength g. It is seen that as expected the condensate fraction is in general an increasing function of time. The effects of interactions are rather small at these low atom numbers. Note that unlike studies of stationary condensates at $T = 0$, where interactions are responsible for the breakdown of a simple product state ansatz for the system and the existence of atoms outside the condensate (see Sec. 2.7), the photodissociation by itself produces atoms both in the condensate and outside the condensate. This production of noncondensed atoms has been dubbed *rogue photodissociation* by Javanainen and Mackie [140] (see also Holland *et al.* [129]) In our calculations, the second-largest eigenvalue accounts for most of the atoms which are not in the condensate.

As for the condensate wavefunction we see an interesting phenomenon: Although the density profile associated with the condensed part of the one-body density matrix is close to that of the trap ground state, the condensate wavefunction is in fact not stationary. The atoms have condensed into a state more resembling a squeezed state[3] and if the incoupling is stopped the wavefunction widths show an oscillating behaviour. In Fig. 5.5 we show $\langle \hat{x}^2 \rangle$ and $\langle \hat{p}^2 \rangle$ of the condensate wavefunction as a function of time. We see that at $\omega t = 2.4$ when the incoupling is stopped, the wavefunction is too wide in momentum space as compared to the ground state of the trap ($\langle \hat{p}^2 \rangle > 1/2$).

One way to avoid this oscillation is to apply δ-kick cooling [141, 142] to the system. This procedure is efficient if there is a linear correlation between position and momentum. In the original suggestion the correlation between position and momentum is brought about by free expansion, but an examination of the condensate wavefunction shows that we have a similar correlation here. The idea is to apply a tight, harmonic trapping potential for a short time interval. If this interval is so short that any changes in position can be ignored, the effect is simply a momentum kick also varying linearly with position. Ideally, this kick brings all the particles to rest. In Fig. 5.5 we demonstrate that the procedure is effective in our problem. The results are shown for $g = 0$, but a similar reduction is achieved for nonvanishing g, except of course that a harmonic wavefunction will then not be stationary.

[3]This position-momentum squeezing should not be confused with the the atom-field squeezing discussed later.

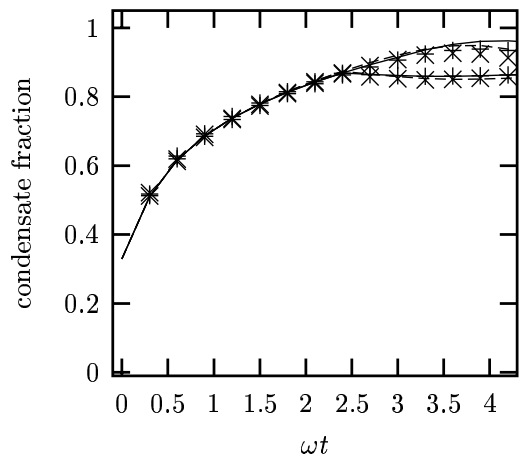

Figure 5.4: The condensate fraction, i.e., the ratio of the largest eigenvalue of the one-body density matrix to the total number of atoms (trace of the one-body density matrix). Solid and dashed curves shown the results of the R&S equations for $g = 0.01\hbar\omega a_0$ and for $g = 0.02\hbar\omega a_0$. The corresponding results of the positive P simulations are indicated by the symbols + and $\times$. The lower sets of data with the same symbols show the results when the incoupling is stopped at $\omega t = 2.4$.

5.4.3 The second order correlation function $g^{(2)}(x, y)$

More detailed information about the quantum state of the system is desired and available, and a natural quantity to consider is the second order correlation function $g^{(2)}$, introduced in Sec. 2.4.2. As $g^{(2)}$ involves the expectation value of a product of four field operators we are faced with similar factorization problem as when we derived the R&S equations. Again we will resort to the Wick prescription although it should be realized that this is only exact for states obtained with $g = 0$. The enumerator of Eq. (2.38) is evaluated in terms of R and S in Appendix C. We end up with

$$g^{(2)}(x, y) = 1 + \frac{|R(x, y)|^2 + |S(x, y)|^2}{R(x, x)R(y, y)}. \tag{5.25}$$

In contrast with the R&S equations, the positive P method has no problems handling 4–operator expectation values and $g^{(2)}$ can be determined exactly up to sampling errors. At relatively short times and low atom numbers we have therefore an excellent tool to obtain exact results even for $g \neq 0$.

In Fig. 5.6 we show a plot of $g^{(2)}(0, 0)$ as a function of time for various values of g. The central value slightly above 3 indicates a strong bunching effect where two atoms are more likely to be found close together than in a coherent or a thermal state. This result can be compared with the analytical expression for a single mode squeezed state, generated by the Hamiltonian $\beta\left(\hat{a}^2 + \hat{a}^{\dagger 2}\right)$:

$$g^{(2)} = \frac{\langle \hat{a}^\dagger \hat{a}^\dagger \hat{a}\hat{a} \rangle}{\langle \hat{a}^\dagger \hat{a} \rangle^2} = 3 + \frac{1}{\langle \hat{a}^\dagger \hat{a} \rangle} \tag{5.26}$$

In the figure we plot both results of the R&S equations using Eq. (5.25) and the exact positive P results. Good agreement is found between the two approaches until $\omega t \cong 2.5$ and hereafter the R&S equations fail to capture a decrease in the value of $g^{(2)}$. This decrease indicates a threshold effect that we will discus in the next section.

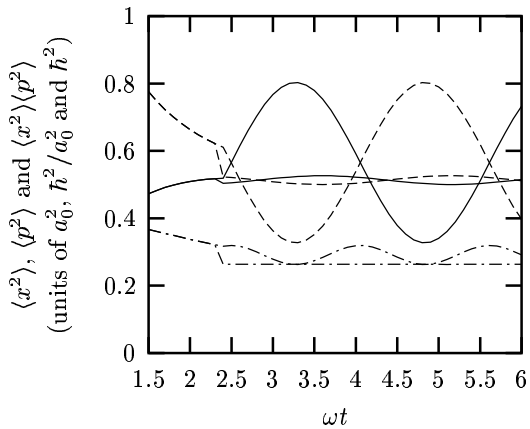

Figure 5.5: The freely evolving expectation values of $\langle x^2\rangle$ (solid curve) and $\langle p^2\rangle$ (dashed curve) are compared to the results obtained after application of a δ-kick to match the wavefunction with the ground state in the trap. If we apply a properly chosen kick just as we stop the incoupling at $\omega t = 2.4$ the oscillations can be almost completely removed. The dash-dotted curves show the product $\langle x^2\rangle\langle p^2\rangle$ in the two cases.

5.4.4 Threshold effect

In the semiclassical treatments of the laser and of the parametric oscillator, one identifies a threshold in the stationary balance between gain and loss; the fields shift from fluctuations around zero to fluctuations around finite intensities [143, 144]. Above threshold these optical systems have smaller relative fluctuations of the intensity, and it is natural to expect a similar threshold behaviour in our model. There is a seemingly important difference between our model and the optical systems in the fact that we do not have an explicit dissipative mechanism. It has been known for a long time, and it has been demonstrated explicitly for a large number of physical systems, however, that quite generically, the interactions in many-body systems lead to ergodicity of eigenstates and a dynamical relaxation without coupling to an external bath. For a recent review, see [145].

The R&S equations with their underlying assumption of a Gaussian Wigner distribution, centered around vanishing atomic field, are clearly unable to describe correctly the system around and above threshold, but the positive P simulations are exact, and the discrepancy between the two methods is thus most likely explained by a threshold effect. To investigate more closely the threshold hypothesis, we show in Fig. 5.7 scatter plots of $\psi_2(0)\psi_1(0)$ at $\omega t = 2.4$, 3.0 and 3.6 for a situation with $g = 0.02\hbar\omega a_0$. From photodetection theory we can deduce the following expression for the atom number distribution

$$P_n(t) = \overline{\frac{[\int \psi_2(x,t)\psi_1(x,t)dx]^n}{n!} \exp\left(-\int \psi_2(x,t)\psi_1(x,t)dx\right)}. \tag{5.27}$$

This expression, however, exhausts the statistical precision of the positive P method, since it involves higher moments of the simulated amplitudes, which yield larger and larger fluctuations. Instead, we heuristically present histograms in the figures of how the real parts, $\mathrm{Re}(\psi_2(0)\psi_1(0))$ are distributed, and these histograms are in good qualitative agreement with our picture of a bifurcation of the solution when we reach threshold in the process. It is seen how the distribution at $\omega t = 2.4$ is strongly peaked at zero with an exponential tail along the the real axis. At $\omega t = 3.0$ this tail extends to larger values, and a shoulder around 120 atoms/a_0 starts to appear, and at $\omega t = 3.6$ a second maximum has developed. This explains the lowering of $g^{(2)}$ seen in Fig. 5.6.

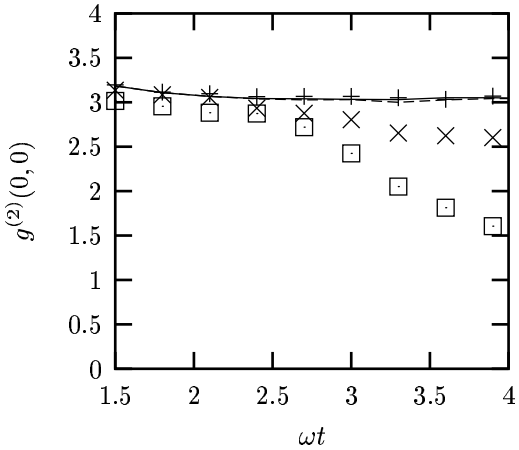

Figure 5.6: The second order correlation function $g^{(2)}(x, y)$ evaluated at $y = x = 0$ as a function of time. The solid and dashed lines show the results of the R&S equations for $g = 0$ (exact) and $g = 0.02\hbar\omega a_0$. The symbols + and × show the results of the positive P simulations with $g = 0.00$ and $g = 0.02\hbar\omega a_0$. The photo-dissociation stops at $\omega t = 2.4$. For $g \neq 0$, here is a strong discrepancy between the results of the R&S equations and the positive P simulations at times beyond $\omega t = 2.5$. The effect is clearly dependent on the interaction. The symbol ⊡ show positive P results obtained when $g = 0.02\hbar\omega a_0$, and when the photodissociation is not interrupted.

5.5 Application of a squeezed condensate

In Sec. 4.3 we presented a realistic quantum beam splitter, capable of splitting a condensate in two parts with almost perfectly matched numbers of atoms. In this section, we use the state created in the photodissociation model to achieve the same goal. Whereas the spin squeezing proposal is in principle close to experimental implementation, splitting atomic condensates will hardly have high priority when initially studying molecular condensates. Nevertheless, to detect the squeezing produced by photodissociation, this technique could be useful. By going through the calculation, we also get a spectacular demonstration of what can be done with even a very small sample of atoms produced by photodissociation.

The proposal is in direct analogy with homodyne detection of a *squeezed vacuum* in quantum optics. In such experiments, a weak quantum field is mixed with a strong field on a beam splitter and by varying the phase of the strong field, we obtain information on the fluctuations by simple photoncounting. A more constructive view on the same experiment is as a special splitting of the strong beam [146]: A beam is never just split, by unitarity it is always mixed with another mode of the light field, and by replacing the ordinary vacuum in the "empty" input mode with a squeezed state we may control the statistical properties of the daughter beams.

5.5.1 Matter wave beam-splitter with squeezed input

In the Bragg interferometer (Sec. 4.3.1), we already saw how the application of two suitably chosen laser beams can constitute a matter wave beam splitter. The input and output arms were different momentum states. We can, however, just as well use two different internal states as in Sec. 4.2. The beam splitter will then be a laser or RF pulse. Without referring to the concrete physical realization, we the denote the coupled states a and b, and a 50/50 beam splitter ($\pi/2$–pulse) will

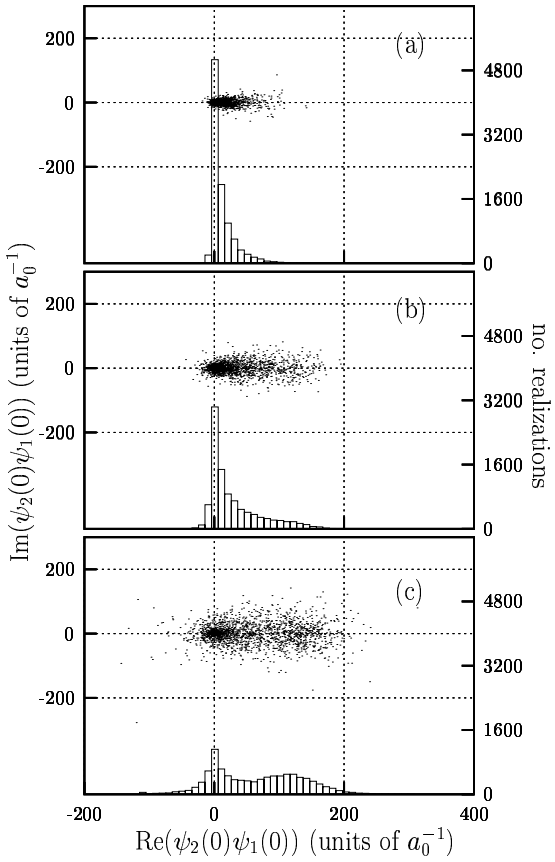

Figure 5.7: Scatter plots of $\psi_2(0)\psi_1(0)$ from the positive P realizations for $\omega t = 2.4$ (a), $\omega t = 3.0$ (b), and $\omega t = 3.6$ (c). The average of this quantity is $\langle \hat{\psi}^\dagger(0)\hat{\psi}(0)\rangle$, the central density in the trap and higher order, normally ordered, moments $\langle \hat{\psi}^{\dagger n}\hat{\psi}^n\rangle$ are similar averages $\overline{(\psi_2(0)\psi_1(0))^n}$. For clarity, we show in the bottom of the plots histograms of Re($\psi_2(0)\psi_1(0)$). It is seen how the character of the state changes with time as a second maximum in the distribution develops at a value different from zero.

in the Heisenberg picture imply

$$\hat{\psi}_a \quad \rightarrow \quad \hat{\psi}'_a = \frac{1}{\sqrt{2}}\left(\hat{\psi}_a + \hat{\psi}_b\right) \tag{5.28}$$

$$\hat{\psi}_b \quad \rightarrow \quad \hat{\psi}'_b = \frac{1}{\sqrt{2}}\left(\hat{\psi}_a - \hat{\psi}_b\right). \tag{5.29}$$

The total number operators of atoms in state a and state b after the splitting are thus given by

$$\begin{aligned}\hat{N}'_a &= \int dx \hat{\psi}'^{\dagger}_a(x)\hat{\psi}'_a(x) \\ &= \frac{1}{2}\hat{N}_a + \frac{1}{2}\hat{N}_b + \frac{1}{2}\int dx \left\{\hat{\psi}^{\dagger}_a(x)\hat{\psi}_b(x) + \hat{\psi}^{\dagger}_b(x)\hat{\psi}_a(x)\right\}\end{aligned} \tag{5.30}$$

$$\begin{aligned}\hat{N}'_b &= \int dx \hat{\psi}'^{\dagger}_b(x)\hat{\psi}'_b(x) \\ &= \frac{1}{2}\hat{N}_a + \frac{1}{2}\hat{N}_b - \frac{1}{2}\int dx \left\{\hat{\psi}^{\dagger}_a(x)\hat{\psi}_b(x) + \hat{\psi}^{\dagger}_b(x)\hat{\psi}_a(x)\right\}.\end{aligned} \tag{5.31}$$

We will now concentrate on the *difference* in the number of atoms in the two states,

$$\hat{N}'_a - \hat{N}'_b \quad = \quad \int dx \left\{\hat{\psi}^{\dagger}_a(x)\hat{\psi}_b(x) + \hat{\psi}^{\dagger}_b(x)\hat{\psi}_a(x)\right\}. \tag{5.32}$$

We will also let $\hat{\psi}_a$ initially describe a large condensate while $\hat{\psi}_b$ describes our photodissociated state. That is, we assume that the photodissociation is to the internal state b, while at the time of the $\pi/2$-pulse these atoms are overlapped with a large normal condensate in the internal state a. The large condensate is assumed to be in a coherent state with a definite phase, $|e^{i\theta}\psi_a\rangle$, with ψ_a real. The mean number of atoms in the large condensate is given by

$$N_a = \langle \hat{N}_a \rangle = \int dx\ \psi_a^2(x). \tag{5.33}$$

Using Eq. (5.32) we find

$$\left\langle \hat{N}'_a - \hat{N}'_b \right\rangle = 0 \tag{5.34}$$

and

$$\left\langle \left(\hat{N}'_a - \hat{N}'_b\right)^2 \right\rangle = N_a + N_b + \iint dxdy\ \psi_a(x)\psi_a(y)\mathrm{Re}\left[R_b(x,y,) + e^{-2i\theta}S_b(x,y,)\right]. \tag{5.35}$$

Ordinary vacuum in the b-state is the special case with $S_b = R_b = N_b = 0$ and we note that the typical imbalance of populations is $\sqrt{\mathrm{Var}(N'_a - N'_b)} = \sqrt{N_a}$. Now we use the nontrivial state created by photodissociation as squeezed vacuum. We imagine to have experimental control over θ and choose this phase optimally in order to reduce $\mathrm{Var}(N'_a - N'_b)$. In Fig. 5.8 we plot this minimum value of $\mathrm{Var}(N'_a - N'_b)/N_a$ as a function of the time of production of the squeezed condensate. It is clearly seen how the noise is rather quickly suppressed almost perfectly. In the particular case shown N_a was taken to be 10^3 and ψ_a was of Gaussian shape. The time-dependent number of atoms in the b-condensate can be approximately read out of Fig. 5.3. The width of ψ_a was chosen to be the same as the equilibrium width of the b-state atoms. It is amazing, but of course already well–known in quantum optics, that this suppression can take place even though the number of atoms initially in the b-state is very small compared to the average number of atoms in the large condensate in the a-state.

5.5.2 Limits to the squeezing

At times beyond $\omega t \cong 2$ the noise suppression is lost in the exact positive P simulations. We recall that for $g = 0$, the R&S equations are also exact, and it is thus natural to ascribe the

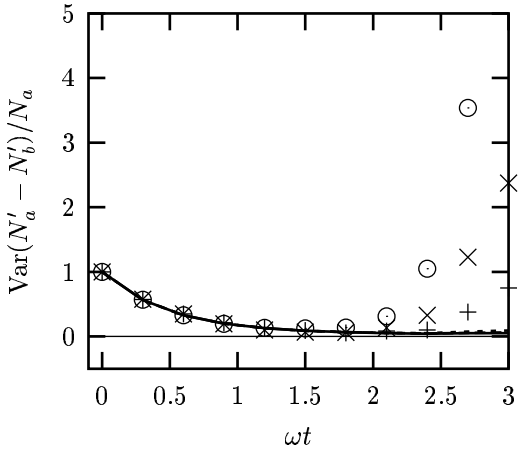

Figure 5.8: The minimum value of $\mathrm{Var}(N'_a - N'_b)/N_a$ as a function of the time of application of the $\pi/2$-pulse. All data are for a situation where incoupling is stopped at $\omega t = 2.4$. Calculations were done with three different interaction strengths ($g = 0.005$, 0.01 and $0.02\hbar\omega a_0$) and the almost overlapping lines (solid, dashed and dotted) show the results of R&S equations while the symbols ($+$, $\times$ and $\odot$) show the results of the positive P simulations.

discrepancy between the two methods to the interactions, which, by analogy with the Kerr-effect in optics, cause a deformation of the Gaussian state [147]. In Fig. 5.9 we show a scatter plot of the amplitudes of the projections, ψ_{1a}, of 3000 positive P realizations of ψ_1 on ψ_a at $\omega t = 2.4$ for $g = 0$ and for $g = 0.02\hbar\omega a_0$. Such plots should be interpreted with care, as in general the *pair* (ψ_1, ψ_2) is needed to calculate all normal-ordered expectations. The Kerr-effect, however, influences the S-function, and to calculate $\langle\hat{\psi}^2\rangle$ we only need to average ψ_1^2. In our case the relevant contributions to this average can thus be depicted by a scatter plot of ψ_{1a} alone.

We see in Fig. 5.9a a Gaussian state represented by points which form an ellipse-like structure. If the distribution had no preferred direction in phase-space $\langle\hat{\psi}^2\rangle = \overline{\psi_1^2}$ would vanish, but this is clearly not the case for our squeezed state. In Fig. 5.9b the the interaction modifies the phase accumulation of points with large values of $|\psi_1|$ and deforms the distribution to an S-like shape, and the mean value of ψ_1^2 is reduced. If the state is centered around a finite field amplitude, the intensity dependent phase shift transforms a circular distribution into a bean-shaped one, and in that case the Kerr effect actually produces squeezing [148].

5.6 Atom–molecule oscillations

The pure photodissociation process cannot be treated with a mean field approximation. This signals strong quantum effects and interesting physics, and it was the our motivation for focusing our analysis in Ref. [1] on these effects and not so much on the prospects for atom–molecule oscillations. In the bright light of hindsight, we should probably have done the analysis without the undepleted pump assumption and added simulations starting from an atomic condensate. In fact, after completing the work presented in the sections above, we did run such simulations. The main difference in the procedure is the explicit inclusion of the molecular field. The positive P Langevin equations are for 4 c-number fields: ψ_1, ψ_2, ψ_{m1}, and ψ_{m2}. The molecular fields, ψ_{m1} and ψ_{m2}, obey equations that are very similar to the ones encountered for atomic fields. The deterministic part contains kinetic energy, possibly an external potential, molecule–molecule and molecule–atom mean field interactions, and terms from the photoassociation/-dissociation. The noise terms are solely due to the collisional interaction as the atom–molecule coupling is linear in

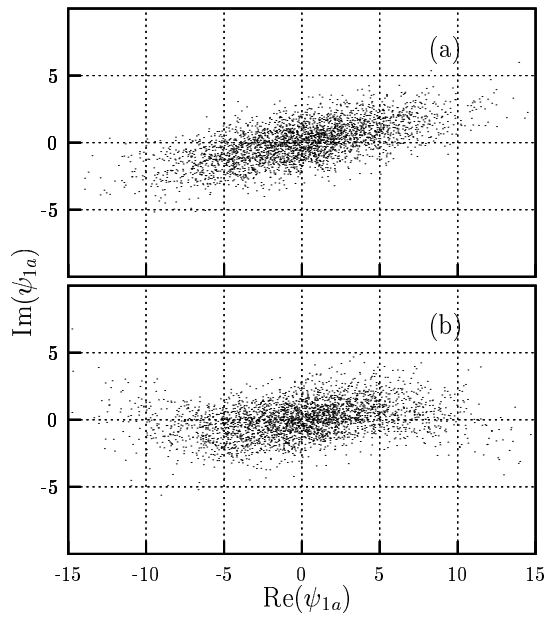

Figure 5.9: Scatter plots of ψ_{1a}, the overlap of ψ_1 with the condensate mode function ψ_a. Plot (a) is for $g = 0.00$ while plot (b) is for $g = 0.02\hbar\omega a_0$. The plots demonstrate the deforming effect of the interactions on the Gaussian state. This deformation reduces the mean of ψ_{1a}^2 which is the decisive factor for the efficiency of the state as squeezed vacuum.

the molecular field.

Fig. 5.10 shows typical results. We observe an almost complete conversion to molecules followed by somewhat irregular oscillations. We have not analyzed the simulations thoroughly, but it seems that there is a spatial dephasing of the oscillations. At the same time as we did these simulations, preprints of the work by Hope *et al.* [126, 149, 127] appeared, and as our preliminary results seemed to agree well with their more complete work, we decided to pursue other projects.

5.7 Discussion

In our work, an important point is that the R&S equations are exact as long as we ignore interactions among atoms, but that the full positive P machinery is needed when $g \neq 0$. The threshold effect (Sec. 5.4.4) and the deterioration of the squeezing (Sec. 5.5.2) cannot be obtained with R&S. The work by Hope *et al.* shows, that the spontaneous contribution indeed is important also when starting from an atomic condensate: Although the conversion to molecules during oscillations is never complete, a mean field (coupled Gross–Pitaevskii equations) treatment fails. This bears strong evidence to the usefulness of exact, albeit numerically quite heavy, methods like the positive P simulations. Subsequently, it would be interesting to analyze in more physical terms especially the threshold effect. The crossover from a squeezed to a coherent condensate would be an interesting parallel to the more familiar condensation process in an evaporatively cooled gases.

We should make a final remark regarding the use of a squeezed condensate as "squeezed vacuum" input in a beam splitter (Sec. 5.5). As described, this process allows the squeezing to be detected by simply counting atoms: the large condensate acts as a strong local oscillator. The method relies crucially on the existence of a well-defined phase between the squeezed sample and the large condensate. In our calculations, this is implied by the assumption of a coherent state for the large condensate. In an experiment, at least two schemes spring to mind: (i) Derive both

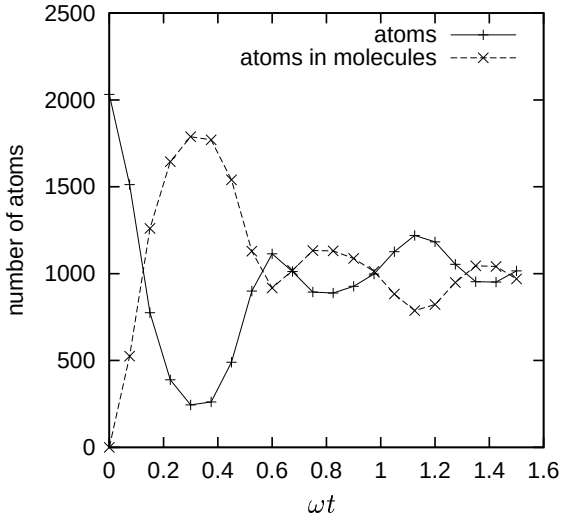

Figure 5.10: Atom-molecule oscillations treated by the positive P method. Initially, only atoms are present, but $\omega t \sim 0.35$ more than 80% has been converted to molecules. It should be noted that to avoid the divergences of positive P, the atom-atom an molecule-molecule interaction was taken to be very weak in this preliminary simulation. In principle, interactions can be included along with the atom-molecule coupling.

the molecular condensate and the local oscillator from one condensate, or (ii) establish a phase between the molecular condensate and the local oscillator. Alternative (i) is of course only viable when the molecules are created coherently, e.g., by photoassociation, while alternative (ii) would require modifications of the methods involved in "ordinary" BEC phase standards [37].

Chapter 6

Scattering of atoms on a BEC

The scattering of atoms on a Bose-Einstein condensate is a process of fundamental interest. Except in the extremely weakly interacting regime considered in Sec. 4.5, the dynamics of the noncondensed atoms in the trap is strongly influenced by the mean field of the condensate. The resulting redistribution of population among "trap-levels" is an important ingredient in quantum kinetic theories of, e.g., the very process of condensation. There are also important scattering effects when two condensates merge. For example, four-wave mixing has been observed in experiments [150]. In this chapter we shall instead deal with the limit of a single or just a few atoms, incident in a well defined momentum state on a condensate, a situation that has been realized experimentally to seed atom lasers [151] and "atomic parametric amplifiers" [152, 153] with a weak atomic beam. Apart from some special effects to be discussed below, a very controlled bombardment of a BEC by atoms could also serve as an interesting probe to condensate properties.

We start the chapter with an introduction in Sec. 6.1. In Sec. 6.2 we discuss the Bogoliubov approach in the special setting we have in mind, and we specify the numerical method we have used. The results are presented in Sec. 6.3 and compared with an approximate analytical model. In Sec. 6.4, we show examples of time dependent wavepacket dynamics. Finally, Sec. 6.5 concludes the chapter and gives an outlook to some of the more quantum optical perspectives that we have yet to explore.

6.1 Introduction

In this chapter we shall analyze a very simple experiment: We imagine to have a BEC made up of a certain kind of atoms and we then try to send a single atom of the same kind through it. Since the atoms of the scatterer are indistinguishable from the scattered particles, exchange effects play an important role. This prompted the suggestion that scattering on a condensate would be very different from scattering on a collection of non-condensed particles. Pictorially, an atom can traverse a condensate by scattering into the condensate on one side and out again on the side. This scattering-in–scattering-out (SISO) effect was proposed as a means for investigating the condensate fraction in the strongly interacting He-4 system [154, 155].

Theoretically, it is much easier to handle weakly interacting systems; for very pure condensates, the Bogoliubov approach presented in Sec. 2.7 is the appropriate tool. To find traces of the condensate mediated transmission, Wynveen *et al.* therefore considered the Bogoliubov scattering states for a dilute condensate held in a finite depth spherical well [156]. By numerically solving the radial Bogoliubov–de Gennes equations for the lowest partial waves, they calculated scattering cross-sections for a range of parameters. They compared their results to the simple Hartree–Fock theory [Eq. (2.15)] and found indeed an enhanced transparency at high incoming momenta. The picture was complicated, though, by the nontrivial behaviour of cross-sections. For lower incoming momenta, both the Hartree–Fock and the Bogoliubov scattering display pronounced resonances and the transparency can be either enhanced or reduced.

Revisiting the SISO picture of condensate mediated transmission, R. Y. Chiao found that one should also consider the opposite time-ordering, i.e., a scattering-out–scattering-in (SOSI) process where the outgoing particle is emitted *before* the incoming particle enters the condensate [157]. The process has analogies in the QED description of, e.g., Compton scattering or the scattering of electrons from the Coulomb field of a nucleus. There higher order Feynman diagrams with identical initial and final states, but with different time-ordering of internal vertices, must be summed coherently.

Inspired by these earlier studies we decided to investigate an even simpler geometry than the spherical well of Wynween *et al.*. We considered a 1D situation with a condensate held in a potential well of finite width and depth. Asymptotically free atoms can then be directed towards the trapped condensate and interact with it in a well defined region of space. The natural quantity to calculate is the transmission probability of the incident particle. If this probability shows a strong dependence on the parameters of the system, scattering of atoms could also be interesting as a measurement method. Bijlsma and Stoof have done a calculation similar to ours for scattering on a cylindrical condensate [158]. They found that the method can be used for nondestructive detection of vortices. In geometries where our 1D description is justified, it should be possible to detect with high efficiency whether the incident atom is reflected or transmitted.[1] In a longer perspective, we imagine such methods to be ingredients in highly nonclassical experiments where the strong atom–atom coupling could be an advantage.

6.2 Scattering in the Bogoliubov approach

As we explained in Sec. 2.7, the Bogoliubov approach assumes the number of particles in the condensate mode to be high and rather well defined. On top of an improved description of the ground state, the problem of small thermal or externally induced excitations can be treated. The picture is one of non-interacting quasi-particles, with a mixed particle-hole character. In the case of scattering, the incoming particle will of course be particle-like asymptotically, but it will move through the condensate as a quasi-particle.

6.2.1 Stationary scattering states

Ordinary single-particle scattering can be treated both in a time-dependent (wavepacket) formulation and in a formulation based on stationary scattering states. One can extract important, general information on the time-dependent behaviour from a few characteristics of the stationary states. We therefore adopt a similar strategy here and start by looking for scattering states of the Bogoliubov–de Gennes equations, (2.69).

For convenience, we shall use a slightly different notation than in Sec. 2.7. First of all, we drop the $\hat{Q}$'s in $\hat{\mathcal{L}}$. As explained in Sec. 2.7.8, this formally means that we are using the symmetry breaking approach. However, there is no effect on the excitation energies and the eigenfunctions of the symmetry preserving approach are found by simple application of $\hat{Q}$ [41]. More so, we shall mostly be interested in the asymptotic behaviour where this projection has a trivial effect. The second difference as compared to Sec. 2.7 will be that we rename $v_k \to -v_k^*$ to get a more symmetric notation. Finally, excitations energies will be expressed as frequencies, $\hbar\omega_k = \epsilon_k$. The Bogoliubov–de Gennes equations then read

$$[\hat{L}(x) - \hbar\omega_k]u_k(x) = gn_0(x)v_k(x) \tag{6.1}$$

$$[\hat{L}(x) + \hbar\omega_k]v_k(x) = gn_0(x)u_k(x), \tag{6.2}$$

where the operator $\hat{L}(x)$ is defined by $\hat{L}(x) = \hat{h}(x) + 2gn_0(x) - \mu$, with $n_0 = N|\phi_0|^2$, the condensate density. The external potential in the single-particle Hamiltonian, $U_{\text{ext}}(x)$, is assumed to vanish

[1] The one dimensional geometry may correspond to either a condensate slab hit by atoms with well defined transverse momenta or to a trapped condensate in a wave guide with a local longitudinal minimum. Especially in the latter case, it is easy to imagine very efficient detection.

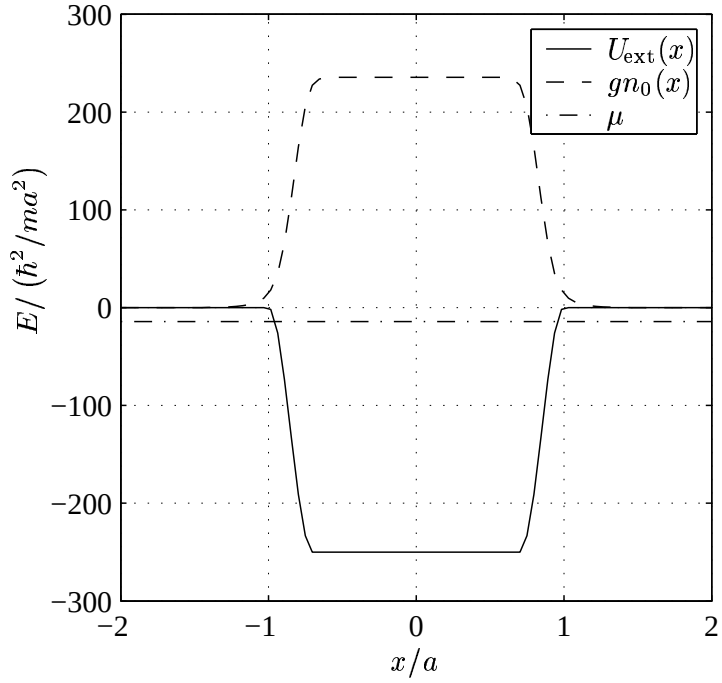

Figure 6.1: Figure showing the potential well and the shape of the condensate. The range of the potential is $[-a, a]$ outside which $U_{\rm ext}(x)$ is identically 0. $U_{\rm ext}(x)$ changes smoothly to $-U_0 = -250\hbar^2/ma^2$ in edge-zones of width $0.3a$. The 1D interaction strength is taken to be $gN = 400\hbar^2/ma$. The solution of the GPE then gives $\mu = -14.4\hbar^2/ma^2$ and a Bogoliubov speed of sound $c = \sqrt{gn_0(0)/m} = 15.4\hbar/ma$ in the inner region of the well.

identically outside a finite range, $x \in [-a, a]$. Eqs. (6.1) and (6.2) should then be solved with the boundary condition $v_k \to 0$ for $x \to \pm\infty$. The spectrum of solutions is divided in two: A part with discrete eigenvalues and localized u_k's, and a continuum part where the u_k's show an oscillatory asymptotical behaviour. It is the scattering states, i.e. the continuum, that we are primarily interested in. As in ordinary scattering theory, there are, however, connections between the two types of solutions, and in Appendix B we show how Levinsons theorem generalizes to Bogoliubov scattering.

6.2.2 Numerical solution

In 1D, the Bogoliubov–de Gennes equations are computationally quite manageable and the choice of method for their solution is not crucial. Nevertheless, for completeness we here briefly summarize our method. First we solve the Gross-Pitaevskii equation (4.13) with the chosen potential. We do this by a simple steepest descent method, i.e., by propagating the corresponding time–dependent equation in imaginary time. In particular, we use a split–step fast–Fourier–transform algorithm [159]. In Fig. 6.1, we show the particular potential we will be using, and we show the corresponding condensate wavefunction.

When $\phi_0(x)$ and μ have been found, the Bogoliubov-de Gennes equations are solved by first defining

$$\begin{aligned} f_k(x) &= \sqrt{\frac{1}{2}}\,[u_k(x) + v_k(x)] \\ h_k(x) &= \sqrt{\frac{1}{2}}\,[u_k(x) - v_k(x)] \end{aligned} \tag{6.3}$$

in terms of which Eqs. (6.1) and (6.2) become

$$[L(x) - gn_0(x)]f_k(x) = \hbar\omega_k h_k(x) \tag{6.4}$$
$$[L(x) + gn_0(x)]h_k(x) = \hbar\omega_k f_k(x) \tag{6.5}$$

We can then avoid diagonalizing a two-component problem by simply applying the operator $[L(x)+gn_0(x)]$ to both sides of Eq. (6.4) to find the necessary condition

$$[L(x) + gn_0(x)][L(x) - gn_0(x)]f_k(x) = [\hbar\omega_k]^2 f_k(x). \tag{6.6}$$

When this one–component eigenvalue problem is solved, $u_k(x)$ and $v_k(x)$ can be found by applying first Eq. (6.4) and then Eq. (6.3).

6.3 Results

6.3.1 Phaseshifts

We assume that $U_{\text{ext}}(x)$ and thus $n_0(x)$ have even spatial symmetry. We can then demand that solutions of Eqs. (6.1) and (6.2) have definite parity. In the discrete part of the spectrum, even and odd solutions alternate, while in the continuum, each energy supports solutions of both parities. In the asymptotic region away from the potential and the condensate, even and odd scattering solutions can then be written

$$\begin{array}{lcl} u_k^{(e)}(x) & \rightarrow & \cos(kx \mp \delta_e(k)) \\ u_k^{(o)}(x) & \rightarrow & \sin(kx \mp \delta_o(k)) \end{array} \quad \text{for } x \rightarrow \pm\infty. \tag{6.7}$$

Note that we identify the label k with the asymptotic wavenumber for the scattering solutions. The phaseshifts, $\delta_e(k)$ and $\delta_o(k)$, contain all the information about the scattering relevant to the asymptotic region. They can be conveniently extracted from our numerical solutions for u_k. The calculations are actually done on a space–interval $[-L, L]$ with periodic boundary conditions (finite lower momentum cutoff). This means that for a given L we only find the subset of the continuum solutions with wavenumbers fulfilling

$$-kL + \delta(k) \equiv kL - \delta(k) \mod 2\pi \tag{6.8}$$

or, equivalently,

$$\delta(k) \equiv kL \mod \pi. \tag{6.9}$$

After the diagonalization this discrete set of k values can easily be determined from the eigenvalues as $\hbar\omega_k = \hbar^2k^2/2m - \mu$. Each k value gives us one point on $\delta(k)$ via Eq. (6.9). This is enough to determine $\delta(k)$ if it is slowly varying on the $1/L$ scale. If not, we just need to change L slightly and repeat the calculation to obtain an additional set of points.

In Fig. 6.2 we show a typical example of $\delta_e(k)$ and $\delta_o(k)$ with parameters as in Fig. 6.1. There is clearly some resonant behaviour with out–of–phase oscillations of $\delta_e(k)$ and $\delta_o(k)$ around a slowly varying average. This behaviour is well known from ordinary, single–particle scattering on a well/barrier, and in the following subsection we shall present an analytical model which yields the same gross features.

6.3.2 Square well model, Thomas–Fermi approximation

Let us consider a condensate trapped in a square well potential

$$U_{\text{ext}}(x) = \begin{cases} -U_0 & , \quad |x| < a_{\text{sw}} \\ 0 & , \quad |x| > a_{\text{sw}}, \end{cases} \tag{6.10}$$

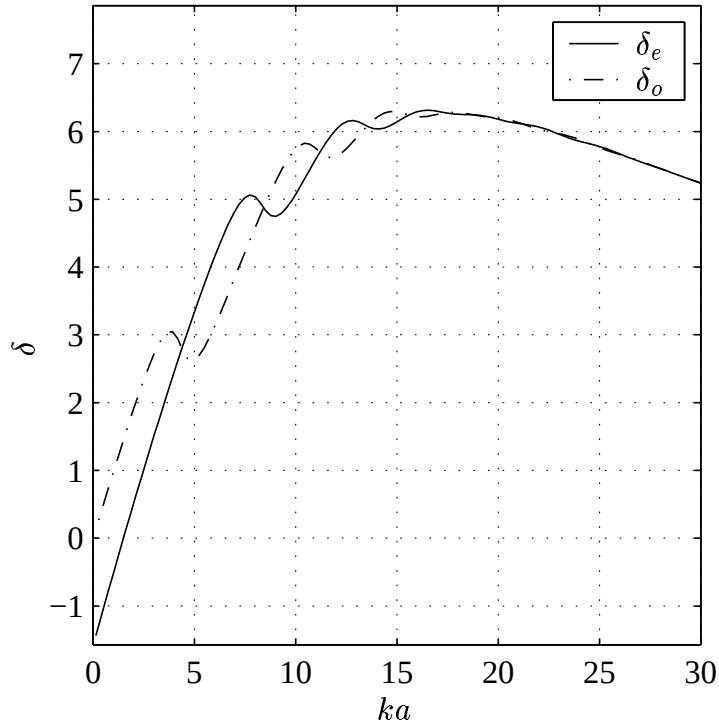

Figure 6.2: Phaseshifts of even and odd solutions as a function of incoming momentum. Parameters as in Fig. 6.1.

where $a_{\rm sw}$ is an appropriately defined effective width. In the Thomas–Fermi approximation the condensate wavefunction is constant in the trap and zero outside

$$\phi_0(x) = \begin{cases} \sqrt{\frac{N}{2a_{\rm sw}}} & , \quad |x| < a_{\rm sw} \\ 0 & , \quad |x| > a_{\rm sw}. \end{cases} \tag{6.11}$$

This $\phi_0(x)$ is naturally not a solution to the Gross–Pitaevskii equation as the kinetic energy term will smoothen the step in density even when the external potential is discontinuous (for solutions of the Gross–Pitaevskii equation in a square well, see [160]). Formally, this introduces linear terms in Eq. (2.66), i.e., the Bogoliubov vacuum is not a steady–state for the system. We are, however, only interested in the scattering behaviour at positive energies and it is reasonable to assume that some insight can be gained by finding solutions to Eqs. (6.1) and (6.2) with the simplifying assumptions expressed by (6.10) and (6.11).

It is amusing to note, that we are now dealing with the Bogoliubov–de Gennes analogy of the undergraduate textbook problem of 1D scattering on a square well. The full solution is found by matching the analytical wavefunctions in the regions, $x \in [-\infty, -a_{\rm sw}]$, $[-a_{\rm sw}, a_{\rm sw}]$, and $[a_{\rm sw}, \infty]$. To the left and to the right of the well, we demand $v(x) = 0$ and let $u(x) = \cos(kx \pm \delta_e(k))$ ($u(x) = \sin(kx \pm \delta_o(k))$) to find even (odd) solutions. Inside the well, we are in a region of constant potential ($U_{\rm ext}(x) = -U_0$) and constant condensate density ($N|\phi_0(x)|^2 = n_0$) so Eqs. (6.1) and (6.2) read

$$\left[-\frac{\hbar^2}{2m}\partial_x^2 - U_0 + 2gn_0 - \mu - \hbar\omega\right] u(x) = gn_0 v(x) \tag{6.12}$$

$$\left[-\frac{\hbar^2}{2m}\partial_x^2 - U_0 + 2gn_0 - \mu + \hbar\omega\right] v(x) = gn_0 u(x). \tag{6.13}$$

To be able to match the boundary conditions, we need four linearly independent solutions and the

ansatz $u(x) = Ue^{i\lambda x}$, $v(x) = Ve^{i\lambda x}$ leads to $\lambda \in \{\pm\lambda, \pm\tilde{\lambda}\}$ where

$$\hbar\lambda(k) = \sqrt{2m\left(\sqrt{[gn_0]^2 + [E-\mu]^2} - 2gn_0 + U_0 + \mu\right)} \tag{6.14}$$

and

$$\hbar\tilde{\lambda}(k) = i\sqrt{2m\left(\sqrt{[gn_0]^2 + [E-\mu]^2} + 2gn_0 - U_0 - \mu\right)} \tag{6.15}$$

where $E = (\hbar k)^2/2m$ is the incoming kinetic energy. Note that $\tilde{\lambda}$ is imaginary and it is normally disregarded in homogeneous condensates. Here, it is needed as we must match the boundary conditions that also v and v' are continuous.

The matching of u and v at $x = a_{\rm sw}$ leads to equations for the phaseshifts. They read

$$\tan\left(ka_{\rm sw} - \delta_e(k)\right) = \frac{\lambda(k)}{k}\tan\left(\lambda(k)a_{\rm sw}\right) \tag{6.16}$$

$$\tan\left(ka_{\rm sw} - \delta_o(k)\right) = \frac{k}{\lambda(k)}\tan\left(\lambda(k)a_{\rm sw}\right). \tag{6.17}$$

These equations are the same as for single particle square well scattering except that the usual $\hbar\lambda = \sqrt{2m(E - U_{\rm ext})}$ is replaced by $\hbar\lambda$ from Eq. (6.14).

In Fig. 6.3 we show results obtained for parameters like in Fig. 6.1: gn_0 is taken as the central density in the smooth trap and $a_{\rm sw}$ is chosen to accommodate the same total number of particles. A comparison with Fig. 6.2 reveals both similarities and differences: The smooth behaviour of the average of the two curves is well reproduced as well as the (quasi-)period of the oscillatory behaviour. However, the positions of curve crossings and the maxima of the phaseshift differences, especially at low k's, are not well reproduced. Also, at high momenta the sharp-edge approximation leads to stronger oscillations in $\delta_e(k)$ and $\delta_o(k)$ than for the smooth well.

6.3.3 Transmission coefficient

The typical scattering situation with an incoming, a reflected, and a transmitted wave specifies the asymptotic form of the wave function

$$u_k(x) \to \begin{cases} e^{ikx} + R(k)e^{-ikx} & \text{for} \quad x \to -\infty \\ T(k)e^{ikx} & \text{for} \quad x \to \infty \end{cases}. \tag{6.18}$$

This defines the reflection- and transmission-coefficients $R(k)$ and $T(k)$. Making the change of basis from the odd and even parity eigenstates (6.7), one finds

$$\begin{aligned} R(k) &= \frac{1}{2}\left(e^{-2i\delta_e(k)} - e^{-2i\delta_o(k)}\right) \\ &= ie^{-i(\delta_o(k)+\delta_e(k))}\sin(\delta_o(k) - \delta_e(k)) \end{aligned} \tag{6.19}$$

$$\begin{aligned} T(k) &= \frac{1}{2}\left(e^{-2i\delta_e(k)} + e^{-2i\delta_o(k)}\right) \\ &= e^{-i(\delta_o(k)+\delta_e(k))}\cos(\delta_o(k) - \delta_e(k)). \end{aligned} \tag{6.20}$$

We see that 100% transmission takes place at k's where $\delta_e(k) = \delta_o(k)$ while 100% reflection requires $\delta_e(k) = \delta_o(k) \pm \pi/2$. In Fig. 6.4 we plot R and T for the same situation as considered above. The curve crossings in Fig. 6.2 are now translated into transmission windows. At very low momenta, we get 100% reflection and at very high momenta we naturally get 100% transmission.

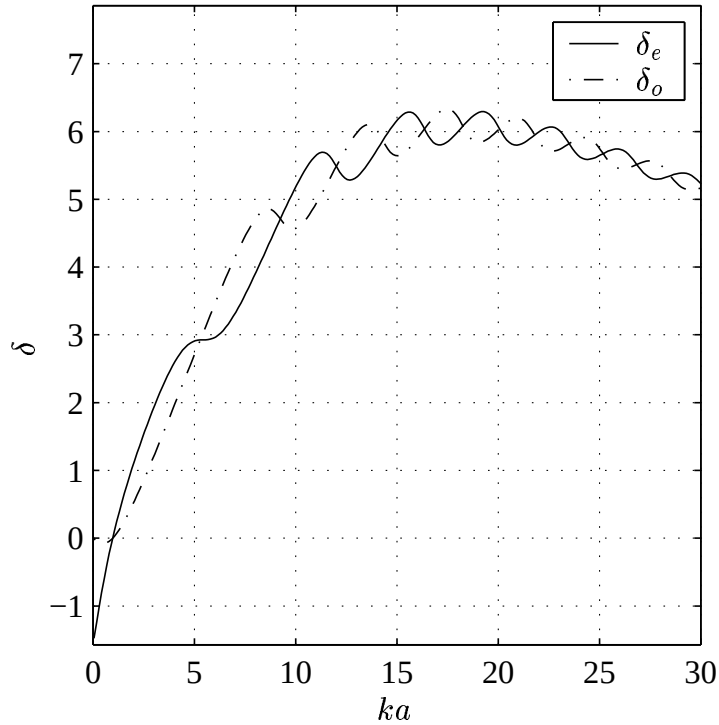

Figure 6.3: Even and odd phaseshifts for a simple square well/square condensate model. The parameters are like in Fig. 6.1 and the curves should be compared to the full numerical calculations presented in Fig. 6.2. There is clearly a qualitative agreement: The smooth behaviour of the average of the two curves is well reproduced and the period of the oscillations around this average is also of the correct order of magnitude. However, the oscillations extend to too high values of k, and the curve crossings are not at the correct positions.

6.4 Time dependent scattering

6.4.1 Wavepacket dynamics

With the complete set of scattering states it is possible to follow scattering of wavepackets in time. To obtain the initial state we add a number of particles to the Bogoliubov vacuum:

$$|t=0\rangle = \frac{1}{\sqrt{n_s!}}\left[\int \phi_{\mathrm{s}}(x)\delta\hat{\psi}^\dagger\right]^{n_s}|\mathrm{vac}\rangle_{\mathrm{bog}} \tag{6.21}$$

where $\phi_{\mathrm{s}}(x)$ is the desired wavepacket mode. The operator term in this equation creates an n_s- particle state, but to benefit from the simple form of Eq. (2.80) we should think of it as creating n_s quasi-particles which at $t=0$ just happen to be localized well away from the condensate. The quasi-particles are created in a superposition of energy eigenstates and the coefficients in this superposition are found as

$$c_k = \int \left[u_k^*(x)\phi_{\mathrm{s}}(x) + v_k^*(x)\phi_{\mathrm{s}}^*(x)\right]dx. \tag{6.22}$$

As ϕ_s is located well away from the condensate region, there is in fact no contribution from the v part of this integral.

The time evolution is entirely given by the relation $\hat{b}_k(t) = e^{-i\omega_k t}\hat{b}_k$ in the Heisenberg picture, and we find the noncondensate part of the total density to be

$$\langle\delta\hat{\psi}^\dagger\delta\hat{\psi}\rangle = n_s\left|U(x,t)\right|^2 + n_s\left|V(x,t)\right|^2 + \sum_k \left|v_k(x)\right|^2 \tag{6.23}$$

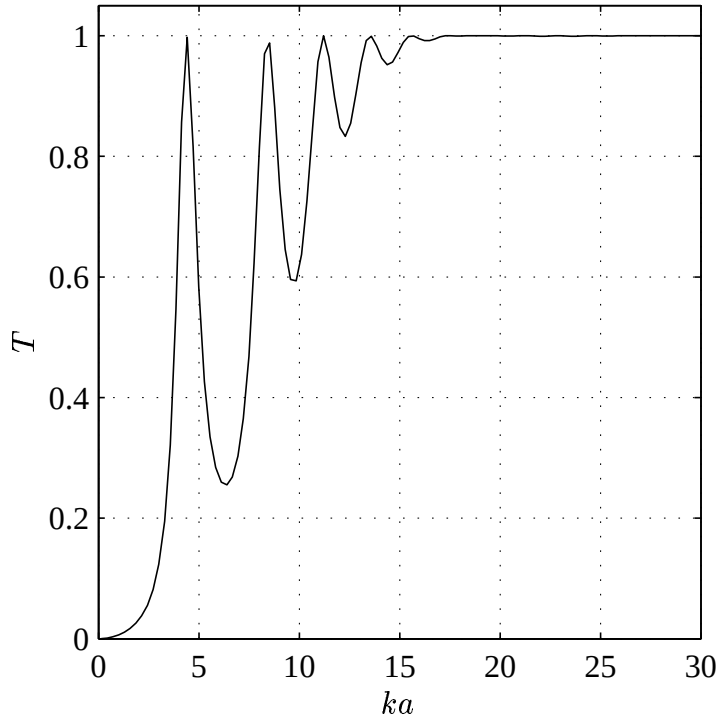

Figure 6.4: Transmission and reflection coefficients for the situation considered in Figs. 6.1 and 6.2. A series of perfect transmissions are seen, corresponding to the crossings of the $\delta_e(k)$ and $\delta_o(k)$ curves in Fig. 6.2.

where

$$U(x,t) = \sum_k c_k e^{-i\omega_k t} u_k(x) \tag{6.24}$$

$$V(x,t) = \sum_k c_k e^{-i\omega_k t} v_k(x). \tag{6.25}$$

The last term in Eq. (6.23) is the quantum depletion of Sec. 2.7.7, which is always present due to the interactions in the condensate, while the first two terms are consequences of the scattering process.

6.4.2 Time-delays

Depending on the spread of k-values in the wavepacket, the asymptotic behaviour of the scattering will be more or less simply described by reading off the reflection and transmission coefficients R and T at the average momentum k_0. In fact, looking at the first form of these coefficients in Eqs. (6.19) and (6.20) we are reminded that the reflected and the transmitted wave can be seen as superpositions of an even part and an odd part. To each of these can be ascribed a time-delay, $\Delta t_{e/o}$ in the arrival of the original wave packet at certain point in space with respect to the free propagation. It is easy to show that these delays are given by

$$\Delta t_e = -\frac{2}{v_g} \frac{\partial \delta_e(k)}{\partial k}\bigg|_{k=k_0} \tag{6.26}$$

$$\Delta t_o = -\frac{2}{v_g} \frac{\partial \delta_o(k)}{\partial k}\bigg|_{k=k_0} \tag{6.27}$$

where $v_g = \hbar k_0/m$ is the (group) velocity of the incoming wavepacket. If these delays are sufficiently different the reflected and transmitted wavepackets are expected to be doublepeaked. In fact, a closer look at Eqs. (6.19) and (6.27) reveals a difference in sign: the reflected wavepacket can easily be double-peaked as it is the difference between the even and odd contribution, while the transmitted wavepacket is the sum and therefore require displacements as large as the wavepacket width for a visible effect.

In Fig. 6.5 we show time series of snapshots from wavepacket simulations. The double peak phenomenon mentioned above is visible in the $k_0 a = 11.50$ time series. This k_0 corresponds to a crossing of $\delta_e(k)$ and $\delta_o(k)$ and thus to both high transmission and a marked difference in Δt_e and Δt_o (cf. Fig. 6.2).

6.4.3 Transmission times

The time–delays of Eqs. (6.26) and (6.27) can also be translated into an effective transmission time, the time spent traversing the condensate region. The well has a width $2a$ so the time spent inside the well can heuristicly be defined as $\tau = \Delta t + 2a/v_g$. In Fig. 6.6 we plot $\tau_e(k)$ and $\tau_o(k)$. The two curves agree for high k, while for ka less than ~ 15, i.e., for v_g less than the Bogoliubov speed of sound in the homogeneous part of the condensate, $c = \sqrt{gn_0/m}$, they show alternating peaks. Such peaks are signatures of resonances where an even or an odd number of oscillations fit inside the condensate.

At low k–values, we observe that τ_e becomes negative over a rather wide range. For wavepackets with momentum components mainly in this range, a peak in the transmitted wavepacket can appear *before* the peak of the incident wavepacket has reached the condensate. This is confirmed by wavepacket simulations.[2] Negative transmission times is a wave phenomenon, which together with superluminal propagation has been observed for light propagation through wave guides and through dispersive atomic media. It is not surprising that the Bogoliubov–de Gennes equations show similar effects.[3]

6.5 Discussion

As explained in Sec. 6.1, we initiated this project with two goals in mind:

(i) We wanted to investigate the suggestion by Halley *et al.* [154] that the system would show a special condensate mediated transmission. In particular, the special features pointed out by Chiao *et al.* [157] seemed interesting.

(ii) Although probing condensate properties with light has proved to be a very versatile tool, it could be of interest to use atoms instead.

In short, we have not moved much closer to goal (i), while our study is certainly a step towards goal (ii).

The geometry that we have considered dramatically demonstrates the difference to the Hartree–Fock approach: The $2gn_0$ mean field would be a truly impenetrable barrier and the transmission windows at low k would be totally absent if there was no v-component. Although this a more clearcut signature than in the earlier study by Wynveen *et al.* [156], we have still not found it easy to connect the Bogoliubov approach directly with the SISO mechanism discussed in Sec. 6.1. In the same way, it is tempting to see the negative transmission times found in Sec. 6.4.3 as support for Chiao's suggestion that the time-reversed SOSI processes play a discernible role, but whether

[2] Analysis of both a real experiment and of wavepacket simulations is more complicated for massive particles than for light: As the transmission coefficient depends strongly on k, there is a velocity filter effect, i.e., the transmitted wavepacket may move at a different speed than the incoming one.

[3] As a curiosity, we note that putting "negative transmission times" in the abstract of preprint-server version of Ref. [6] earned us more publicity than ever intended: The article became a news item on the popular "geeks" news-site, `www.slashdot.org`, and we were even contacted by Science.

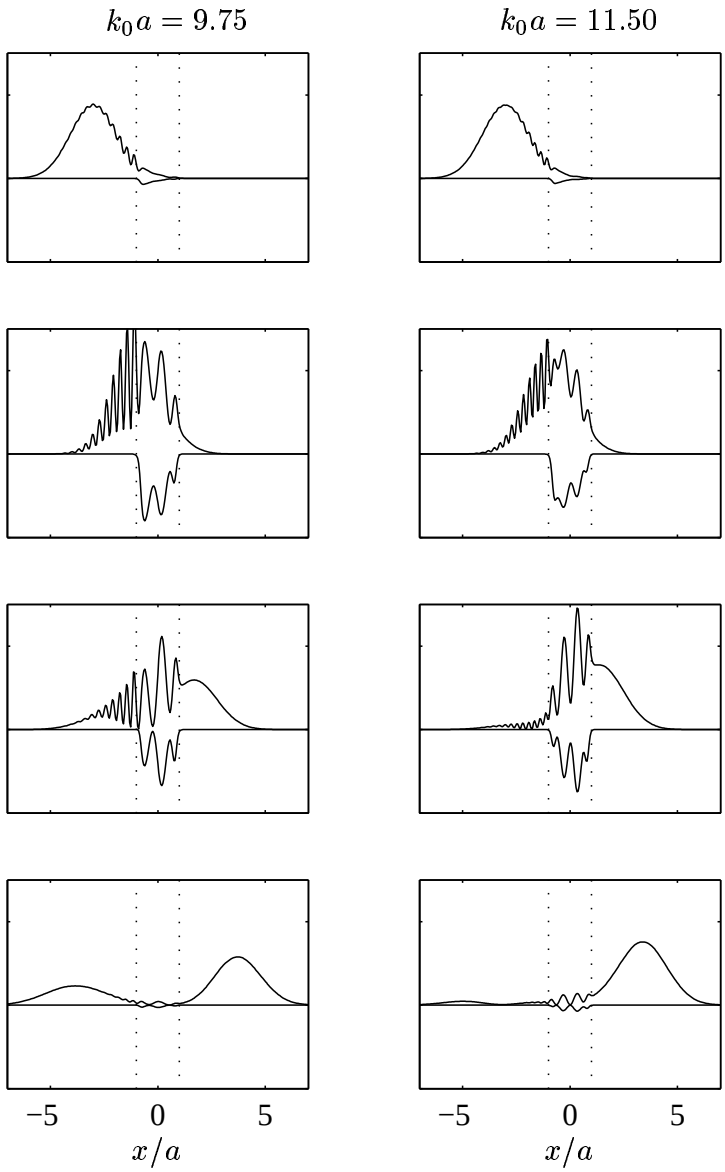

Figure 6.5: Wavepacket scattering on a BEC. Time series are shown for two different incoming momenta: At mean wavenumber $k_0a = 9.75$, the initial packet propagates towards the potential well containing the BEC and reflected and transmitted wavepackets appear. In accordance with Fig. 6.4 transmission is approximately 62% at this k_0. At $k_0a = 11.5$ we are in a transmission window and the reflected wavepacket has small amplitude and a double–peaked envelope.The figures show both $|U(x)|^2$ and $-|V(x)|^2$, the particle contribution and $(-)$ the hole contribution to the total density of scattering atoms. Note that the ground state quantum depletion also contributes to the density of atoms out of the condensate mode. This contribution is located inside the well and is not plotted here.

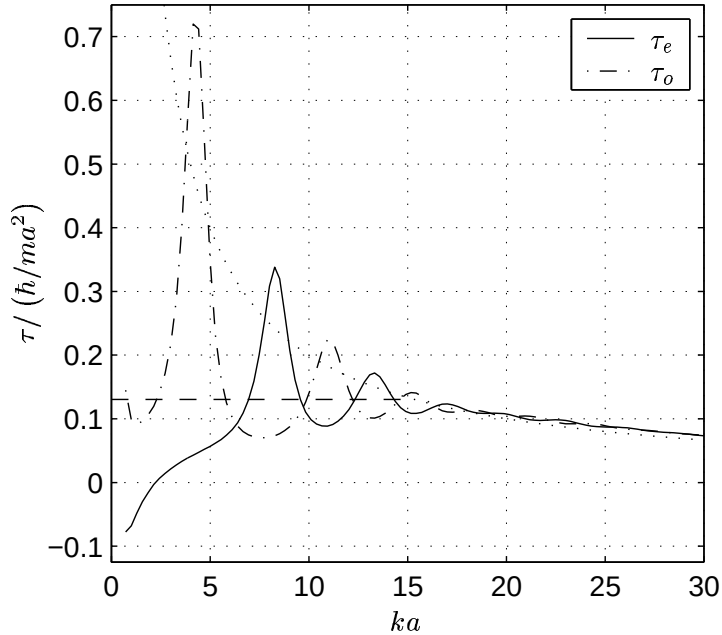

Figure 6.6: Time spent in the condensate region. Curves are shown for both even and odd solutions. Where these curves approximately coincide, the retardation can be seen directly in wavepacket scattering. When they are very different, the translation to a time-dependent wavepacket formulation is less direct. Note the negative values of τ_e in the region around $ka \lesssim 2$: Wavepacket simulations show that here the peak of the transmitted wavepacket appears *before* the peak of the incident wavepacket has reached the condensate. For comparison, the two dashed curves show respectively the free motion and the sound wave transmission times, $2a/v_g$ and $2a/c$.

it is at all possible to separate out such special effects from all the "normal" wavedynamics of the problem remains an open question.

The wavedynamics is, however, interesting in itself. Particles incident on the condensate propagate as phonons through the condensate, where they may be reflected back and forth between the condensate edges, and eventually they re-emerge as reflected or transmitted particles. We have determined the reflection and transmission probabilities and the phase shifts, which enable us to derive time-dependent results from our stationary formulation. The double peaked distributions reflected from the condensate and the negative transmission times come as interesting (but not mysterious) results. Independently of goal (i), an experimental demonstration of the these phenomena would be an interesting supplement to similar studies for light transmission.

The rich structure found in transmission coefficients etc. is important when striving for goal (ii). If low energy atoms are to be used as probes on condensates, detailed knowledge of, e.g., the position of transmission windows is useful. In addition to the simple transmission/reflection experiments, interferometric methods can also be envisaged. Such experiments should be able to show that coherence is preserved by the intermediate phonon excitation. One could even imagine to use quantum correlated atoms to show that entanglement can be communicated through the phonons. This would be in analogy with recent experiments where surface plasmons propagate quantum correlated photon pairs through sub wavelenght hole arrays [161]. One could also consider experiments using two-level atoms, both in the condensate and in the probe beam, resulting in an atomic "Faraday effect". Perhaps powerful measurement induced state engineering can be performed this way.

In conclusion, scattering experiments as analyzed here seem to have a large potential for studying interesting physics. They seem as a natural ingredient in the study of controlled atomic dynamics. In particular for atoms and condensates trapped on chip architectures, [162, 163, 164],

“integrated” scattering experiments would a realistic and worthwhile challenge to undertake.

Chapter 7

Conclusion and outlook

In this short, concluding chapter we summarize the most important results of the thesis. We also comment on what we find to be the most interesting directions in which to extend the work presented.[1]

Spin squeezing

In Sec. 4.2 we used the exact positive P method to investigate the applicability of the simple two-mode picture. The results were very encouraging for the situations we focussed on: the one of favourable interaction strengths and the separated-components scenario. Due to the statistical nature of the positive P simulations, the regime of really strong squeezing could not easily be treated. It is a challenge for the future to extend the treatment, possibly to the cases where two-component Bogoliubov theory predicts a breakdown of the two-mode model.

In Sections 4.3 and 4.4 we suggested two applications of spin squeezing in BEC: a quantum beam splitter and a source of squeezed light. The beam splitter proposal we believe to be a very realistic one, and observation of the squeezed counting statistics is mainly prevented by experimental inability to observe even the standard, binomial distribution. We analyzed this proposal in some detail, checking, e.g., that it is not overly sensitive to the quality of mode matching. Our work on producing squeezed light from spin squeezed atoms is probably still some way from experimental realization. A 3D calculation with realistic physical parameters would be a necessary theoretical prelude. Our 1D calculation was, however, very promising, not least the perfect mapping of atomic spin operators onto light field operators. The extension of the previous treatments to inhomogeneous media and the suggested method for probing a particular spatial integral of the spin variables were also useful results.

Finally, in Sec. 4.5 we investigated with an analytical toy-model calculation the effect of non-condensed particles on the observation of phase revivals. These revivals are particularly interesting as they serve as proof of the existence of an intermediate Schrödinger cat state. Preliminary work suggests that our toy-model describes well the extremely weakly interacting regime for trapped gases. Almost independently of this, the possibility to calculate nontrivial expectation values analytically within a nontrivial model is always noteworthy, and the proposed model has been used in praxis to check another simulation scheme.

Photodissociation of a molecular condensate

The main part of our work on molecules in BEC had a slightly different focus than the majority of the literature in this very active field. By choosing a molecular condensate as initial state, we got a very direct analogy with degenerate downconversion of photons. The inadequacy of mean field methods and the squeezed character of the created atomic field were easily demonstrated. The ability of the positive P method to include also collisional interactions revealed some interesting

[1] This is one of the places where the "we" should probably be exchanged for an "I".

phenomena, not least the observed thresholdlike effect. An obvious extension of the work would be to do a closer analysis of the transition from squeezed vacuum to the classical matter wave regime.

We also presented simulations in the more general setting of atom–molecule oscillations. Again the positive P method showed its strength by being able to include all important terms of the Hamiltonian, but we didn't pursue the analysis far, as other authors have done more extensive work in this area. We believe that Monte Carlo methods have a role to play also in the future of the field, but talking from experience we also raise a general note of caution that, e.g., the phase space doubling of positive P can interfere with the use of physical intuition in the interpretation of equations and single realizations. One should not loose sight of the fact that the Hamiltonian includes interactions via effective terms and that positive P is never better than the quality of these approximations.

Scattering of atoms on a BEC

The last topic covered in the thesis is identical particle scattering on BECs. We presented Bogoliubov calculations for the 1D well of finite width and depth, and we extracted relevant scattering information from the results. In the regime of a really slow incoming atoms (velocity $\sim$ the Bogoliubov speed of sound), the physics was found to be rich with transmission windows, double peaked reflected wavepackets, and even negative transmission times. Our results spectacularly demonstrated the difference between Bogoliubov and Hartree–Fock scattering, but the precise connection to condensate mediated transmission remained unclear.

The perspective of using slow atoms as probes on BECs is promising and many interesting experiments can be envisage. In particular, experiments with incoming atoms that are entangled or in superpositions of different internal states were suggested.

Appendix A

Coherent states

For a single mode with creation operator $\hat{a}^\dagger$ and annihilation operator $\hat{a}$, coherent states are usually known as the eigenstates for $\hat{a}$,

$$\hat{a}|\alpha\rangle = \alpha|\alpha\rangle. \tag{A.1}$$

In analogy with the c-number exponential function they can be written

$$|\alpha\rangle = \exp\bigl(-|\alpha|^2/2\bigr) \sum_{N=0}^{\infty} \frac{1}{N!} \left[\alpha\hat{a}^\dagger\right]^N |\mathrm{vac}\rangle, \tag{A.2}$$

or even

$$|\alpha\rangle = \exp\bigl(\alpha\hat{a}^\dagger - \alpha^*\hat{a}\bigr)|\mathrm{vac}\rangle. \tag{A.3}$$

The vacuum, $|\mathrm{vac}\rangle$, is the special coherent state with $\alpha = 0$.

From Eq. (A.2) it is clear that a coherent state is a superposition of number states, the distribution of $N = \langle\hat{a}^\dagger\hat{a}\rangle$ being Poissonian with mean value $|\alpha|^2$. In the thesis we repeatedly refer to the fact that this coherence between states of different N is washed out when considering an incoherent mixture of coherent states with a uniform phase distribution. The corresponding density operator is thus equivalent to a mixture of number states with Poissonian number distribution. This can be seen explicitly by the following calculation:

$$\begin{aligned}
\hat{\rho} &= \int \frac{d\theta}{2\pi}\, |\alpha e^{i\theta}\rangle\langle\alpha e^{i\theta}| \\
&= e^{-|\alpha|^2} \sum_{M,N} \frac{1}{M!N!} \int \frac{d\theta}{2\pi} e^{i\theta(N-M)} \left[\alpha\hat{a}^\dagger\right]^N |\mathrm{vac}\rangle\langle\mathrm{vac}| \left[\hat{a}\alpha^*\right]^M \\
&= e^{-|\alpha|^2} \sum_{N} \frac{1}{(N!)^2} \left[\alpha\hat{a}^\dagger\right]^N |\mathrm{vac}\rangle\langle\mathrm{vac}| \left[\hat{a}\alpha^*\right]^N \\
&= e^{-|\alpha|^2} \sum_{N} |\alpha|^{2N} \frac{1}{N!}\, |N\rangle\langle N|.
\end{aligned} \tag{A.4}$$

Coherent states can also be defined in a multi-mode setting. An important consequence of the "exponential" character of coherent states should then be noticed:

$$\prod_j \exp\bigl(\alpha_j\hat{a}_j^\dagger - \alpha_j^*\hat{a}_j\bigr)|\mathrm{vac}\rangle = \exp\bigl(\beta\hat{b}^\dagger - \beta^*\hat{b}\bigr)|\mathrm{vac}\rangle \tag{A.5}$$

where $\hat{b} = \sum_j \alpha_j\hat{a}_j/\beta$ and $\beta = \sqrt{\sum_j |\alpha_j|^2}$. We see that coherent states in all modes can be simplified via a change of basis to a coherent state in just the mode with annihilation operator $\hat{b}$ and vacuum in all other modes. Conversely, a coherent state will look as a coherent state even when split in smaller parts.

A particular multi-mode case is the coherent states for the field operator, $\hat{\psi}$,

$$\hat{\psi}(\mathbf{r})|\psi\rangle = \psi(\mathbf{r})|\psi\rangle. \tag{A.6}$$

The state $|\psi\rangle$ can be constructed analogously to (A.2):

$$|\psi\rangle = \exp\big(-\frac{1}{2}(\psi|\psi)\big)\sum_{n=0}^{\infty}\frac{1}{n!}\left[\int d^3\mathbf{r}\ \psi(\mathbf{r})\hat{\psi}^\dagger(\mathbf{r})\right]^n|\text{vac}\rangle. \tag{A.7}$$

Notice the $(\psi|\psi) = \int\psi^*\psi\ d^3\mathbf{r}$ appearing in the normalization: ψ is not a normalized mode function. Its norm is connected with the mean number of particles. In fact we find

$$\begin{aligned}\langle\psi|\hat{N}|\psi\rangle &= \int\langle\psi|\hat{\psi}^\dagger(\mathbf{r})\hat{\psi}(\mathbf{r})|\psi\rangle d^3\mathbf{r}\\ &= \int\psi^*(\mathbf{r})\psi^\dagger(\mathbf{r})\ d^3\mathbf{r}\ \langle\psi|\psi\rangle\\ &= (\psi|\psi).\end{aligned} \tag{A.8}$$

Appendix B

Levinsons theorem for Bogoliubov scattering

Levinsons theorem [165] connects the number of bound states to the low energy limit of the phase–shift. It is most often quoted in a 3D, spherically symmetrical setting, where it can be applied in each partial wave. The theorem can be derived from the analytical properties of the scattering matrix, but we shall instead use a simple method based on the completeness of the set of Bogoliubov modes. This approach to Levinsons theorem is due to Jauch [166]. The presentation here follows the 1D, single-particle derivation given by Sassoli de Bianchi in Ref. [167].

In the $U(1)$ gauge invariant version of the Bogoliubov theory, we have following decomposition of unity in the two-component, (u, v), space

$$= SS^{-1} = \begin{pmatrix} |\phi_0\rangle \\ 0 \end{pmatrix} \left(\langle\phi_0|, 0\right) + \begin{pmatrix} 0 \\ |\phi_0^*\rangle \end{pmatrix} \left(0, \langle\phi_0^*|\right) + \sum_k \left[\begin{pmatrix} |u_k\rangle \\ |v_k\rangle \end{pmatrix} \left(\langle u_k|, -\langle v_k|\right) + \begin{pmatrix} |v_k^*\rangle \\ |u_k^*\rangle \end{pmatrix} \left(-\langle v_k^*|, \langle u_k^*|\right) \right]. \quad \text{(B.1)}$$

In particular, we get a decomposition of one-component unity from the diagonal components.

We now specialize to 1D, and we assume a spatially symmetrical external potential. For simplicity, we assume the potential to be non-zero only in a finite region around $x = 0$. Then a stationary condensate density will also be spatially symmetric and we can split the problem in even and odd components. If we assume ϕ_0 to be even, we get for the even part of the problem

$$\frac{1}{2}\left[\delta(x - x') + \delta(x + x')\right] = \phi_0(x)\phi_0^*(x') + \sum_j \left[u_{e,j}(x)u_{e,j}^*(x') - v_{e,j}^*(x)v_{e,j}(x')\right] + \frac{1}{2\pi}\int_0^\infty dk \left[u_e(k,x)u_e^*(k,x') - v_e^*(k,x)v_e(k,x')\right], \quad \text{(B.2)}$$

where $(u_{e,j}(x), v_{e,j}(x))$ belongs to the discrete part of the spectrum and are normalized in the usual sense,

$$\int_{-\infty}^{\infty} dx \left[u_{e,j}^*(x)u_{e,j'}(x) - v_{e,j}(x)v_{e,j'}^*(x)\right] = \delta_{jj'}, \quad \text{(B.3)}$$

while $(u_e(k,x), v_e(k,x))$ are continuum solutions with

$$\int_{-\infty}^{\infty} dx \left[u_e^*(k,x)u_e(k',x) - v_e(k,x)v_e^*(k',x)\right] = \delta(k - k'). \quad \text{(B.4)}$$

The continuum solutions have the asymptotic behaviour,

$$\begin{array}{lcl} u_e(k,x) & \to & \sqrt{2}\cos(kx \mp \delta_e(k)) \\ v_e(k,x) & \to & 0 \end{array} \qquad \text{for } x \to \pm\infty. \tag{B.5}$$

The idea is now to compare (B.2) with the corresponding relation for the free solutions,

$$\frac{1}{2}\left[\delta(x-x') + \delta(x+x')\right] = \frac{1}{2\pi}\int_0^\infty dk\ \psi_e(k,x)\psi_e^*(k,x'), \tag{B.6}$$

where simply $\psi_e(k,x) = \sqrt{2}\cos(kx)$. Subtracting Eq. (B.6) from Eqs. (B.2), putting $x = x'$, and integrating, we get

$$\lim_{R\to\infty}\int_{-R}^{R} dx \int_0^\infty dk\ \left[|u_e(k,x)|^2 - |v_e(k,x)|^2 - |\psi_e(k,x)|^2\right] = -2\pi n_{\mathrm{e}}, \tag{B.7}$$

where n_e is the number of discrete even states, including the condensate mode, $|\phi_0\rangle$.

To relate the integral expression on the left hand side of Eq. (B.7) to the phase shifts, we need to move the evaluation to the asymptotic region. By taking the derivative with respect to k of both the Bogoliubov-de Gennes equations and of the free motion equation, we get

$$\begin{aligned} |u_e(k,x)|^2 - |v_e(k,x)|^2 - |\psi_e(k,x)|^2 = & \\ & +\frac{1}{2k}\frac{\partial}{\partial x}\left\{\frac{\partial u_e^*}{\partial x}\frac{\partial u_e}{\partial x} - u_e^*\frac{\partial^2 u_e}{\partial x \partial k}\right\}(k,x) \\ & +\frac{1}{2k}\frac{\partial}{\partial x}\left\{\frac{\partial v_e^*}{\partial x}\frac{\partial v_e}{\partial x} - v_e^*\frac{\partial^2 v_e}{\partial x \partial k}\right\}(k,x) \\ & -\frac{1}{2k}\frac{\partial}{\partial x}\left\{\frac{\partial \psi_e^*}{\partial x}\frac{\partial \psi_e}{\partial x} - \psi_e^*\frac{\partial^2 \psi_e}{\partial x \partial k}\right\}(k,x) \\ & +\mathcal{W}_e(k,x), \end{aligned} \tag{B.8}$$

where $\mathcal{W}_e(k,x)$ is a correction due to the nonlocal character of the projection operators needed in the gauge invariant Bogoliubov approach,

$$\begin{aligned} \mathcal{W}_e(k,x) = \quad & gN\ \langle u_e(k)|\left[\ |x\rangle\langle x|\ , Q|\phi_0|^2 Q\ \right]|\partial_k u_e(k)\rangle \\ & +gN\ \langle u_e(k)|\left[\ |x\rangle\langle x|\ , Q\phi_0^2 Q^*\ \right]|\partial_k v_e(k)\rangle \\ & +gN\ \langle v_e(k)|\left[\ |x\rangle\langle x|\ , Q^*(\phi_0^*)^2 Q\ \right]|\partial_k u_e(k)\rangle \\ & +gN\ \langle v_e(k)|\left[\ |x\rangle\langle x|\ , Q^*|\phi_0|^2 Q^*\ \right]|\partial_k v_e(k)\rangle. \end{aligned} \tag{B.9}$$

Eq. (B.8) can now be plugged into Eq. (B.7), and the integral over x can be done immediately for all terms except $\mathcal{W}$. It is, however, not difficult to see that the integral of the commutators in $\mathcal{W}$ will vanish as $R \to \infty$. Also the terms of (B.8) containing only v_e will vanish in this limit, so we only need to consider the u_e term and the free solutions. For R in the asymptotic region we can use Eq. (B.5) to write

$$\begin{aligned} \frac{1}{2k}\Bigg\{ & \left[\frac{\partial u_e^*}{\partial x}\frac{\partial u_e}{\partial x} - u_e^*\frac{\partial^2 u_e}{\partial x \partial k}\right]_{x=-R}^{x=R} - \left[\frac{\partial \psi_e^*}{\partial x}\frac{\partial \psi_e}{\partial x} - \psi_e^*\frac{\partial^2 \psi_e}{\partial x \partial k}\right]_{x=-R}^{x=R}\Bigg\} \\ & = \frac{1}{k}\Big\{\sin[2kR - 2\delta_e(k)] - \sin[2kR] - 2k\delta_e'(k)\Big\} \\ & = -\frac{\cos[2kR]}{k}\sin[2\delta_e(k)] - 2\pi\frac{\sin[2kR]}{\pi k}\sin^2[\delta_e(k)] - 2\delta_e'(k). \end{aligned} \tag{B.10}$$

When this expression is inserted in Eq. (B.7), we should get a finite limit of the integral over k as R goes to infinity. This requires the first term of Eq. (B.10) to be integrable at $k \to 0$ and thus $\sin[2\delta_e(0)] = 0$. The second term in Eq. (B.10) approaches a Dirac δ–function and we get

$$\delta_e(0) - \delta_e(\infty) = -\pi n_e + \frac{\pi}{2}\sin^2[\delta_e(0)]. \tag{B.11}$$

We define $\delta_e(\infty) = 0$ and except for the case of a $k = 0$ resonance [167], we get

$$\delta_e(0) = \left(\frac{1}{2} - n_e\right)\pi \tag{B.12}$$

In a completely analogous way, we can find the limit of the phaseshift for odd mode. The result is (again assuming no $k = 0$ resonance):

$$\delta_o(0) = -n_o\pi. \tag{B.13}$$

Appendix C

Wick's theorem

For convenience we give here a brief sketch of the simple version of Wicks theorem (see e.g. Ref. [138]) that we use.

If we put $g = 0$ in the Heisenberg equation of motion for the field operator, (5.6), the right hand side is a linear combination of $\hat{\psi}$ and $\hat{\psi}^\dagger$. This implies that $\hat{\psi}(x,t)$ can at all times be expressed as a linear combination of the initial values

$$\hat{\psi}(x,t) \quad = \quad \int dy \, \left\{ f(x,y,t)\hat{\psi}(y,0) + g(x,y,t)\hat{\psi}^\dagger(y,0) \right\}. \tag{C.1}$$

Eq. (C.1), its hermitian conjugate and the fact that our system starts in the vacuum state then suggest the following scheme for calculation of any operator product at arbitrary t: Use the commutation relation (2.25) to move all $\hat{\psi}(x,0)$ to the right of any $\hat{\psi}^\dagger(y,0)$ (normal ordering). Of all the terms produced in this process only the ones consisting entirely of c-numbers are nonzero as the vacuum expectation of any normal ordered product of operators vanishes in the vacuum state. To evaluate the c-number terms we formally need to calculate integrals of products of the f and g functions of Eq.(C.1). It is, however, not difficult to see that these integrals factorize and that the factors are exactly the ones involved in calculating expectation values of products of only two field operators. The end result is that the average of any operator product is replaced by a sum of all possible factorizations into two-operator expectations

$$\begin{aligned} \langle \hat{\psi}^\dagger(x_1)\hat{\psi}^\dagger(x_2)\hat{\psi}(x_3)\hat{\psi}(x_4)\rangle = & \langle \hat{\psi}^\dagger(x_1)\hat{\psi}^\dagger(x_2)\rangle\langle \hat{\psi}(x_3)\hat{\psi}(x_4)\rangle \\ & + \langle \hat{\psi}^\dagger(x_1)\hat{\psi}(x_3)\rangle\langle \hat{\psi}^\dagger(x_2)\hat{\psi}(x_4)\rangle \\ & + \langle \hat{\psi}^\dagger(x_1)\hat{\psi}(x_4)\rangle\langle \hat{\psi}^\dagger(x_2)\hat{\psi}(x_3)\rangle. \end{aligned} \tag{C.2}$$

Appendix D

Synthesis of correlated noise

In order to numerically simulate Eqs. (5.17) and (5.18) we discretize time and space, and we synthesize noise terms, $dW_{1,2}(x_n, t_i)$, that obey discretized versions of Eqs. (5.19)–(5.22). It is well-known how independent (pseudo) random numbers from different distributions can be created. For example a Gaussian distribution can be created starting from uniformly distributed numbers via the Box-Müller method, i.e. we know how to produce $\{dU_{1,2}(x_n, t_i)\}$ so that

$$\langle dU_{1,2}(x_n, t_i)\rangle = 0 \tag{D.1}$$

$$\langle dU_\alpha(x_n, t_i) dU_\beta(x_m, t_j)\rangle = \delta_{\alpha\beta}\delta_{nm}\delta_{ij}. \tag{D.2}$$

We see that the correlation functions, Eqs. (5.21) and (5.22), contain two terms: one from the interaction and one from the incoupling. These can be treated separately if we split the noise in two independent contributions

$$dW_{1,2}(x_n, t_i) = dW^g_{1,2}(x_n, t_i) + dW^b_{1,2}(x_n, t_i) \tag{D.3}$$

Due to the contact form of the interaction, the corresponding noise term poses no difficulties; we simply choose

$$dW^g_{1,2}(x_n, t_i) = \sqrt{\frac{\pm ig\psi(x_i)dt}{dx}} dU^g_{1,2}(x_n, t_i), \tag{D.4}$$

where $dU^g_{1,2}$ is chosen with the properties expressed by (D.1) and (D.2). The incoupling term is more involved. The corresponding noise terms are created by multiplication and convolution of uncorrelated noise, $dU^b_{1,2}$, obeying (D.1) and (D.2) with suitable Gaussian functions:

$$dW^b_{1,2}(x_n, t_i) = \mathcal{N} \exp(\pm it_i\Delta) \exp\left(-\frac{x_n^2}{2\sigma_a^2}\right) \times \\ \times \sum_{n'} dx\; dU^b_{1,2}(x_{n'}, t_i) \exp\left(-\frac{(x_n - x_{n'})^2}{2\sigma_b^2}\right) \tag{D.5}$$

It turns out that choosing

$$\sigma_a^2 = 2\sigma_{cm}^2, \qquad \sigma_b^2 = \frac{2\sigma_{cm}^2\sigma_r^2}{4\sigma_{cm}^2 - \sigma_r^2}, \qquad \mathcal{N} = \sqrt{\frac{\pm idtB}{dx\sqrt{\pi}\sigma_r\sigma_{cm}\sigma_b}} \tag{D.6}$$

is sufficient to fulfill Eq. (5.19) with b given by Eq. (5.5). σ_r and σ_b are rather small, and in practice the sum in Eq. (D.5) only needs to involve a few terms.

Bibliography

[1] U. V. Poulsen and K. Mølmer, Phys. Rev. A **63**, 023604 (2001).

[2] U. V. Poulsen and K. Mølmer, C. R. Acad. Sci. Paris **, Série IV**, 687 (2001).

[3] U. V. Poulsen and K. Mølmer, Phys. Rev. A **64**, 013616 (2001).

[4] U. V. Poulsen and K. Mølmer, Phys. Rev. Lett. **87**, 123601 (2001).

[5] U. V. Poulsen and K. Mølmer, Phys. Rev. A **65**, 033613 (2002).

[6] U. V. Poulsen and K. Mølmer, (2002), cond-mat/0207029, submitted to Phys. Rev. A.

[7] U. V. Poulsen and K. Mølmer, Euro. Phys. J. D **11**, 151 (2000).

[8] A. S. Parkins and D. F. Walls, Phys. Rep. **303**, 1 (1998).

[9] F. Dalfovo, S. Giorgini, and S. Stringari, Rev. Mod. Phys. **71**, 463 (1999).

[10] A. J. Leggett, Rev. Mod. Phys. **73**, 307 (2001).

[11] C. Pethick and H. Smith, *Bose–Einstein Condensation in Dilute Gases* (Cambridge University Press, Cambridge, 2002).

[12] K. Huang, *Statistical Mechanics*, 2 ed. (John Wiley & Sons, Singapore, 1987).

[13] E. Timmermans, P. Tommasini, M. Hussein, and A. Kerman, Phys. Rev. **315**, 199 (1999).

[14] S. L. Cornish *et al.*, Phys. Rev. Lett. **85**, 1795 (2000).

[15] C. C. Bradley, C. A. Sackett, J. J. Tollett, and R. G. Hulet, Phys. Rev. Lett. **75**, 1687 (1995).

[16] C. C. Bradley, C. A. Sackett, J. J. Tollett, and R. G. Hulet, Phys. Rev. Lett. **79**, 1170 (1997).

[17] E. A. Donley *et al.*, Nature **412**, 295 (2001).

[18] E. P. Gross, J. Math. Phys. **4**, 195 (1963).

[19] V. L. Ginzburg and L. P. Pitaevskii, Sov. Phys. JETP **7**, 858 (1958), [Zh. Eksp. Teor. Fiz. **34**, 1240-1245 (1958)].

[20] L. P. Pitaevskii, Sov. Phys. JETP **13**, 451 (1961), [Zh. Eksp. Teor. Fiz. **40**, 646-651 (1961)].

[21] Y. Castin and R. Dum, Phys. Rev. Lett. **77**, 5315 (1996).

[22] Y. Castin, in *Coherent atomic matter waves*, *Les Houches Session LXXII*, edited by R. Kaiser, C. Westbrook, and F. David (Springer, Berlin, 2001), pp. 1–136, cond-mat/0105058.

[23] C. Gardiner and P. Zoller, *Quantum Noise*, Vol. 56 of *Springer series in synergetics*, 2 ed. (Springer–Verlag, Berlin, 2000).

[24] C. Herzog and M. Olshanii, Phys. Rev. A **55**, 3254 (1997).

[25] F. Illuminati, P. Navez, and M. Wilkens, J. Phys. B: At. Mol. Opt. Phys. **32**, L461 (1999).

[26] W. Ketterle and H.-J. Miesner, Phys. Rev. A **56**, 3291 (1997).

[27] R. J. Dodd, C. W. Clark, M. Edwards, and K. Burnett, Optics Express **1**, 284 (1997).

[28] Y. Kagan, B. V. Svistunov, and G. V. Shlyapnikov, Pis'ma Zh. Eksp. Teor. Fiz. **42**, 169 (1985), [JETP Lett. **42**, 209 (1985)].

[29] E. A. Burt *et al.*, Phys. Rev. Lett. **79**, 337 (1997).

[30] J. I. Cirac, C. W. Gardiner, M. Naraschewski, and P. Zoller, Phys. Rev. A **54**, R3714 (1996).

[31] E. V. Goldstein, O. Zobay, and P. Meystre, Phys. Rev. A **58**, 2373 (1998).

[32] W. Ketterle, D. S. Durfee, and D. M. Stamper-Kurn, in *Bose–Einstein condensation in atomic gases*, *Proceedings of the international school of physics – Enrico Fermi*, edited by M. Inguscio, S. Stringari, and C. E. Wieman (IOS Press, Amsterdam, 1999), pp. 67–176.

[33] A. Browaeys *et al.*, Phys. Rev. A **64**, 034703 (2001).

[34] M. R. Andrews *et al.*, Science **275**, 637 (1997).

[35] J. Javanainen and S. M. Yoo, Phys. Rev. Lett. **76**, 161 (1996).

[36] Y. Castin and J. Dalibard, Phys. Rev. A **55**, 4330 (1997).

[37] J. A. Dunningham and K. Burnett, Phys. Rev. Lett. **82**, 3729 (1999).

[38] K. Mølmer, Phys. Rev. A **65**, 021607(R) (2002).

[39] N. Bogoliubov, J. Phys. (Moscow) **11**, 23 (1947).

[40] C. W. Gardiner, Phys. Rev. A **56**, 1414 (1997).

[41] Y. Castin and R. Dum, Phys. Rev. A **57**, 3008 (1998).

[42] P. Öhberg *et al.*, Phys. Rev. A **56**, R3346 (1997).

[43] J. M. Vogels, K. Xu, J. R. Abo-Shaeer, and W. Ketterle, Phys. Rev. Lett. **88**, 060402 (2002).

[44] A. Brunello, F. Dalfovo, L. Pitaevskii, and S. Stringari, Phys. Rev. Lett. **85**, 4422 (2000).

[45] M. Lewenstein and L. You, Phys. Rev. Lett. **77**, 3489 (1996).

[46] K. Mølmer, Phys. Rev. A **58**, 566 (1998).

[47] W. Krauth, Phys. Rev. Lett. **77**, 3695 (1996).

[48] C. W. Gardiner, *Handbook of Stochastical Methods* (Springer-Verlag, Berlin, 1983).

[49] P. D. Drummond and C. W. Gardiner, J. Phys. A: Math. Gen. **13**, 2353 (1980).

[50] S. L. Braunstein, C. M. Caves, and G. J. Milburn, Phys. Rev. A **43**, 1153 (1991).

[51] I. Carusotto and Y. Castin, J. Phys. B: At. Mol. Opt. Phys. **34**, 4589 (2001).

[52] A. M. Smith and C. W. Gardiner, Phys. Rev. A **39**, 3511 (1989).

[53] P. E. Kloeden and E. Platen, *Numerical Solution of Stochastic Differential Equations* (Springer-Verlag, New York/Berlin, 1992).

[54] M. J. Werner and P. D. Drummond, J. Comp. Phys. **132**, 312 (1997).

[55] G. Collecutt and P. D. Drummond, `xmds`: eXtensible Multi-Dimensional Simulator, `http://www.physics.uq.edu.au/xmds/`, 2001.

[56] I. Carusotto, Y. Castin, and J. Dalibard, Phys. Rev. A **63**, 023606 (2001).

[57] A. Gilchrist, C. W. Gardiner, and P. D. Drummond, Phys. Rev. A **55**, 3014 (1997).

[58] M. J. Steel *et al.*, Phys. Rev. A **58**, 4824 (1998).

[59] A. Sinatra, Y. Castin, and C. Lobo, J. Mod. Optics **47**, 2629 (2000).

[60] A. Sinatra, C. Lobo, and Y. Castin, Phys. Rev. Lett. **87**, 210404 (2001).

[61] P. D. Drummond and J. F. Corney, Phys. Rev. A **60**, R2661 (1999).

[62] M. Fleischhauer, private communication.

[63] L. I. Plimak, M. Fleischhauer, M. K. Olsen, and M. J. Collett, (2001), cond-mat/0102483.

[64] H. T. C. Stoof, in *Coherent atomic matter waves*, *Les Houches Session LXXII*, edited by R. Kaiser, C. Westbrook, and F. David (Springer, Berlin, 2001), pp. 219–315, cond-mat/9910441.

[65] P. Deuar and P. D. Drummond, Comp. Phys. Comm. **142**, 442 (2001).

[66] I. Carusotto and Y. Castin, (2002), cond-mat/0206211.

[67] M. K. Olsen, L. I. Plimak, and M. J. Collett, Phys. Rev. A **64**, 063601 (2001).

[68] J. J. Sakurai, *Modern Quantum Mechanics* (Addison-Wesley Publishing Company, Reading, Massachusetts, 1994).

[69] A. Perelomov, *Generalized Coherent States and Their Application*, *Texts and Monographs in Physics* (Springer-Verlag, Berlin, 1986).

[70] M. Kitagawa and M. Ueda, Phys. Rev. A **47**, 5138 (1993).

[71] *Atom Interferometry*, edited by P. Berman (Academic Press, New York, 1997).

[72] D. J. Wineland, J. J. Bollinger, W. M. Itano, and D. J. Heinzen, Phys. Rev. A **50**, 67 (1994).

[73] G. S. Agarwal and R. R. Puri, Phys. Rev. A **41**, 3782 (1990).

[74] A. Kuzmich, K. Mølmer, and E. S. Polzik, Phys. Rev. Lett. **79**, 4782 (1997).

[75] J. Hald, J. L. Srensen, C. Schori, and E. S. Polzik, Phys. Rev. Lett. **83**, 1319 (1999).

[76] A. E. Kozhekin, K. Mølmer, and E. Polzik, Phys. Rev. A **62**, 033809 (2000).

[77] A. Kuzmich, N. P. Bigelow, and L. Mandel, Europhys. Lett. **42**, 481 (1998).

[78] K. Mølmer, Euro. Phys. J. D **5**, 301 (1999).

[79] A. Kuzmich, L. Mandel, and N. P. Bigelow, Phys. Rev. Lett. **85**, 1594 (2000).

[80] K. Mølmer and A. Sørensen, Phys. Rev. Lett. **82**, 1835 (1999).

[81] A. Sørensen and K. Mølmer, Phys. Rev. Lett. **83**, 2274 (1999).

[82] I. Bouchoule and K. Mølmer, Phys. Rev. A **65**, 041803(R) (2002).

[83] H. Pu and P. Meystre, Phys. Rev. Lett. **85**, 3987 (2000).

[84] L.-M. Duan, A. Sørensen, J. I. Cirac, and P. Zoller, Phys. Rev. Lett. **85**, 3991 (2000).

[85] A. Sørensen, L.-M. Duan, I. Cirac, and P. Zoller, Nature **409**, 63 (2001).

[86] J. A. Dunningham, K. Burnett, and M. Edwards, Phys. Rev. A **64**, 015601 (2001).

[87] S. Raghavan, H. Pu, P. Meystre, and N. Bigelow, Opt. Comm. **188**, 149 (2001).

[88] D. S. Hall *et al.*, Phys. Rev. Lett. **81**, 1539 (1998).

[89] E. V. Goldstein, M. G. Moore, H. Pu, and P. Meystre, Phys. Rev. Lett. **85**, 5030 (2000).

[90] A. Sinatra and Y. Castin, Euro. Phys. J. D **8**, 319 (2000).

[91] A. S. Sørensen, Phys. Rev. A **65**, 043610 (2002).

[92] C. Menotti, J. R. Anglin, J. I. Cirac, and P. Zoller, Phys. Rev. A **63**, 023601 (2001).

[93] E. W. Hagley *et al.*, Phys. Rev. Lett. **83**, 3112 (1999).

[94] J. Denschlag *et al.*, Science **287**, 97 (2000).

[95] J. E. Simsarian *et al.*, Phys. Rev. Lett. **85**, 2040 (2000).

[96] F. Chevy, K. W. Madison, V. Bretin, and J. Dalibard, Phys. Rev. A **64**, R031601 (2001).

[97] S. Inouye *et al.*, (2001).

[98] F. P. D. Santos *et al.*, Phys. Rev. Lett. **86**, (2001).

[99] A. Robert *et al.*, Science **292**, 461 (2001).

[100] N. Treps *et al.*, Phys. Rev. Lett. **88**, 203601 (2002).

[101] P. Kok *et al.*, Phys. Rev. A **63**, 063407 (2001).

[102] G. Björk, L. L. Sanchez-Soto, and J. Söderholm, Phys. Rev. A **64**, 013811 (2001).

[103] K. Mattle, H. Weinfurter, P. G. Kwiat, and A. Zeilinger, Phys. Rev. Lett. **76**, 4656 (1996).

[104] D. Bouwmeester *et al.*, Nature **390**, 575 (1997).

[105] A. Furusawa *et al.*, Science **282**, 706 (1998).

[106] C. Fabre and E. Giacobino (eds.), *Quantum Noise Reduction in Optical Systems*, Special issue of Appl. Phys. B **55**, (1992).

[107] P. R. Hemmer *et al.*, Opt. Lett. **20**, 982 (1995).

[108] M. D. Lukin, P. R. Hemmer, M. Löffler, and M. O. Scully, Phys. Rev. Lett. **81**, 2675 (1998).

[109] M. D. Lukin, A. B. Matsko, M. Fleischhauer, and M. O. Scully, Phys. Rev. Lett. **82**, 1847 (1999).

[110] M. G. Raymer and J. Mostowski, Phys. Rev. A **24**, 1980 (1981).

[111] M. G. Raymer, I. A. Walmsley, J. Mostowski, and B. Sobolewska, Phys. Rev. A **32**, 332 (1985).

[112] R. L. Carman, F. Shimizu, C. S. Wang, and N. Bloembergen, Phys. Rev. A **2**, 60 (1970).

[113] C. Liu, Z. Dutton, C. H. Behroozi, and L. V. Hau, Nature **409**, 490 (2001).

[114] D. F. Phillips *et al.*, Phys. Rev. Lett. **86**, 783 (2001).

[115] M. Fleischhauer and M. D. Lukin, Phys. Rev. Lett. **84**, 5094 (2000).

[116] C. W. Gardiner, Phys. Rev. Lett. **70**, 2269 (1993).

[117] C. W. Gardiner and S. Parkins, Phys. Rev. A **50**, 1792 (1994).

[118] I. S. Averbukh and N. F. Perelman, Phys. Lett. A **139**, 449 (1989).

[119] E. Wright *et al.*, Phys. Rev. A **56**, 591 (1997).

[120] A. Sinatra and Y. Castin, Euro. Phys. J. D **4**, 247 (1998).

[121] A. Sinatra and Y. Castin, private communication.

[122] H. R. Thorsheim, J. Weiner, and P. S. Julienne, Phys. Rev. Lett. **58**, 2420 (1987).

[123] W. C. Stwalley and H. Wang, J. Mol. Spect. **195**, 194 (1999).

[124] R. Wynar *et al.*, Science **287**, 1016 (2000).

[125] M. Mackie, R. Kowalski, and J. Javanainen, Phys. Rev. Lett. **84**, 3803 (2000).

[126] J. J. Hope, M. K. Olsen, and L. I. Plimak, Phys. Rev. A **63**, 043603 (2001).

[127] J. J. Hope, Phys. Rev. A **64**, 053608 (2001), 8 pages.

[128] P. S. Julienne, K. Burnett, Y. P. Band, and W. C. Stwalley, Phys. Rev. A **58**, R797 (1998).

[129] M. Holland, J. Park, and R. Walser, Phys. Rev. Lett. **86**, 1915 (2001).

[130] P. D. Drummond, K. V. Kheruntsyan, and H. He, Phys. Rev. Lett. **81**, 3055 (1998).

[131] V. A. Yurovsky, A. Ben-Reuven, P. S. Julienne, and C. J. Williams, Phys. Rev. A **62**, 043605 (2000).

[132] M. Koštrun, M. M. R. Côté, and J. Javanainen, Phys. Rev. A **62**, 063616 (2000).

[133] K. Góral, M. Gajda, and K. Rzążewski, Phys. Rev. Lett. **86**, 1397 (2000).

[134] D. J. Heinzen, R. Wynar, P. D. Drummond, and K. V. Kheruntsyan, Phys. Rev. Lett. **84**, 5029 (2000).

[135] S. Kokkelmans and M. Holland, (2002), cond-mat/0204504.

[136] E. A. Donley, N. R. Claussen, S. T. Thompson, and C. E. Wieman, Nature **417**, 529 (2002).

[137] T. Haugset and H. Haugerud, Phys. Rev. A **57**, 3809 (1998).

[138] K. Huang, *Quantum Field Theory* (John Wiley & Sons, New York, 1998).

[139] M. Kitamura and T. Tokihiro, J. Opt. B: Quantum Semiclass. **1**, 546 (1999).

[140] J. Javanainen and M. Mackie, Phys. Rev. Lett. **88**, 090403 (2002).

[141] H. Ammann and N. Christensen, Phys. Rev. Lett. **78**, 2088 (1997).

[142] S. H. Myrskog *et al.*, Phys. Rev. A **61**, 053412 (2000).

[143] M. Sargent III, M. O. Scully, and W. E. Lamb, *Laser Physics* (Addison Wesley, Reading Massachusetts, 1974).

[144] L. A. Lugiato *et al.*, Nouvo Cimento **D 10**, 959 (1988).

[145] T. Guhr, A. Müller-Groeling, and H. A. Weidenmüller, Phys. Rev. **299**, 189 (1998).

[146] W. G. Unruh, in *Quantum Optics, Experimental Gravitation and Measurement Theory*, edited by P. Meystre and M. O. Scully (Plenum, New York, 1983), p. 647.

[147] J. A. Dunninghama, M. J. Collett, and D. F. Walls, J. Mod. Optics **245**, 49 (1998).

[148] S. Reynaud, C. Fabre, E. Giacobino, and A. Heidemann, Phys. Rev. A **40**, 1440 (1989).

[149] J. J. Hope and M. K. Olsen, Phys. Rev. Lett. **86**, 3220 (2001).

[150] L. Deng *et al.*, Science **398**, 218 (1999).

[151] J. Vogels, K. Xu, and W. Ketterle, Phys. Rev. Lett. **89**, 020401 (2002).

[152] S. Inouye *et al.*, Nature **402**, 641 (1999).

[153] S. Inouye *et al.*, Phys. Rev. Lett. **85**, 4225 (2000).

[154] J. W. Halley, C. E. Campbell, C. F. Giese, and K. Goetz, Phys. Rev. Lett. **71**, 2429 (1993).

[155] A. K. Setty, J. W. Halley, and C. E. Campbell, Phys. Rev. Lett. **79**, 3930 (1997).

[156] A. Wynveen *et al.*, Phys. Rev. A **62**, 023602 (2000).

[157] R. Y. Chiao, C. Ropers, D. Solli, and J. M. Hickmann, in *Coherence and Quantum Optics VIII*, edited by J. H. Eberly and E. Wolf (Plenum Press, New York, to appear).

[158] M. J. Bijlsma and H. T. C. Stoof, Phys. Rev. A **62**, 013605 (2000).

[159] J. A. Fleck, Jr., J. R. Morris, and M. D. Feit, Appl. Phys. B **10**, 129 (1976).

[160] L. D. Carr, K. W. Mahmud, and W. P. Reinhardt, Phys. Rev. A **64**, 033603 (2001).

[161] E. Altewischer, M. van Exter, and J. Woerdman, Nature **418**, 304 (2002).

[162] R. Folman *et al.*, Phys. Rev. Lett. **84**, 4749 (2000).

[163] D. Cassettari *et al.*, Phys. Rev. Lett. **85**, 5483 (2000).

[164] W. Hänsel, P. Hommelhoff, T. Hänsch, and J. Reichel, Nature **413**, 498 (2001).

[165] N. Levinson, Kgl. Danske Videnskab. Selskab **25**, 9 (1949).

[166] J. Jauch, Helv. Phys. Acta **30**, 143 (1957).

[167] M. S. de Bianchi, J. Math. Phys. **35**, (1994).